UNIVERSITETET
I OSLO

Masteroppgave

Functional Characterization of Bardet Biedl associating protein-IFT27

Simen Roland Aronsson

Biomolecules and Biomaterials
60 Credits

Department of Chemistry
Faculty of Mathematics and Natural Sciences

2024

Functional Characterization of Bardet-Biedl associating Protein-IFT27

Simen Roland Aronsson

http://www.duo.uio.no/

Printing by Reprosentralen, Universitetet i Oslo

Acknowledgments

A big thank you must be given to my supervisor Assoc. Prof. Nikolina Sekulic[1], for giving me this project. I appreciate all the time and effort you have put into this project, and I have learnt a lot from the many discussions we have had about each step of project. I would also like to thank my co-supervisor Dr. Ahmad Ali-Ahmad[2], for always having time for answering questions and teaching me how to properly use techniques and equipment. I truly appreciate both of yours seemingly endless knowledge of biochemistry.

I also greatly appreciate the rest of the group members of the Sekulic lab, Dr. Dario Seguera[3], Anna Mørch[4], Hemanga Gogoi[5] and Ole Magnus Fløgstad[6]. A special thanks goes to Hemanga for answering the smaller everyday questions about the lab. I appreciate all the fun moments in the lab with Ole and Hemanga especially. A final thank you to Dr. Cinzia Anita Maria Progida[7], for her input on this project.

The support from friends and family has been greatly appreciated, especially my parents who have supported me through my time as a student.

UiO, February 2024

Simen Roland Aronsson

[1] Associated Professor, Group Leader, Structural Biology and Chromatin, Centre for Molecular Medicine Norway, NCMM, University of Oslo

[2] Postdoctoral Researcher, Sekulic Group Structural Biology and Chromatin, Centre for Molecular Medicine Norway, NCMM, University of Oslo

[3] Postdoctoral Researcher, Sekulic Group Structural Biology and Chromatin, Centre for Molecular Medicine Norway, NCMM, University of Oslo

[4] Former Master student, Sekulic Group Structural Biology and Chromatin, Centre for Molecular Medicine Norway, NCMM, University of Oslo

[5]Research Assistant, Sekulic Group Structural Biology and Chromatin, Centre for Molecular Medicine Norway, NCMM, University of Oslo

[6]PhD Candidate, Sekulic Group Structural Biology and Chromatin, Centre for Molecular Medicine Norway, NCMM, University of Oslo

[7]Professor, Progida Group Cell Dynamics, Department of Biosciences, University of Oslo

Abstract

Bardet-Biedl Syndrome (BBS) is a ciliopathy, a severe genetic disorder that negatively affects the primary cilia, an organelle the cell uses to sense the environment around it. Patients with BBS have genetic mutations in the intraflagellar transport proteins which are normally responsible for the function of the primary cilia. Two mutations in Intraflagellar transport protein 27 (IFT27), IFT27^{Y35C} and IFT27^{C99Y} are identified in Bardet-Biedl syndrome patients but how these mutations could cause disease is not clear.

Recent results from Porgida's laboratory have shown that IFT27 localizes to the midbody during cell division along with centromere-associated protein (CENP-J) and Aurora B kinase. Personal communication and preliminary data suggest that IFT27 mutations associated with BBS affect the final stages of cell division by retaining chromatin in the midbody. This leads to prolonged cytokinesis and increased cell mortality, but the molecular mechanism behind this phenomenon is not well understood.

Here, I have successfully expressed and purified IFT27 with its binding partner IFT25 (IFT25/IFT27^{WT}) as well as BBS-associated mutant IFT25/IFT27^{Y35C} but IFT25/IFT27^{C99Y} was not soluble. Using size exclusion chromatography (SEC) and GTPase activity tests, I have found that both purified protein complexes are well folded. I have also expressed and purified active Aurora B$^{60-360}$ kinase and using pull-down assay I confirmed that both GST-IFT25/IFT27^{WT} and GST-IFT25/IFT27^{Y35C} directly bind Aurora B$^{60-360}$ kinase but further experiments are needed to confirm if they differentially affect the enzymatic activity. Finally, I expressed and purified CENP-J$^{412-897}$ and using pull-down experiments, I found that neither IFT25/IFT27^{WT} nor IFT25/IFT27^{Y35C} directly bind CENP-J$^{412-897}$. Results of this thesis are the first step in understanding the role of IFT27 and how BBS related mutations might lead to the disease.

Abbreviations

3C protease	**Human rhinovirus 3C protease**
Amp	Ampicillin
AuB	Aurora B kinase
BBS	Bardet-Biedl Syndrome
BME	2-Mercaptoethanol
bp	Base pair
C-terminal	Carboxyl-terminal
Cam	Chloroamphenicol
CDC	Cilium disassembly complex
CPC	Chromosomal Passenger Complex
cDNA	Copy DNA
CENP-J	Centromere protein J
CV	Column Volume
Da	Dalton
dNTP	Deoxy nucleoside triphosphate
DTT	Dithiothreitol
E. coli	*Escherichia coli*
EDTA	Ethylenediamine tetraacectate
EGTA	Egtazic Acid
GDP	Guanosine triphosphate
GTP	Guanosine diphosphate
GST	Glutathione S-transferase
His-tag	Histidine tag
IFT25	Intraflagellar transport protein 25
IFT27	Intraflagellar transport protein 27
IPTG	Isopropyl β-D-1-thiogalactopyranoside
KLD	Kinase, Ligase, DnpI
LB	Lysogeny Broth
LDH	Lactose Dehydrogenase
mAu	Milli absorbance unit

MilliQ water	Milli-Q filtered water
MWCO	Molecular weight cut-off
NADH	Nicotinamide adenine dinucleotide
N-terminal	Amino-terminal
NEB	New England Biolabs
OD_{600}	Optical density at 600 nm
PCR	Polymerase Chain Reaction
PEP	Phosphoenolpyruvate
pI	Isolectric point
PK	Pyrovate Kinase
PTM	Post translational modifications
RPM	Rounds per Minute
SDS-PAGE	Sodium Dodecyl Sulphate Polyacrylamide electrophoresis
SEC	Size Exclusion Chromatography
TEV	Tobacco Etch Virus
Tm	Melting temperature
Tris	Tris(hydroxymethyl)aminomethane
UiO	Universitetet i Oslo
UV	Ultraviolet
WT	Wild type

Table of contents

1. Introduction

1.1 Bardet Biedl Syndrome

Bardet-Biedl syndrome (BBS) and can manifest itself as polydactyly, obesity, rod/cone dystrophy, hypogonadism and reduced function of the kidneys (Beales et al. 1999) BBS is a very rare condition with roughly 60 people diagnosed in Norway (Kvam, 2022). Since BBS is a genetic disorder, it is impossible to cure the disease, and treatment usually consists of alleviating symptoms and patients must learn to live with the disabilities as best as possible. Patients often experience secondary symptoms stemming from the primary symptoms, for example, many BBS patients develop diabetes type II and cardiovascular problems caused by obesity (Pomeroy, Offenwanger, and Timmler 2023) (Forsythe et al. 2015).

Genetic disorders that negatively affects the cilia and its formation, disassembly or function, are called ciliopathies. BBS falls in this category, and patients with BBS show genetic mutations within proteins that are employed in cilia. In the next paragraphs I will explain the basic scientific terms that are necessary for understanding BBS.

1.2 Primary Cilia

Cilia are hair like organelle protruding out from the membrane of most eukaryotic cells. There are two classes of cilia, motile and non-motile. Almost all non-motile cilia function as sensory organelle, and most vertebrate cells contain a single non motile cilium called the primary cilia. The determining factor of whether a cilium is motile or non-motile is the structure of their axoneme. The axoneme is the internal skeleton of primary cilia. In the primary cilia, that are non-motile, the axoneme consists of nine microtubule pairs (9+0 axoneme), while in motile cilia axoneme also has the microtubule pair in the centre (9+2 axoneme) and this is responsible for motility (Nicastro et al. 2006). The axoneme is connected to the basal body, a foundation found inside the larger body of the cell. Between the basal body and the axoneme is the transition zone, an area found at the very base of the cilia parturition, that controls the intraflagellar transport (IFT) of proteins up and down the cilia (Wang et al. 2022).

Primary cilia serve as sensory organelles that detect mechanical and chemical cues from the environment. They also regulate various cellular processes including cell differentiation, proliferation, and migration. Primary cilia play a crucial role in signal transduction pathways. Signalling pathways

coordinated by the primary cilia are varied, and are often determined by the cell type (Eggenschwiler and Anderson 2007). Through customization of the primary cilia, it can inhabit functions required for specific cells, like mechanoreceptors for epithelial cells sensing urine flow, or as a photoreceptor, transporting rhodopsin pigment (Hildebrandt and Otto 2005).

The main overall function of the primary cilium is therefore to sense the exterior environment around the cell and send the information gathered to the interior. Dysfunction or absence of primary cilia impairs the cells' ability to sense the environment, and has been linked to a variety of developmental and genetic disorders including polycystic kidney disease, Bardet-Biedl syndrome, and retinal degeneration (Elawad et al. 2022).

1.3 Intraflagellar Transport

Cilia assembly, maintenance and regular usage requires transport of material up and down the cilium. To accomplish this, eukaryotic cells have developed a system to transport material, as there are no ribosomes inside the cilia to produce necessary proteins (Lechtreck et al. 2017).

Between the basal body and the cilium itself, there is an area called the transition zone that serves as diffusion barrier, restricting access to the cilia for particles that happened to wander in. If actual cargo appears at the transition zone, they will be transported by two protein complexes, IFT-A and IFT-B. Together these form IFT trains. However, it isn't these trains that locomote the cargo up to the cilia tip. This is performed by a kinesin attached to IFT-B, that moves up the axonemal microtubules (Nonaka et al. 1998), leaving the IFT trains as mere passports to ensure safe passage to the cilia tip. When arriving at the tip a reshuffling happens to the trains making them able to travel down the cilia. The biggest change now being that dynein is connected to IFT-A, transports the complex down. A third protein complex, BBSome, can connect to the train but is not required for travelling down the cilia. BBSome is a cargo adaptor, able to connect to and transport membrane protein, but not required for protein transport. (Wingfield, Lechtreck, and Lorentzen 2018). Figure 1.3.1 illustrates this process. BBS can interact with membrane proteins that function as receptors, and this mechanism is reason that the cilium can act as sensor of the extracellular environment (Nakayama and Katoh 2020). At the base of the cilium, a protein called IFT27 promotes the exit of the BBSome from cilia, together with its cargo (Liew et al. 2014).

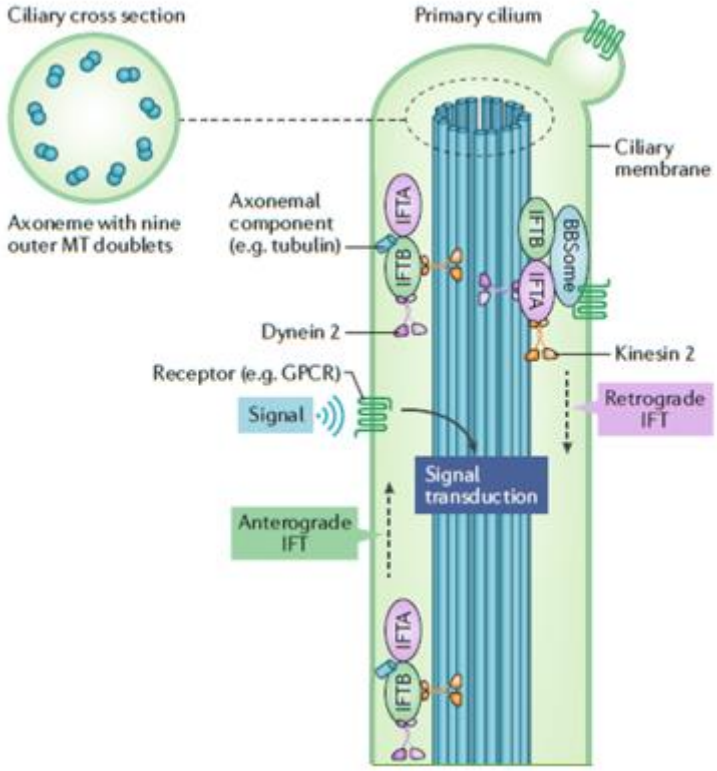

Figure 1.3.1: IFT transport goes up and the down along the axoneme, which consists of a ring made up of nine microtubule pairs. The BBSsome can interact with receptor membrane proteins while it is transported down the cilium, which is the proposed method behind the primary cilia's ability to sense the environment. Figure modified from (Anvarian et al. 2019).

1.4 IFT27

One of the proteins involved the intraflagellar transport is IFT27 (intraflagellar transport protein 27). This protein is a 21 kDa Rab-like small G protein that is part of the IFT-B subcomplex and shows detectable levels of GTPase activity (Huet et al. 2014). The protein is shown to play a vital role in not only IFT-B, but also the entirety of IFT trains, as removal of IFT27 reduces the amount of IFT-A and IFT-B complexes in *Chlamydomonas* (Qin et al. 2007). Cells with IFT27 knockdown have been shown to destabilize the IFT trains, which in turn made cells grow slower and increased the amount of cell defects and cell mortality rate (Qin et al. 2007). For IFT27 to interact with the rest of the IFT-B complex it must bind GTP (Huet et al. 2014). The IFT27 binds to another protein IFT25, and it is this IFT25/IFT27 subcomplex that becomes part of the larger IFT-B complex (Wang et al. 2009).

1.5 Mutations in IFT27 are linked to Bardet Biedl Syndrome

Not only has mutations in IFT transport proteins been linked to BBS (Zhou et al. 2022), two point mutations in IFT27 has been linked to the disease, those being Y35C and C99Y (Schaefer et al. 2019), (Aldahmesh et al. 2014). Both point mutations are located on the protein surface but not in the GTP binding site, nor on the surface interacting with IFT25, illustrated by figure 1.5.1. Thus it is not clear why these mutations result in diseases.

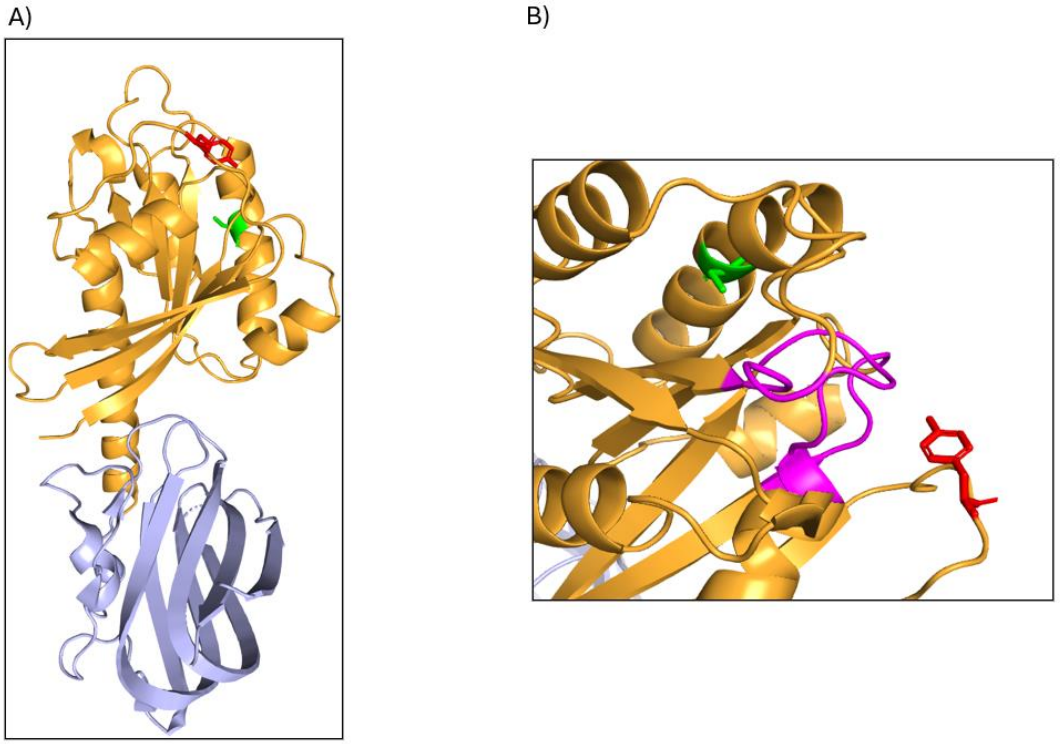

Figure 1.5.1: A) Shows IFT27 (orange) interacting with IFT25 (blue). Mutation IFT27^{C99Y} (green) and mutation IFT27^{Y35C} (red) are far from the interaction phase between IFT25 and IFT27. B) The amino acids involved in GTPase activity (12-19, 64-68, 123-126) activity are in magenta. Both mutations are not interfering with the active site. Figure made in PyMol.

Some studies have shown that IFT27 affects the localization of Aurora kinase B within the cell (Taulet et al. 2017), and the Progida lab has identified interaction between IFT27 and CENP-J that localizes to the centrosome in unpublished results. Since Aurora B and CENP-J play an important role in orchestrating different steps in cell division, this indicates that IFT27 could also have a role beyond the well characterized process in cilia (Qin et al. 2007). However, the functions of IFT outside of the cilia, are mostly unknown (Pan and Snell 2007).

1.6 Cell cycle and cell division

The cell cycle is a series of events that reorganizes the interior of the cell in preparation of mitosis, with the goal of replicating itself, and producing two identical daughter cells (Hunt, Nasmyth, and Novák 2011) illustrated by figure 1.6.1.

When the cell is not actively pursuing cell replication, it is in the G_0 phase or resting phase. The majority of a cell's lifespan is spent in this phase. The cell cycle can be divided in to four main phases in eucaryotic cells, each with specific goals. G_1 is the first step where the cell grows in size and ups its productions of bio materials and organelles that will be used in the reshuffling of the interior of the cell. The following stage, is the S phase, where the cell initiates replication of all its genome, making two sets of chromosomes. When the entirety of the genome is replicated, the next phase, G_2 can commence. Here the cell continues its rapid growth and starts the formation of spindles. These are made of microtubules that are attached to the centrosome on each end of the cell. The final step is the M phase or mitosis. In this phase the microtubules attached on duplicated chromosomes are pulling each sister chromatid away from each other and towards the spindle on the opposing sides of the cell. The mitosis ends with the cytokinesis phase, where the mother cell will divide into two genetically identical daughter cells and assembly of primary cilia may occur.

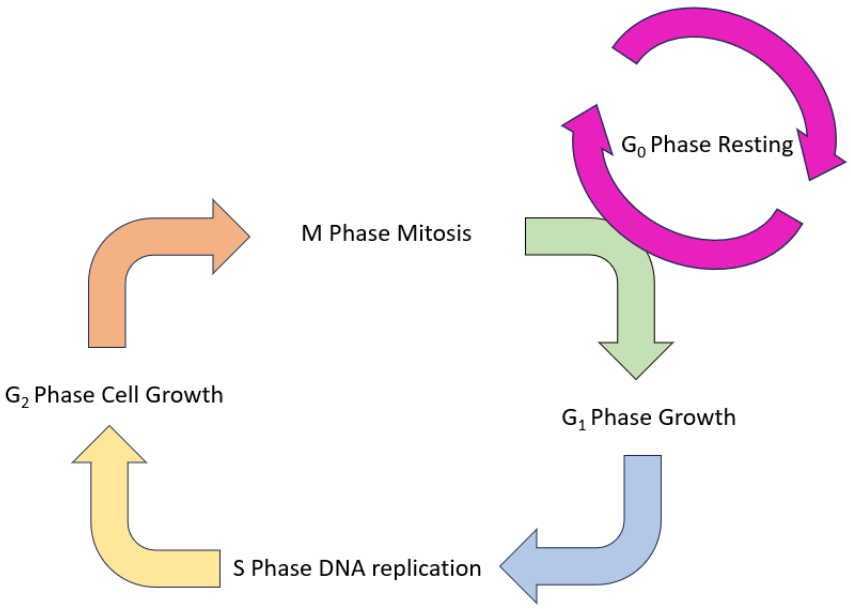

Figure 1.6.1: The cell cycle has four phases, G_1, S, G_2 and M. G_0 resting phase is when the cell is not actively preparing for mitosis. Figure made in PowerPoint.

1.7 Centrosomes, Cilia and Cell cycle

Centrosomes are organelles that serves as an organizing centre for microtubule, and are therefore a regulator of the cell cycle (Lawo et al. 2012). The centrosome is composed of two centrioles connected at a 90^{o} angle, surrounded by a mass of protein called the pericentriolar material (PCM). During the G_1 phase of the cell cycle, the centrosome has one mother centriole, connected to an undeveloped daughter centriole. As the cell prepares to enter the S phase, the daughter centriole is grown to a fully mature centriole and can now serve as platforms to create two new centrosomes. In the G_2 phase the cell prepares for the separation of chromosomes and the mother and daughter centrioles now sprouting pro-centrioles at a 90^{o} angle, separate, making two centrosomes that then migrate to opposing sides of the cell (Basten and Giles 2013). After cell division each daughter cells contain one mother centriole with an incomplete daughter centriole, making a centrosome (Nigg and Stearns 2011). If the cell is not actively pursuing cell duplication and thus enters phase G_0, the mother centriole can localize to the membrane, becoming the basis of the primary cilia (Breslow and Holland 2019). Therefore it is crucial that the primary cilia is disassembled before S phase, to ensure the centrosome can be duplicated (Plotnikova, Pugacheva, and Golemis 2009) (Figure 1.7.1). Since the appearance and disappearance of primary cilia is so tightly linked to cell cycle stages, many proteins first linked to the primary cilia, has been shown to also play other roles in regulation the cell cycle and vice versa (Wang, Wu, and Kirschner 2014).

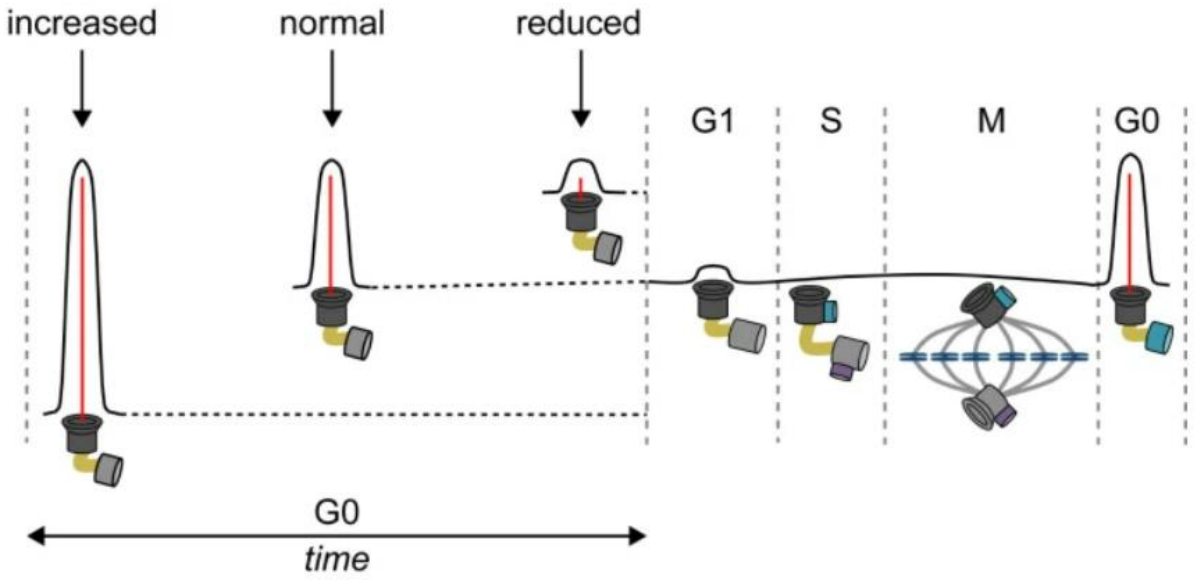

Figure 1.7.1: The primary cilia are completely disassembled before S phase, and is reassembled during the resting phase. The mother centriole is shown in black, the daughter centriole in grey and the procentriole carried over into G_0 in blue. Figure taken from (Basten and Giles 2013).

1.8 Centromere Protein J

CENP-J is confusingly named as a CENP protein (Centromere associating protein) even though it is mainly associated with the centrosome and not centromeres. It is also known as Centrosomal P4.1-associated protein (CPAP) and is a protein with an important role in cell cycle regulation, localizing within the centrosome (Kleylein-Sohn et al. 2007). CENP-J is a 153 kDa protein with versatile function involved in different processes in the centrosome, maintaining spindle poles structural integrity (Chou et al. 2016), functioning as a scaffold for the cilium disassembly complex (CDC) (Gabriel et al. 2016), and finally it is involved in centriole elongation where it is also employed as a scaffold, helping the centriole shackle PCMs (Zheng et al. 2014).

CENP-J is predicted to be mainly unfolded with several predicted long helices and G-box (a helix of beta sheet) at the C-terminus that was successfully crystalized (Hatzopoulos et al. 2013). The unstructured parts allow CENP-J to be highly functionally flexible, being able to take up a multitude of different conformations depending on the characteristics of differing proteins or complexes it is supposed to interact with. This is a feature many unstructured protein seem to inhabit (Dunker et al. 2005). It also seems to be able to form oligomers to further allow for structural and function flexibility, possibly dictated by concentration (Alvarez-Cabrera et al. 2017).

1.9 Aurora B Kinase

IFT27 has been shown to interact with Aurora B, a protein involved in mitotic regulation (Taylor and Peters 2008). Aurora B is a serine/threonine protein kinase, a class for proteins that transfers phosphate from ATP to serine or threonine residues on a protein target. It phosphorylates multiple protein in mitosis and thus regulate its progression. Aurora B kinase is part of the bigger complex called chromosomal passenger complex (CPC). (Wheatley et al. 2001) (Yasui et al. 2004). This complex plays an important part in controlling spindle assembly (Honda, Körner, and Nigg 2003), as well as attachment of duplicated chromosomes to microtubules (Mo et al. 2016). CPC inhabits three other proteins, Survivin, Borealin and INCENP. Aurora B directly interacts with INCENP, and this interaction is essential for catalytic activity of Aurora B. The C-terminal of INCENP is called IN-box and directly interacts with Aurora B. For the full activity of Aurora B/IN-box complex it is necessary that both activation loop on Aurora B and TSS motif in IN-Box are phosphorylated (Segura-Peña et al. 2023). During metaphase, CPC with Aurora B localizes to centromeres of duplicated chromosomes but in cytokinesis it stays at the cleavage furrow and gets deactivated through dephosphorylation (Mallampalli et al. 2013).

1.10 Understanding the molecular mechanisms behind Bardet Biedl Syndrome

Although many mutations have been linked to BBS, it is still unknown how these mutations alter the function of the wild type protein. Preliminary results from Progida's lab indicate that the BBS-causing mutants in IFT27 will delay cytokinesis, by retaining the chromatin at the midbody, an organelle with a principal function of localizing the site of abscission. The Progida lab has also found that CENP-J and Aurora B kinase co-localize with IFT27 and preliminary experiments show that mutants modulate Aurora B activity. In order to better understand the underlying cause of the disease, the cross-talk between cell cycle and IFT27 needs to be explored in more detail.

2. Aim of thesis

Primary cilia are eucaryotic sensory organelles that play important roles in cell signalling, homeostasis and tissue formation. Ciliopathies are genetic diseases linked with ciliary dysgenesis and dysfunction. The Bardet-Biedl syndrome (BBS) is an autosomal recessive ciliopathy characterized by vision loss, obesity, polydactyly and infertility. Molecular basis for the disease is not clear, but mutants in ciliary protein-encoding genes, particularly IFT27 are found in many patients. The exact function of IFT27 is still elusive but recent results from Progida's laboratory have shown that IFT27 localizes to the midbody during cell division along with centromere-associated protein J (CENP-J) and Aurora B kinase, an important regulator of cell division.

The main goal of this thesis is to explore if CENP-J and Aurora B kinase are direct binding partners of IFT27 and if IFT27 modulates Aurora B kinase activity. The thesis follows behaviour of wild type protein ($IFT27^{WT}$) as well as mutants identified in BBS patients ($IFT25^{Tyr35Cys}$ and $IFT27^{Cys99Tyr}$).

This thesis has 3 main objectives

1. Obtain pure proteins: $IFT27^{WT}$ and BBS-associated mutants, central domain of CENP-J ($CENP\text{-}J^{412\text{-}897}$ and Aurora B kinase
2. Test if IFT27 and BBS-associated mutants directly bind CENP-J or Aurora B
3. Test if IFT27 and BBS-associated mutants affect kinetic activity of Aurora B

Results of this study will contribute towards understanding the function of IFT27 and how mutants associated with the disease are impairing this function.

3. Methods

3.1.1 Cloning of His-MBP-TEV-IFT27 and IFT27-TEV-MBP constructs

In order to increase both the solubility and the expression level, IFT27 cDNA, originally cloned in *pET16B* plasmid with a N-terminal 6x His-tag and a TEV protease cleavage site, was amplified by Polymerase Chain Reaction (PCR), using Q5 High Fidelity DNA polymerase, and cloned into *pMAL-6ct* plasmid harbouring a N-terminal 6x His-tag followed by maltose binding domain (MBP) and TEV protease cleavage site. The PCR reaction, containing 500 nM of each primer (AA392 and AA391), 20 ng of template DNA, 200 µM of deoxy nucleotide phosphates (dNTP), 1 x reaction buffer and 1 x GC enhancer, conducted by heating to 95 °C for 30 seconds, followed by 28 of the following cycle: denaturation at 98 °C for 10 seconds, annealing at an annealing temperature that was calculated using Tm calculator (60 °C) by NEB and finally elongation at 72 °C for 1 minute. The PCR product was run on a 1% agarose gel electrophoresis and the fragment corresponding to IFT27s size was extracted using QIAquick Gel Extraction Kit (Qiagen)

The purified fragment and 2 µg of *pMAL-c6T* plasmid were separately digested with BamHI HF (NEB) and HindIII HF (NEB) for three hours at 37 °C, and the products were purified using a PCR cleaning kit (Qiagen), and gel extraction kit (Qiagen), respectively. Restriction cloning was then performed between the digested IFT27 fragment and the digested *pMAL-c6T* vector. A molar ratio of 1:3 of the digested plasmid and the insert were added together with, 1 x T4 DNA Ligase Buffer and T4 DNA ligase in a 20 µL reaction. The reaction proceeded for 10 minutes at room temperature, before deactivation of the ligase at 65 °C for 15 minutes. 12.5 ng of the ligated plasmid was transformed into 50 µL of highly competent XL10 cells. The cells were plated on LB-agar supplemented with 100 µg/mL ampicillin and grown overnight at 37 °C. 3 colonies were picked to start 3x 8 mL 2x YT ON preculture at 37 °C. The next day the plasmids were extracted using Qiagen miniprep kit (Qiagen), and sent for sequencing.

IFT27 cDNA was also cloned using the same strategy into another *pET16b* plasmid harbouring a C-terminal TEV cleavage site, followed by a 6x His-tag, using XhoI HF (NEB) and NcoI HF (NEB) restriction enzymes

3.1.2 Adding a 13 amino acid extra linker to His-MBP-TEV-IFT27 construct

To test if an extra amino acid linker would improve the MBP-tag cleaving, Q5-mutagensis was used to add an extra 13 amino acids linker (SGSSGGGSGGGGT) between the TEV cleavage site and IFT27. The PCR reaction, containing 500 nM of each primer harbouring the DNA coding for the extra linker (AA397 and AA398), 20 ng of *pET16b-HIS-MBP-TEV-IFT27* plasmid, 200 µM of deoxy nucleotide phosphates (dNTP), 1 x reaction buffer and 1 x GC enhancer, conducted by heating to 95 °C for 30 seconds, followed by 28 of the following cycle: denaturation at 98 °C for 10 seconds, annealing at an annealing temperature that was calculated using Tm calculator (60 °C) by NEB and finally elongation at 72 °C for 1 minute. To see if the product had the correct mass, 5 µL was run on a 1% agarose gel electrophoresis. The remaining reaction was treated with DnpI (NEB), for 1 hour at 37 °C to digest the methylated DNA template with the KLD mixture (kinase, ligase, DpnI) for 10 minutes at room temperature. The total reaction containing the ligated plasmid was then transformed into 50 µL of highly competent XL10 cells. The cells were plated on LB-agar plates supplemented with 100 µg/mL ampicillin and grown overnight at 37 °C. 3 colonies were picked for 3x 8 mL 2x YT ON precultures at 37 °C. The next day the plasmids were extracted by miniprep (Qiagen), and sent for sequencing.

3.1.3 Cloning of IFT25/IFT27 construct

The cDNA coding for IFT25 was purchased from Horizon Dharmacon in a non-expression plasmid (MHS6278-202839449). IFT25 was amplified by Polymerase Chain Reaction (PCR), utilizing Q5 High Fidelity DNA polymerase and cloned into *pGEX-6P* containing a N-terminal GST tag and a 3C protease cleavage site. The PCR reaction, containing 500 nM of each primer (AA416 and AA415), 20 ng of template DNA, 200 µM of deoxy nucleotide phosphates (dNTP), 1 x reaction buffer and 1 x GC enhancer, conducted by heating to 95 °C for 30 seconds, followed by 28 of the following cycle: denaturation at 98 °C for 10 seconds, annealing at an annealing temperature that was calculated using Tm calculator (59 °C) by NEB and finally elongation at 72 °C for 1 minute. The PCR product was run on a 1% agarose gel electrophoresis and the fragment corresponding to IFT25s size was extracted using QIAquick Gel Extraction Kit (Qiagen). The fragment was then cloned into *pGEX-6P* plasmid using In-Fusion enzyme mix through infusion cloning. The reaction containing 50 ng of the linearized plasmid, 2 x molar insert, 1 X In-Fusion Snap Assembly Master Mix at a total of 5 µL. The reaction proceeded for 15 minutes at 50 °C, after which it was transformed into XL10 cells and plated on LB-agar plates supplemented with 100 ng/µL and incubated overnight at 37 °C.

HIS-TEV-IFT27 originally in a *pET16b* plasmid with a N-terminal 6x His-tag and a TEV protease cleavage site along with the T7 promotor, lac operon and RBS, was amplified by PCR, using Q5 High Fidelity DNA polymerase and cloned into *pGEX-6P* plasmid already containing GST-IFT25 using T4 ligation. The reaction totalled 50 µL, 500 nM of each primer (AA417 and AA418), 20 ng of template DNA, 200 µM of deoxy nucleotide phosphates (dNTP), 1 x reaction buffer and 1 x GC enhancer. The PCR reaction, containing 500 nM of each primer, 20 ng of template DNA, 200 µM of deoxy nucleotide phosphates (dNTP), 1 x reaction buffer and 1 x GC enhancer, conducted by heating to 95 °C for 30 seconds, followed by 28 of the following cycle: denaturation at 98 °C for 10 seconds, annealing at an annealing temperature that was calculated using Tm calculator (57 °C) by NEB and finally elongation at 72 °C for 1 minute. (AA417 and AA418). The PCR product was run on a 1% agarose gel electrophoresis and the fragment corresponding to IFT27 size was extracted using QIAquick Gel Extraction Kit (Qiagen)

The purified fragment was digested with PacI HF (NEB) and NotI HF (NEB) for three hours at 37 °C. The sample was then purified using a Qiagen PCR cleaning kit (Qiagen). At the same time, 2 µg of *pGEX* already containing IFT25 plasmid was cleaved with PacI HF (NEB) and NotI (NEB) for 3 hours at 37 °C and purified using a Qiagen gel extraction kit (Qiagen). Restriction cloning was then performed between the digested IFT27 fragment and the digested *pET16b* vector. A molar ratio of 1:3 of the digested plasmid and the insert were added together with 1 x T4 DNA ligase buffer and T4 DNA ligase in a 20 µL reaction. The reaction proceeded for 10 minutes at room temperature, before deactivation of the ligase at 65 °C for 15 minutes. 12.5 ng of the ligated plasmid was transformed into 50 µL of highly competent XL10 cells. The cells were plated on LB-agar plated supplemented with 100 µg/mL ampicillin and grown overnight at 37 °C. 3 colonies were picked for a 3x 8 mL 2x YT ON preculture at 37 °C. The next day the plasmids were extracted by miniprep (Qiagen), and sent for sequencing.

3.1.4 Cloning of CENP-J$^{412\text{-}897}$ construct

The cDNA coding for CENP-J was purchased from (Horizon Dharmacon) in a non-expression plasmid (MHS6278-202826966). The DNA coding for CENP-J$^{412\text{-}897}$ was amplified by Polymerase Chain Reaction (PCR), utilizing Q5 High Fidelity DNA polymerase and cloned into *pMAL-c6T* containing a N-terminal 6x His-tag, MBP and a TEV protease cleavage site. The PCR reaction, containing 500 nM of each primer (AA284 and AA390), 20 ng of template DNA, 200 µM of deoxy nucleotide phosphates (dNTP), 1 x reaction buffer and 1 x GC enhancer, conducted by heating to 95 °C for 30 seconds, followed by 28 of the following cycle: denaturation at 98 °C for 10 seconds, annealing at an annealing temperature that was calculated using Tm calculator (64 °C) by NEB and finally elongation at 72 °C for 1 minute.

The PCR product was run on a 1% agarose gel electrophoresis and the fragment corresponding to CENP-J$^{412-897}$ size was extracted using QIAquick Gel Extraction Kit (Qiagen).

Both the purified fragment and 2µg of *pMAL-c6T* were separately digested with BamHI HF (NEB) and PstI (NEB) for three hours at 37 °C and run on 1/ agarose gel. The bands corresponding to the digested plasmid and insert were then purified using a Qiagen gel extraction kit (Qiagen). Restriction cloning was performed as previously described using a 1:3 molar ratio of plasmid to insert. 12.5 ng of the ligated plasmid was transformed into 50 µL of higly competent XL10 cells. The cells were plated on LB-agar plated supplemented with 100 µg/mL ampicillin and grown overnight at 37 °C. 3 colonies were picked for a 3x 8 mL 2x YT ON preculture at 37 °C. The next day the plasmids were extracted by miniprep (Qiagen), and sent for sequencing.

3.2 Transformation Protocol

Cells stored at -80 °C were thawed on ice for 10 minutes after which approximately 20 to 80 ng of the construct of choice was carefully mixed into the cells. The mixture was incubated on ice for 30 minutes, and then heat shocked at 42 °C for 60 seconds and immediately put on ice for 2 minutes. 600 µL of 2x YT media was added to the sample, which was later incubated for 1 hour at 37 °C. The cells were plated on LB-agar plates supplemented with the right antibiotic and incubated overnight at 37 °C.

3.3.1 Expression Protocol of GST-IFT25/His-IFT27

Using the protocol for transformation, *pGEX-6P* plasmid containing IFT25/IFT27 was transformed into Rosetta 2 cells. Three separate colonies were added to a 125 m of 2x YT preculture containing 50 µg/mL ampicillin (amp Sigma Aldrich) and 34 µg/mL chloroamphenicol (cam (Sigma Aldrich)) The preculture was then left overnight to grow at 37 °C and 120 RPM. The following day, 6x 5L-baffled flasks, each containing 1.5 L of media along with 50 µg/mL amp and 34 µg/mL cam, were inoculated with 20 mL of preculture and left to grow at 37 °C and 85 RPM until OD_{600} = 0.6. Isopropyl β-D-1-thiogalactopyranoside (IPTG (Fisher Scientific)) was added to each flask, to a final concentration of 0.33 mM to induce IFT25 and IFT27 overexpression. The cells were left to grow overnight at 18 °C at 85 RPM. The following day the cells were harvested through centrifugation at 4500 RPM for 15 minutes at 4 °C (Avanti J-26 XP, JLA-8.1, Beckman Coulter). 20 mL of lysis buffer B (50 mM Tris pH 7.5 (Sigma Aldrich Merck), 150 mM NaCl (Fisher Scientific), 5 mM $MgSO_4$ (Sigma Aldrich) and 1 mM $CaCl_2$

(Sigma Aldrich)) was used to resuspend the cells, after which the cells were frozen at -80 °C until an appropriate time for purification.

3.3.2 Purification Protocol GST-IFT25/His-IFT27

The cells were thawed at 37 °C and lysed by sonication (Branson 550) using 30 second cycles of 0.7 seconds on and 0.3 seconds off at 65% amplitude. 1 x of Turbonuclease (*Serratia Marcesens* Sigma Aldrich) was added to the lysate and incubated for 15 minutes, before clarification to remove cell debris by centrifugation, at 40000 x G for 45 minutes at 4 °C (Avanti J-26 XP, JA 25.50, Beckman Coulter). IFT25 is expressed with a GST tag, a tag that may improve solubility, but more importantly, can be used in purification as GST binds its substrate, glutathione with high affinity. The supernatant was loaded on a GST affinity column (GSTrap 4B 5 mL Cytiva) at 1.5 ml/min and then washed with washing buffer B (50 mM Tris pH 7.5, 300 mM NaCl) for 10 CV at 2.0 ml/min. Elution proceeded using elution buffer D (50 mM Tris pH 7.5, 300 mM NaCl and 10 mM Glutathione (Sigma Aldrich)) The fractions were run on SDS-PAGE gel (Mini Protean TGX Gels 5-20% (Biorad)) to determine their content. Fractions containing IFT25 and IFT27 were pooled together and dialysed overnight at 4 °C against washing buffer B in the presence of 3C protease (1 mg) to cleave off the GST tag.

IFT27 is expressed with a His tag. This is a very common tag used for purification, as it is a small, mostly unintrusive tag that have high affinity for immobilized nickel. The dialysis product was loaded on a (His Trap HP 5 mL Cytiva) His affinity column at 1.5 ml/min, and then three steps of washing were performed using buffer B supplemented with 0 mM, 25 mM or 50 mM imidazole (Sigma Aldrich) for 5 CV each at 2.0 ml/min. His-IFT27/IFT25 complex was coeluted using elution buffer B (50 mM Tris pH 7.5, 300 mM NaCl and 300 mM Imidazole). The fractions were run on SDS-PAGE gel to determine the content. The elution fractions containing IFT25 and IFT27 were dialysed overnight at 4 °C against SEC buffer B (10 mM Tris pH 7.5, 150 mM NaCl and 1 mM DTT (Thermo Scientific)) in the presence of TEV protease (0.5 mg) to cleave off the his-tag.

The following day the sample was clarified by spinning at 40000 x G for 15 minutes at 4 °C to remove precipitation and concentrated using Amicon Ultra 10K MWCO 15 mL Regenerated Cellulose at 4000 x G at 4 °C (Sorvall Legend X1R (Thermo Scientific)). After concentrating, the sample was clarified by spinning at 17000 x G for 10 minutes at 4 °C (Accuspin Micro 17 (Fisher Scientific)), and injected on size exclusion chromatography (SEC) column (HiLoad 16/600 Superdex 200 pg 120 mL (GE Healthcare)) connected to a Äkta Purifier. SEC columns are packed with spherical bead with different pore diameters. Molecules larger than the pores do not enter the beads, so they elute first.

Molecules smaller than the smallest of the pores will enter the total pore volume and elute last, and molecules that range in size between very big and very small are eluted in between based on their size and shape. The SEC column was used at 0.700 mL/min for 1.2 CV to perform the separation. Relevant fraction was run on SDS-PAGE gel to confirm their contents. Fractions containing pure IFT27/IFT25 complex were pooled and concentrated until 1-2 mg/mL and used immediately or stored in 20% glycerol at -80 °C

3.4.1 Expression Protocol MBP-CENP-J$^{412-897}$

Using the protocol for transformation, *pMAL-c6T* plasmid containing MBP-CENP-J$^{412-897}$ was transformed into Rosetta 2 cells. Three separate colonies were added to a 125 mL of 2x YT preculture containing 50 µg/mL amp and 34 µg/mL cam. The preculture was left overnight to grow at 37 °C and 120 RPM. The following day, 6x 5L-baffled flasks, each containing 1.5 L of media along with 50 µg/mL amp and 34 µg/mL cam were inoculated with 20 mL of preculture each, and then left to grow at 37 °C and 85 RPM until OD_{600} = 0.6. IPTG was added to each flask, to a final concentration of 0.33 mM to induce protein overexpression. The cells were left to grow overnight at 18 °C at 85 RPM. The following day the cells were harvested through centrifugation at 4500 RPM for 15 minutes at 4 °C (Avanti J-26 XP, JLA-8.1, Beckman Coulter). 20 mL of lysis buffer A (50 mM Tris pH 8, 500 mM NaCl, 8 mM $MgSO_4$, 10 mM BME (Sigma Aldrich) and 5% glycerol (Fisher BioReagents)) was used to resuspend the cells, after which the cells were frozen at -80 °C until an appropriate time for purification.

3.4.2 Purification Protocol of MBP-CENP-J$^{412-897}$

The cells were thawed at 37 °C and lysed by sonication (Branson 550) using 30 second cycles of 0.7 seconds on and 0.3 seconds off at 65% amplitude. 1 x of Turbonuclease (*Serratia Marcesens* Sigma Aldrich) was added to the lysate and incubated for 15 minutes, before clarification to remove cell debris by centrifugation, at 40000 x G for 45 minutes at 4 °C (Avanti J-26 XP, JA 25.50, Beckman Coulter).

CENP-J$^{412-897}$ is expressed with a N-terminal His tag followed by a maltose binding domain and a TEV protease cleavage site. Maltose Binding Domain is a larger tag that is mostly used to increase solubility of a protein, but can also be used for purification, as it has an affinity for amylose. The supernatant was loaded on a (His Trap HP 5 mL Cytiva) His affinity column at 1.5 ml/min, and then

three washing steps were performed with washing buffer A (50 mM Tris pH 8.0, 500 mM NaCl, 5% glycerol and 5 mM BME) containing 0 mM, 25 mM or 50 mM imidazole for 5 CV each at 2.0 ml/min. The elution was performed using elution buffer A (50 mM Tris pH , 500 mM NaCl, 5% glycerol, 5 mM BME and 500 mM Imidazole). The fractions were run on SDS-PAGE gel to determine their content. The Fractions containing MBP-CENP-J were pooled together and dialysed overnight at 4 °C against SEC buffer A (50 mM Tris pH 8.0, 300 NaCl, 5% glycerol and 5 mM BME).

The following day the sample was clarified by spinning at 40000 x G for 15 minutes at 4 °C to remove precipitation. Concentrating the sample was done using Amicon Ultra 10K MWCO 15 mL concentrator at 4000 x G at 4 °C (Sorvall Legend X1R (Thermo Scientific)) The sample was clarified by spinning at 17000 x G for 10 minutes at 4 °C. (Accuspin Micro 17 (Fisher Scientific)), and injected on a HiLoad 16/600 Superdex 200 pg SEC column at 0.700 mL/min flowrate. Relevant fractions were run on SDS-PAGE gel to confirm their contents. Fractions containing CENP-J were pooled together and concentrated until 1-2 mg/mL. The samples were stored in 20% glycerol at -80 °C

3.5.1 Expression Protocol for Aurora B^{60-360} and $INCENP^{798-858}$

Any mention of a Aurora B^{60-360} sample also contain $INCENP^{798-858}$ even though its not explicitly stated. Three separate colonies were added to a 125 mL of 2x YT preculture containing 50 µg/mL kanamycin (kan(Sigma Aldrich)) and 34 µg/mL cam The preculture was then left overnight to grow at 30 °C and 120 RPM. The following day, 10 mL of preculture media was transferred to 300 mL of media containing 50 µg/mL kan and 34 µg/mL cam and grown to OD_{600} = 1.0 at 30 °C. 3x 5L-baffled flasks, each containing 1.5 L of media along with 50 µg/mL kan and 34 µg/mL cam, were inoculated with 75 mL of intermediate culture, and then left to grow at 30 °C and 85 RPM until OD_{600} = 0.6. IPTG was added to each flask, to a final concentration of 0.2 mM. The cells were left to grow overnight at 18 °C at 85 RPM. The following day the cells were harvested through centrifugation at 4500 RPM for 15 minutes at 4 °C (Avanti J-26 XP, JLA-8.1, Beckman Coulter). 20 mL of lysis buffer C (25 mM Tris pH 7.5, 300 mM NaCl, 50 mM Imidazole and 1 mM PMSF (Sigma Aldrich)), was used to resuspend the cells, after which the cells were frozen at -80 °C until an appropriate time for purification.

3.5.2 Purification Protocol for Aurora B^{60-360} and $INCENP^{790-858}$

The cells were thawed at 37 °C and lysed by sonication (Branson 550) using 30 second cycles of 0.7 seconds on and 0.3 seconds off at 65% amplitude. 1 x of Turbonuclease (*Serratia Marcesens*) was

added to the lysate and incubated for 15 minutes, before clarification to remove cell debris by centrifugation, at 30000 x G for 45 minutes at 4 °C (Avanti J-26 XP, JA 25.50, Beckman Coulter).

Aurora B^{60-360} is expressed with a His tag. The dialysis product was loaded on a His affinity column (His Trap HP 5 mL Cytiva) at 1.5 ml/min and then three washing steps were performed using washing buffer C (25 mM Tris HCl pH 7.5, 300 mM NaCl) supplemented with 0 mM, 25 mM or 50 mM imidazole for 5 CV each at 2.0 ml/min. Elution proceeded using elution buffer C (50 mM Tris pH 7.5, 150 mM NaCl and 500 mM Imidazole). The fractions were run on SDS-PAGE gel to determine the content. The elution fractions containing Aurora B^{60-360} were pooled and dialysed overnight at 4 °C against SEC buffer C (25 mM Tris pH 7.5, 300 mM NaCl and 2 mM DTT) in the presence of TEV protease (0.5 mg) to cleave off the his-tag.

The following day the sample was clarified by spinning at 40000 x G for 15 minutes at 4 °C to remove precipitation, and concentrated using Amicon Ultra 10K MWCO 15 mL concentrator (Sigma Aldrich)) at 4000 x G at 4 °C (Sorvall Legend X1R (Thermo Scientific)). The sample was clarified by spinning at 17000 x G for 10 minutes at 4 °C before being injected on (HiLoad 16/600 Superdex 200 pg (GE Healthcare)) SEC column, connected to a Äkta Purifier. The SEC column was used at 0.700 mL/min for 1.2 CV to perform the separation. Relevant fractions were run on SDS-PAGE gel to confirm their content. Fraction containing Aurora B^{60-360} /$INCENP^{790-858}$ were pooled, concentrated until 1-2 mg/mL and immediately used or stored in 50% glycerol at -80 °C.

3.6.1 Expression of different constructs of IFT27 alone with different tags

Different constructs of IFT27, His-TEV-IFT27, His-FaX-IFT27, His-MBP-TEV-IFT27, IFT27-TEV-MBP-HIS and His-MBP-TEV-IFT27 with linker between TEV and IFT27, were all expressed and purified in the following fashion. All plasmids were transformed into Rosetta 2 cells according to the protocol. Three separate colonies were picked and added to a 125 mL 2x YT preculture containing 50 µg/mL amp and 34 µg/mL cam. The preculture was then left overnight to grow at 37 °C and 120 RPM. The following day 5L-baffled flasks, each containing 1.5 L of media along with 50 µg/mL amp and 34 µg/mL cam, were inoculated with 20 mL of preculture and then left to grow at 37 °C and 85 RPM until OD_{600} = 0.6. IPTG was added to each flask, to a final concentration of 0.33 mM. The cells were left to grow overnight at 18 °C at 85 RPM. The following day the cells were harvested through centrifugation at 4500 RPM for 15 minutes at 4 °C (Avanti J-26 XP, JLA-8.1, Beckman Coulter). 20 mL of lysis buffer A was used to resuspend the cells, after which the cells were frozen at -80 °C until an appropriate time for purification.

3.6.2 Purification Protocol of different constructs of IFT27 alone with other tags

The cells were thawed in a water bath until liquid. Lysing the cells was done by sonication (Branson 550 with Medium tip) for 30 seconds 30 off 70 on at amplitude 65%. 1 x of Turbonuclease (*Serratia Marcesens* Sigma Aldrich) was added to the lysate and incubated for 15 minutes, before it was centrifuged to remove cell debris, at 40000 x G for 45 minutes at 4 °C using a (Avanti J-26 XP, JA 25.50, Beckman Coulter).

All of the aforementioned proteins are expressed with a His tag, so the supernatants were loaded on a His Trap HP 5 mL Cytiva His affinity column at 1.5 ml/min and then three washing seps were performed using washing buffer A containing 0 mM, 25 mM or 50 mM imidazole for 5 CV each at 2.0 ml/min. The protein elution was proceeded using elution buffer A. The fractions were run on SDS-PAGE gel to determine the content. The elution fractions containing IFT27, if any, were pooled and dialysed overnight at 4 °C against SEC buffer A.

The following day the sample was clarified by spinning at 40000 x G for 15 minutes at 4 °C to remove precipitation, concentrated using Amicon Ultra 10K MWCO 15 mL concentrator (Sigma Aldrich) and clarified again by spinning, before the sample was injected on (Superdex S75 10/300 GL) SEC column connected to a Äkta Purifier. The SEC column was used at 0.700 mL/min for 1.2 CV to perform the separation. Relevant fractions were run on SDS-PAGE gel to confirm their contents.

3.7 Sodium Dodecyl Sulphate-Polyacrylamide Gel Electrophoresis (SDS-PAGE) Protocol

Sodium Dodecyl Sulphate will bind to amino acids, making the protein negatively charged and therefore giving all protein the same charge to mass ratio. Together in the presence of BME, the proteins disulfide bonds are broken and secondary structure lost. A positive charge is applied to the gel, making the protein travel through the polyacrylamide, with the largest proteins encountering the most resistance. This separates the protein based on the linear size of the protein, which can be equated to the mass of the protein.

4X SDS loading solution containing (2% SDS (VWR), 0.6 M BME, a dash of Bromphenol Blue, 40% glycerol, 50 mM EDTA (Sigma Aldrich) and 50 mM Tris HCl pH 6.8) was added to each protein sample,

at a final concentration of 1 x. Cell samples were prepared as following: 1 mL of culture at OD_{600} = 0.5 was spun down at 4000 x G for 10 minutes (Accuspin Micro 17). The supernatant was discarded and 100 µL 4X SDS loading dye were added to the pelleted cells. All samples were then heated at 95 °C for 5 minutes to completely denature the protein. The samples were spun down at low RPM, and 10 µL of each sample was loaded in each well, along with a pre stained protein ladder (Precision Plus Protein Dual Standards (Bio Rad)) that acts as a benchmark. The gels were run at 200 Volts for 36 minutes (Power Pac Basic) and stained overnight (InstaBlue (Abcam)). The gels were scanned using ChemiDoc MP Imaging System (Bio Rad).

3.8 GTPase Test Protocol

IFT27 is a GTPase, which means that it can catalyse removal of phosphate from GTP and generate GDP and inorganic phosphate.

$GTP \rightarrow GDP + P_i$

The inorganic phosphate released can be measured through the following reaction:

$(NH_4)_6Mo_7O_{24} + P_i \rightarrow (NH_4)_3PMo_{12}O_{40}$

The reagents in this reaction are transparent and the product is blue, so formation of the product can be measured spectrophotometrically at λ = 690 nm.

300 µL of 12 µM protein is incubated at 37 °C for 10 minutes. Then GTP is added to the sample with a final concentration of 1 mM and reaction is further incubated at 37 °C for 1 hour. After this, 75 µL of solution II (166 µM solution I, 0.162 M Asorbic acid (Sigma Aldrich), 2.86% SDS and 0.47 M HCl (Sigma Aldrich)) is added and the sample is put on ice for 10 minutes, following with the addition of 125 µL of solution III (88 mM Bismuth Citrate (Sigma Aldrich), 135 mM Sodium Citrate (Sigma Aldrich) and 1 M HCl) incubation of 10 minutes at room temperature. UV absorbance is measured (Agilent Technologies Cary 60 UV-Vis) at 690 nm.

3.9 DNA and Protein Quantification

DNA and protein quantification was done with a NanoDrop One^C instrument (Thermo Scienftic). The aromatic amino acids, phenylalanine, tryptophan and tyrosine can absorb UV light at 280 nm wavelength which can be exploited to quantify the concentration of a protein sample using Beer-

Lambert Equation A = εbc, were ε is the molar absorptivity of the individual molecule, b is the path length through the sample and c is the concentration.

When measuring DNA concentration, the instrument will provide the concentration in ng/µL as well as the 260/280 ratio which should be around 1.8 for pure DNA.

For measuring pure protein, we always use the exact extinction coefficient that is calculated for each protein based on aminoacid sequence (program used – ProtParam), for estimating protein during different steps of purification. We add the coefficient ε 1% value into to measurement for more accurate quantifiaction. Additionally, the instrument will provide the A260/A280 value, which indicates if the protein sample has been contaminated by DNA. A value of less than 1 is considered good.

3.10 Pull Down Assay between IFT25/IFT27 and MBP-CENP-J$^{412-897}$

A pull-down assay works by having a bait protein bind to a resin of choice and adding a prey protein that does not bind to the resin by itself but only if it interacts with the bait protein. Here we use amylose beads (NEB) that are binding MBP tagged CENP-J (so CENP-J will act as the bait). 100 µL of beads were washed with 1 mL of water for 15 minutes at 12 RPM, after which 1 mL SEC buffer B was used to equilibrate the beads for 15 minutes. The bait protein MBP-CENP-J was added to the beads at a concentration of 8 µM and incubated for 30 minutes at 12 RPM. Then 1 mL of SEC buffer B was used to wash away any contaminants, incubated at 12 RPM for 15 minutes. This was done twice. The bait protein IFT25/His-IFT27 was then incubated for 1 hour at 12 RPM. The sample was washed twice with SEC buffer B to wash away any non-specific binders and 50 µL of 4x SDS loading dye were added to the beads. 20 µL were then run on SDS-PAGE gel to determine if any interaction has occurred.

3.11 Pull Down Assay between GST-IFT25/His-IFT27 and Aurora B$^{60-360}$/INCENP$^{790-858}$

In this experiment Aurora B$^{60-360}$ /INCENP$^{790-858}$ served as the prey, and GST-IFT25 with His-IFT27 attached to glutathione beads, was used as the bait protein. 100 µL of glutathione beads (NEB) were washed with 1 mL of water for 15 minutes at 12 RPM, after which 1 mL SEC buffer B was used to equilibrate the beads for 15 minutes. The bait protein GST-IFT25/His-IFT27 was added to the beads at a concentration of 8 µM and incubated for 30 minutes at 12 RPM. Then 1 mL of SEC buffer B was used

to wash away any non-specific binding, centrifuged at 12 RPM for 15 minutes. This process was repeated twice. The beads where then incubated with the bait protein Aurora B^{60-360} /$INCENP^{790-858}$ for 1 hour at 12 RPM. The sample was washed twice with SEC buffer B and the sample was then run on SDS-PAGE gel to determine if any interaction has occurred.

3.12 Kinase Activity Assay

Kinase activity assay was performed to determine the activity of Aurora B^{60-360}/$INCENP^{790-858}$ in the absence and in the presence of IFT27. The kinetic assay is an enzyme coupled assay that uses helper enzymes pyruvate kinase (PK) and lactate dehydrogenase (LDH) to relate amount of generated ADP to the amount of consumed NADH that can be followed spectrophotometrically at λ = 340 nm

$$\text{Aurora B + peptide + ATP} \xrightarrow{Aurora\ B\ kinase} \text{ADP + Phosphorylated peptide}$$

$$\text{ADP + PEP} \xrightarrow{PK} \text{ATP + Pyruvate + Phosphate}$$

$$\text{Pyruvate + NADH} \xrightarrow{LDH} \text{Lactate + } NAD^{+}$$

The peptide with the sequence: Ac-ALRRFSLHGA-NH_2 was used as AuroraB^{60-360}/$INCENP^{790-858}$ substrate. Since the consumption of ATP will be equivalent to the formation of ADP, which will again be equivalent to the consumption of NADH, it is possible to measure the decrease of NADH at 340 nm to determine the activity of Aurora B.

First a Kmg-100 buffer was prepared containing, 100 mM KCl (EMSURE), 2mM $MgCl_2$ (EMSURE), 1 mM EGTA (Sigma Aldrich), 2 mM DTT, 25 mM Tris-HCl pH 7.4 and 0.01% Brij 35. Then the "5x cocktail" was made with the following ingredients, 0.8 mM NADH (Sigma Aldrich), 2.5 mM PEP (Sigma Aldrich), 100 u/mL LDH (Sigma Aldrich), 100 u/mL PK (Sigma Aldrich) and brought to their final concentration by diluting with the Kmg-100 buffer. Finally, the Kinase Assay Buffer (KAB) was made with the following ingredients: 200 µL of 5x cocktail, peptide, ATP (Thermo fisher), diluted with Kmg-100 buffer to a final volume of 1080 µL. The final concentration of peptide and ATP being 200 µM and 1 mM respectively. The absorbance was measured at 340 nm (Agilent Technologies Cary 60 UV-Vis) continually with 250 µL KAB buffer in the cuvette, until a protein sample was inoculated in the KAB and mixed with a 200 µL pipette. Aurora B^{60-360} from a 6 µM stock solution was added to the cuvette, with 4.2 µL added for 100 nM concentration, and 6.3 µL added for 150 nM concentration. The absorbance was measured for 8 minutes, and the slope was calculated for absorbance decrease in the first minutes after mixing. All experiments were conducted in triplicates using different molar

ratios of Aurora B^{60-360} to IFT27: 1:1, 1:4 and 0:4, where the final sample did not contain Aurora B^{60-360} (used a negative control) The same molar ratios were also used for IFT27 mutant (Y35C).

4. Results and Discussion

4.1 Protein Expression and Purification

Many constructs expressing IFT27 with different tags were cloned in order to increase its solubility and expression level in *E. coli*. The tested constructs are listed in table 4.1.1, together with a short summary of the problems faced for each construct. Briefl, at the beginning of this project, two constructs were available, His-TEV-IFT27 and His-FaX-IFT27. Both constructs were mainly expressed in inclusion bodies, with almost no soluble His-TEV-IFT27, and only a small amount of His-FaX-IFT27 being soluble. A bigger tag (His-MBP) was then added to IFT27 at the N-terminal to increase solubility. His-MBP-TEV-IFT27 was expressed with good yield and most of the protein was soluble, but the MBP-tag could not be cleaved off, probably because of inaccessible TEV protease cleavage site. To solve this problem, two new constructs of IFT27 were designed, with the first having His-MBP tag cloned at the C-terminal (IFT27-TEV-His-MBP), and the second having longer linker between the N-terminal His-MBP-tag and IFT27 to allow more exposure of the TEV protease site. While IFT27-TEV-His-MBP construct did not show big improvement of the His-MBP tag cleavage after incubation with TEV over-night, the tag was successfully cleaved in His-MBP-TEV-IFT27 construct with longer linker. However, removing the His-MBP tag resulted in IFT27 precipitating in solution, suggesting that IFT27 cannot be soluble by itself. That is why, in this thesis, I ended up cloning and co-purifying IFT25/IFT27 heterodimer, and I conducted all the biochemical experiments using IFT25/IFT27

Table 4.1.1: List of generated IFT27 clones with notes on their expression and purification.

Construct	**Expressed**	**Solubility**	**Comments**
His-TEV-IFT27	Yes	Inclusion bodies	- Not soluble
His-FaX-IFT27	Yes	Low solubility, mainly in inclusion bodies	- Very low yield - Uncleavable - The final product was purified with impurities
His-MBP-TEV-IFT27	Yes	Good solubility	- High yield - MBP tag cleavage was not efficient

IFT27-TEV-His-MBP	Yes	Good solubility	- High yield - MBP tag cleavage was not efficient
His-MBP-TEV-IFT27	Yes	Good solubility	- High Yield - MBP tag cleavage was efficient - IFT27 precipitated after tag cleavage

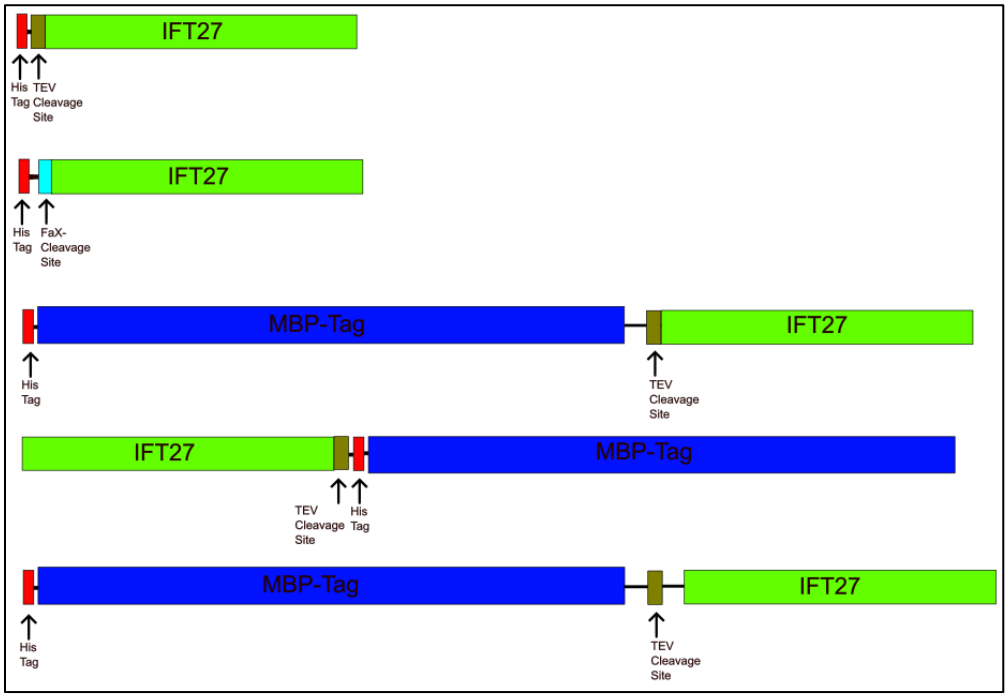

Figure 4.1.1: Shows the tested constructs of IFT27 expressed and purified, scaled proportionally with their length. From top to bottom: His-TEV-IFT27, His-FaX-IFT27, His-MBP-TEV-IFT27, IFT27-TEV-HIS-MBP and His-MBP-TEV-IFT27 extra linker

4.1.1 Expression and Purification of HIS-TEV-IFT27

His-TEV-IFT27 was expressed in Rosetta 2 cells overnight at 18°C. Cells were harvested, lysed with sonication and the cell debris spun down at 40000 x G. The pellet and supernatant were analysed on SDS-PAGE for the presence of ~23 kDa band corresponding to the protein of interest. Although there was a thick band close to corresponding MW present in the supernatant (Figure 4.1.1.1, A) nothing bound Ni-column (Figure 4.1.1.1, B), so we concluded that the His-TEV-IFT27 is either insoluble or is

not expressed. Different expression conditions were tested for this construct, by varying the temperature and time of growth, but never observed soluble protein.

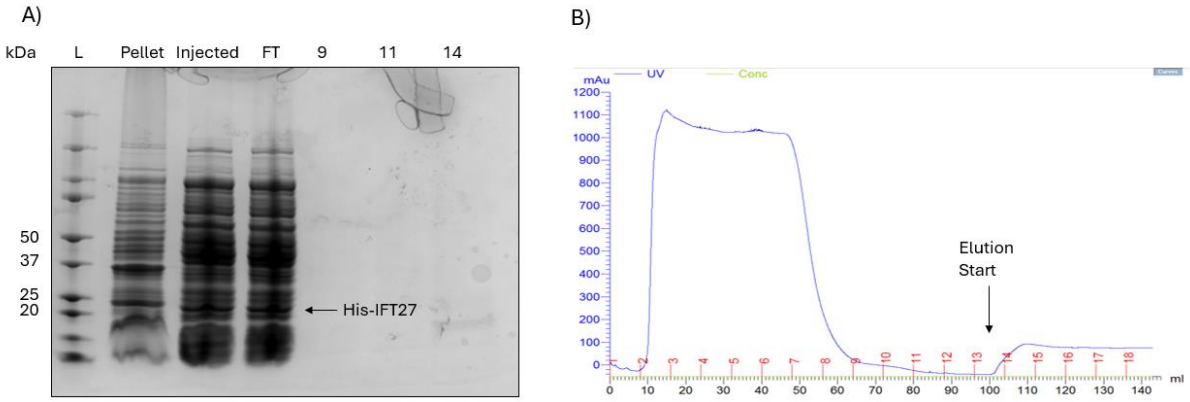

Figure 4.1.1.1: A) The SDS-PAGE gel for His-TEV-IFT27 purification. Fractions from left to right: Ladder, Pellet after cell lysis, Supernatant after cell lysis (also input for the Ni^+-column), Flow through from the Ni^+ column, fractions 9, 11 and 14 from Ni^+-column. Fraction 14 was eluted with high imidazole gradient. B) Chromatogram of the Ni-Affinity purification of His-TEV-IFT27.

4.1.2 Expression and Purification of His-FaX-IFT27

This construct is almost identical to His-TEV-IFT27, the only difference being a FaX cleavage site, instead of TEV cleavage site, and a shorter linker between the His-tag and FaX site (SSG linker instead of SSGGGGG linker in the His-TEV-IFT27 construct). FaX protease was not available, so cleavage of the tag was not achieved.

His-FaX-IFT27 was expressed in Rosetta 2 cells overnight at 18°C. Cells were harvested, lysed with sonication and the cell debris spun down at 40000 x G. The supernatant was injected on the Ni-affinity column and eluted with high imidazole concentration. In figure 4.1.2.1 B no elution peak is visible from the Ni-affinity purification, although the SDS-PAGE gel (figure 4.1.2.1, A) reveals a band between 20 and 25 kDa that might correspond to IFT27 (23 kDa). The pellet seems to inhabit a band around 23 kDa, indicating that His-FaX-IFT27 was expressed but ended up in inclusion bodies, although this cannot be said for certain due to the saturation. Elution fractions (F9-F14) were pooled and dialyzed to remove imidazole.

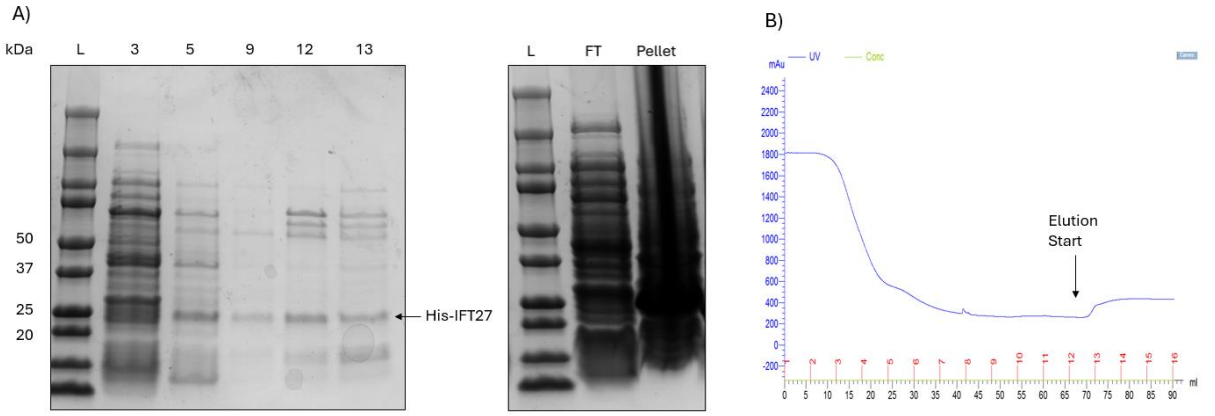

Figure 4.1.2.1: A) Shows the SDS-PAGE gel for His-FaX-IFT27 purification. From left to right: Ladder, fractions 3, 5, 9, 12 and 13 from Ni^{+} column along with the flowthrough and the pellet. Fraction 12 and 13 was eluted with high imidazole gradient. B) Shows the Ni-affinity purification of His-FaX-IFT27.

Because the elution had impurities corresponding to higher molecular weights, we used Size exclusion chromatography (SEC; Superdex 75 10/300 GL) to further purify the proteins. SEC purification did not remove all the contaminants. The SDS-PAGE gel in figure 4.1.2.2 A shows that, fractions B11 and B10 from the SEC mainly contains His-FaX-IFT27, although there are still multiple contaminants. His-FaX-IFT27 did not elute in a peak (figure 4.1.2.2 B), but rather a plateau tailing out from the larger peak. Fractions B12-B9 were pooled, and the final yield was 0.9 mg of protein form 9 liters of culture. 20% glycerol was added to the sample and, it was flash frozen and stored at -80 °C.

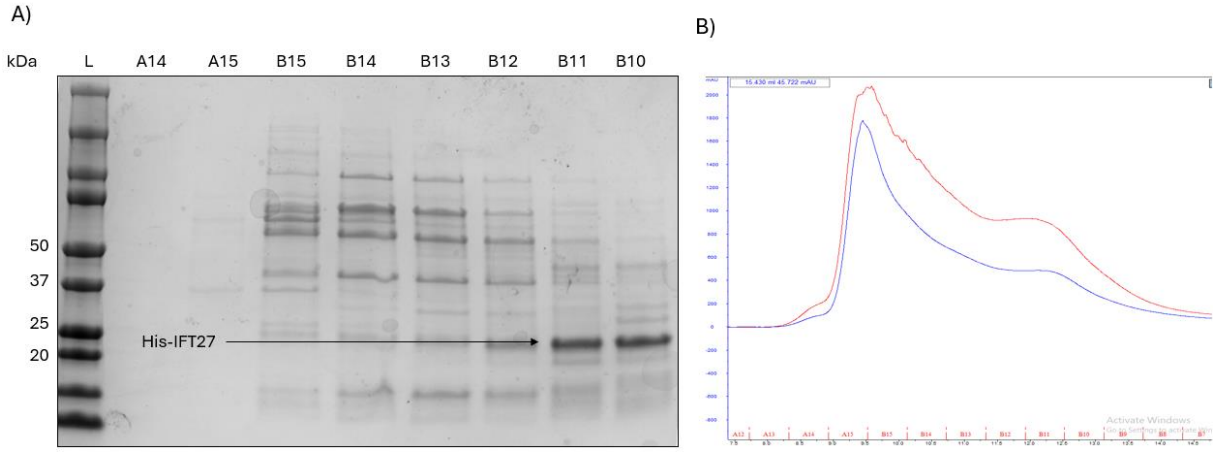

Figure 4.1.2.2: A) Shows the SDS-PAGE gel run after SEC purification from left to right: fraction A14, fraction A15, fraction B15, fraction B14, fraction B13, fraction B12, fraction B11 and fraction B10. B) Shows the SEC purification of His-FaX-IFT27 using Superdex 75 10/300 GL.

4.1.3 Expression and Purification of His-MBP-TEV-IFT27

To improve expression and solubility of the protein we decided to express it with a bigger soluble tag – maltose binding protein (MBP). The presence of MBP should help with solubility and the presence of a TEV cutting site provides the possibility to remove the MBP tag.

His-MBP-TEV-IFT27 was expressed in Rosetta 2 cells overnight at 18°C. Cells were harvested, lysed with sonication and the cell debris spun down at 40000 x G. The supernatant was injected on the Ni-affinity column and eluted with high imidazole concentration. Figure 4.1.3.1 B shows a majority of the protein eluted in fraction 20 and when run on SDS-PAGE gel (figure 4.1.2.1 A), this fraction shows protein of ˜65 kDa which corresponds to expected MW of His-MBP-TEV-IFT27, 64.6 kDa. Notice that the protein gives two bands, most likely due to proteolysis. Fractions 19-24 were pooled and dialyzed overnight with TEV protease to cleave off the His-MBP tag.

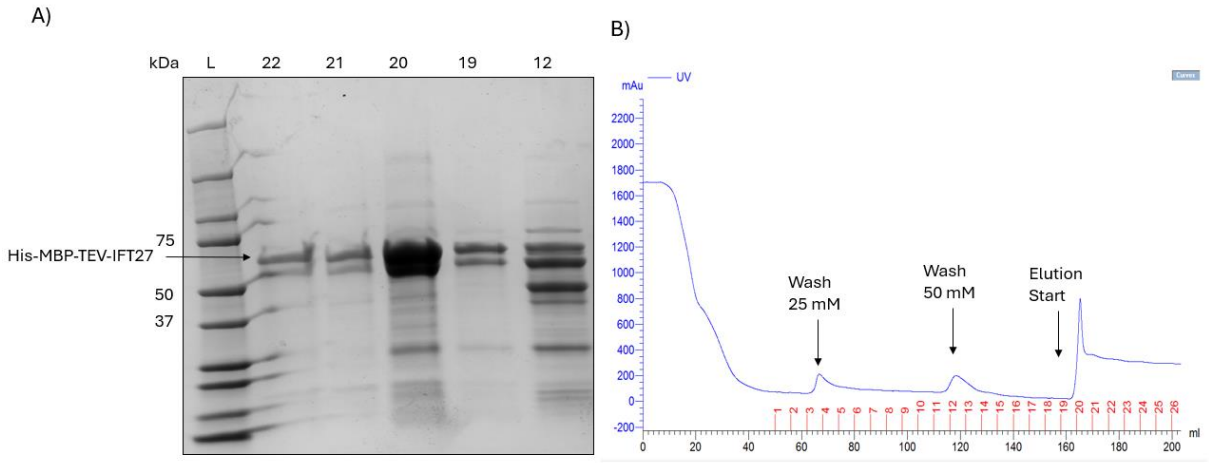

Figure 4.1.3.1: A) Shows the SDS-PAGE gel for His-MBP-TEV-IFT27 purification. FFrom left to right: Ladder, fractions 22, 21, 20, 19 and 12 from Ni^{+} column. B) Shows the Ni-affinity purification of His-MBP-TEV-IFT27

To further purify protein, we performed SEC using Superdex 75 10/300 GL. Two peaks eluted from the column. The first peak (A14 and A15) contains an overwhelming amount of uncleaved protein (64.6 kDa) and the second peak (B13 and B12) contains mostly free MBP (44.1 kDa), along with other contaminants. The expected band for IFT27 (20.6 kDa) could be visible co-eluting with uncleaved protein, between 20 and 25 kDa

In conclusion, expressing IFT27 with a MBP tag has helped the solubility but it was difficult to remove the bulky tag from the protein. Since we are not sure if presence of MBP at the N-terminus would affect properties we are testing, we designed two new construct with hopes to be able to remove the MBP-tag. Firstly, we reasoned that removal of the tag was not possible due to steric hindrance of the TEV cutting site, so we decided to move the MBP tag to the C-terminus of the protein. Secondly, to

allow for more space for TEV protease to cut, we made another construct that included a linker between the TEV site and the N-terminal of IFT27.

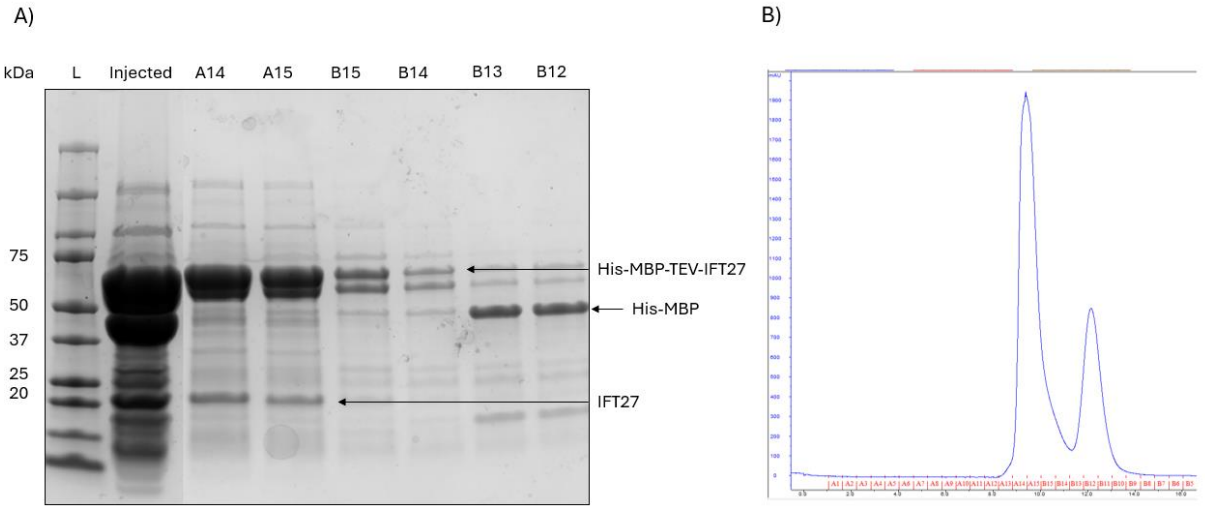

Figure 4.1.3.2: A) Shows the SDS-PAGE gel run after SEC purification of cleaved His-MBP-TEV-IFT27. From left to right: ladder, fraction A14, fraction A15, fraction B15, fraction B14, fraction B13, fraction B12, fraction B11 and fraction B10. Fractions A14-B14 are in peak 1, Fraction B13-B12 are in the second peak B) Shows the SEC purification of His-MBP-TEV-IFT27 using Superdex 75 10/300 GL.

4.1.4 Expression and Purification of IFT27-TEV-HIS-MBP

IFT27-TEV-HIS-MBP was expressed in Rosetta 2 cells overnight at 18°C. Cells were harvested, lysed with sonication and the cell debris spun down at 40000 x G. The supernatant was injected on the Ni-affinity column and eluted with high imidazole concentration. The majority of the protein eluted in fraction 20 (Figure 4.1.4.1 B) and SDS-PAGE gel (figure 4.1.4.1 A) of the fraction shows to bands between 50 and 75 kDa, most likely corresponding to IFT27-TEV-His-MBP (expected MW 63.5 kDa). The lower of the two band is probably the product of cellular proteolysis. Fractions 19-23 were pooled and at the same time incubated with TEV to remove the tag and dialyzed overnight to remove imidazole.

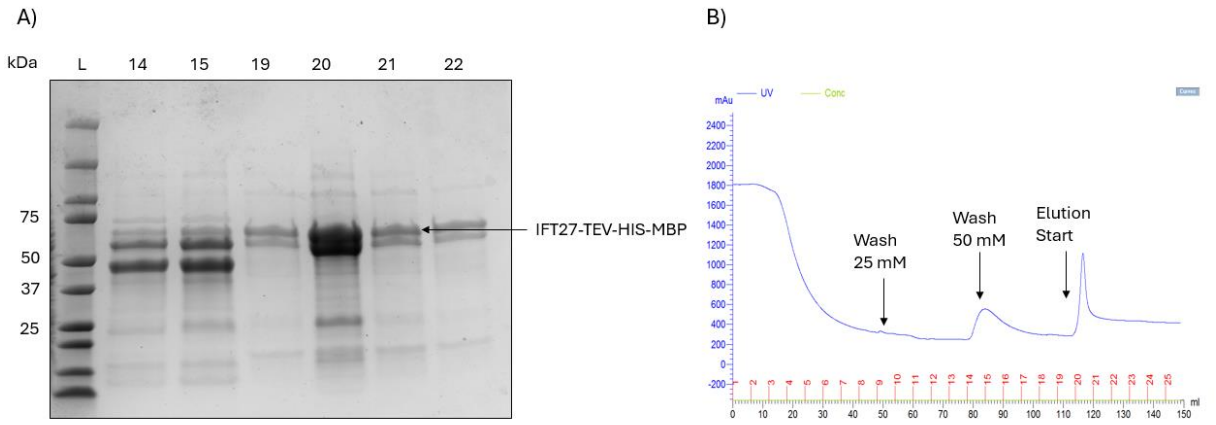

Figure 4.1.4.1: A) Shows the SDS-PAGE gel from purification of IFT27-TEV-His-MBP. From left to right: Ladder, fractions 14, 15, 19, 20, 21 and 22 from Ni^{+} column. B) Shows the Ni-affinity purification of IFT27-TEV-HIS-MBP.

To remove cut-off MBP and other impurities we performed SEC using HiLoad 16/600 Superdex 75 pg. We observed two peaks (Figure 4.1.4.2 B). When content of the first peak was run on SDS-PAGE gel (figure 4.1.4.2 A), it revealed two major bands – one corresponding to˜65 kDa and the second one corresponding to ˜20 kDa. The first band is most likely uncleaved IFT27-TEV-HIS-MBP (expected size 63.5 kDa) and the second band is most likely cleaved IFT27 (expected MW 20.6 kDa). The second peak contains on dominant band between 37 kDa and 50 kDa, and this is most likely cleaved MBP (expected MW 44.2 kDa)

In conclusion, this construct also showed good expression and protein solubility, but removal of the tag was not successful.

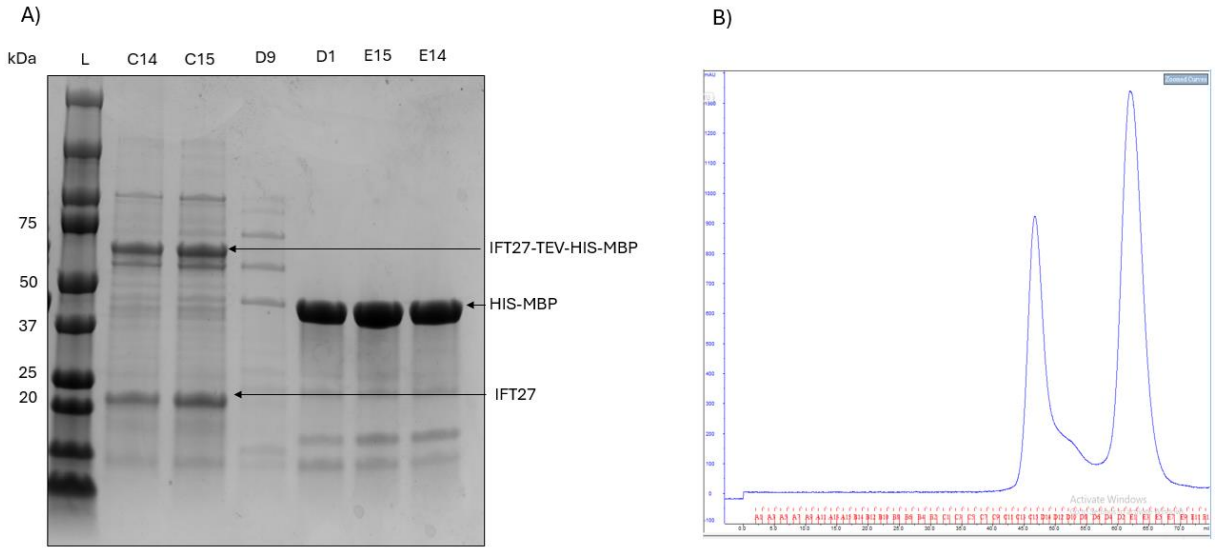

Figure 4.1.4.2: A) Shows the SDS-PAGE gel from purification of IFT27-TEV-His-MBP run after SEC purification. From left to right: fraction C14, fraction C15, fraction D9, fraction D1, fraction E15 and fraction E14. Fractions C14-C15 are in peak 1, Fraction D1-E14 are in the second peak.Shows the SEC purification of IFT27-TEV-His-MBP using HiLoad 16/600 Superdex 75 pg. B) Shows the SEC purification of IFT27-TEV-His-MBP using HiLoad 16/600 Superdex 75 pg.

4.1.5 Expression and Purification of His-MBP-TEV-IFT27 with extra linker

This construct is the same as His-MBP-TEV-IFT27 except it got an extra linker of amino acids (GSGSSGGGSGGGGT) between TEV and IFT27. This was added to try and improve the cleaving between MBP and IFT27. IFT27-TEV-HIS-MBP with longer linker was expressed in Rosetta 2 cells overnight at 18°C. Cells were harvested, lysed with sonication and the cell debris spun down at 40000 x G. The supernatant was injected on the Ni-affinity column and eluted with high imidazole concentration. When the wash and elution fraction were run on SDS-PAGE gel (figure 4.1.5.1 A), we could see that a protein between 75 kDa and 50 kDa was eluting both in wash and in elusion. After elution with imidazole, the protein eluted mainly in fraction 16 (figure 4.1.5.1 B). This is likely our protein (expected MW 65.4 kDa) and fractions 16-19 were pooled and dialyzed overnight with TEV protease to cleave off the His-MBP tag.

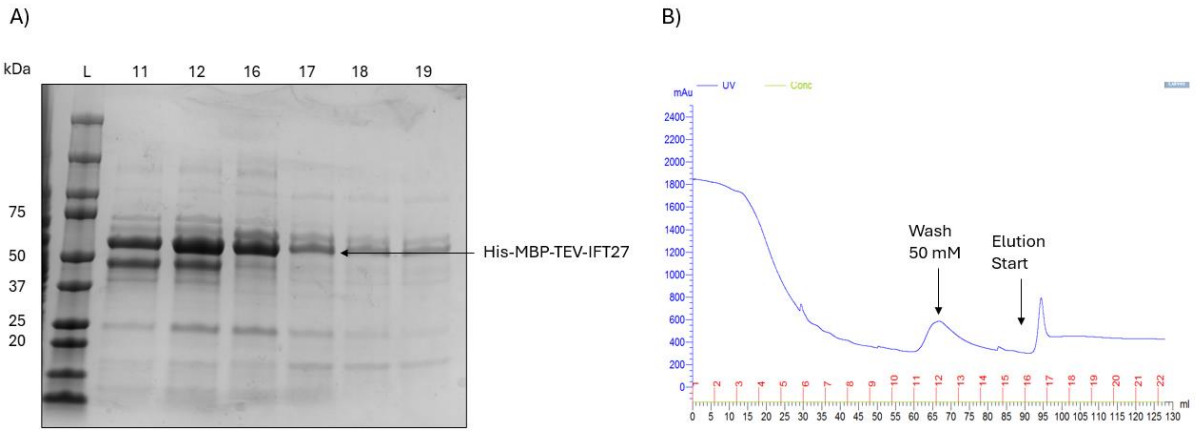

Figure 4.1.5.1: A) Shows the SDS-PAGE gel for His-MBP-TEV-IFT27 with loner linker purification. From left to right: Ladder, fractions 11, 12, 16, 17, 18 and 19 from Ni^{+} column. B) Shows the Ni-affinity purification of His-MBP-TEV-IFT27 extra linker.

In the next step we used SEC using Superdex 75 10/300 GL to further purify the protein. The protein eluted into two peaks (Figure 4.1.5.2 B) An SDS-PAGE gel was run (Figure 4.1.5.2 A), and the first peak (A15 and B15) contains protein contaminants that bound unpacifically to the Ni-beads, and the second peak (B12, B11, B10, B11) contains mostly cleaved MBP (expected MW 44.1 kDa), but we could not identify a strong band corresponding to IFT27 (expected MW 20.6 kDa) in neither peaks.

In conclusion, the construct expressed well and the protein was soluble until the tag was removed. The tag removal leads to protein aggregating and precipitation. From here we concluded that monomer IFT27 is not soluble, and it must have a binding partner to stabilize it in cells.

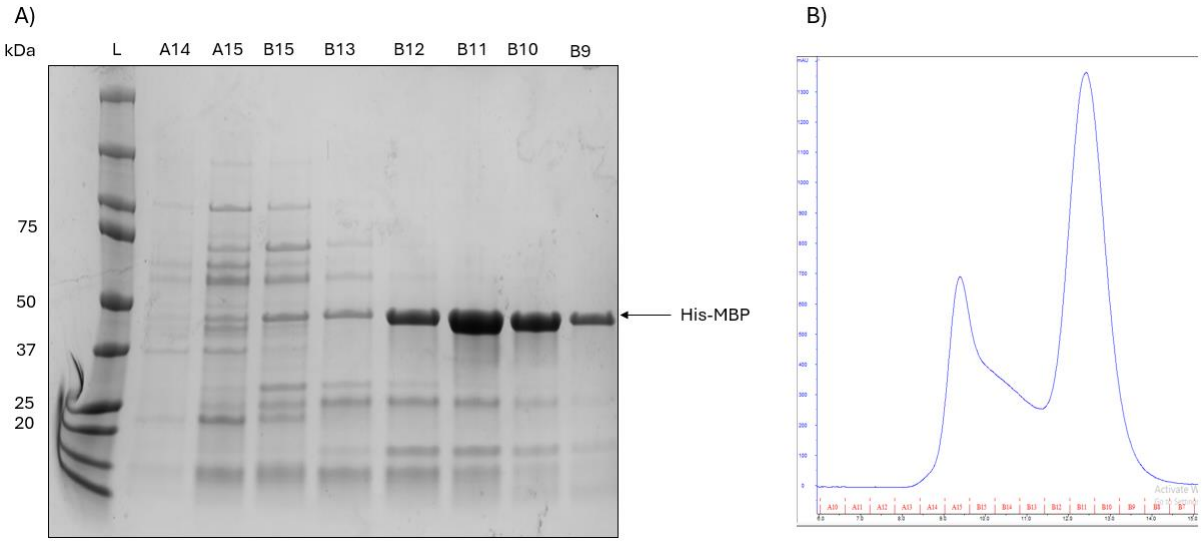

Figure 4.1.5.2: A) Shows the SDS-PAGE gel run after His-MBP-TEV-IFT27 SEC purification from left to right: fraction A14, fraction A15, fraction B15, fraction B13, fraction B12, fraction B11, fraction B10 and fraction B9. Fractions A14-B15 are in peak 1, Fraction B12-B19 are in the second peak. B) Shows the SEC purification of His-MBP-TEV-IFT27 extra linker using Superdex 75 10/300 GL

4.1.6 Expression and Purification of GST-IFT25/His-IFT27^{WT} heterodimer

After searching the literature, we found that IFT27 from Chlamydomonas was also reported to be insoluble alone, and it needed to form a complex with partner IFT25 in order to be correctly folded Bhogaraju et al. 2011. So we engineered a plasmid to co-express GST-IFT25 and His-IFT27. The construct was expressed in Rosetta 2 cells overnight at 18°C. Cells were harvested, lysed with sonication and the cell debris spun down at 40000 x G. The supernatant was injected on a GST-column. The column was washed with several volumes of buffer and the protein was eluted with 10 mM glutathione. The majority of the protein eluted in fraction 8 (figure 4.1.6.1 B) that showed two bands in the SDS-PAGE gel (figure 4.1.6.1 A). A band between 37 and 50 kDa agrees with expected MW for GST-IFT25 (41.7 kDa), while the lower band between 20 and 25 kDa agrees with both His-TEV-IFT27 and free GST (expected MW 25 kDa). In order to remove free GST from the solution we run the sample on a Ni-affinity column. Fractions 8 and 9 from the elution were pooled and then split in half and dialyzed overnight to remove glutathione from the sample. One part was cleaved using 3C protease, to remove the GST tag from IFT25. The cleaved batch of protein would be used for pull-

down assay between MBP-CENP-J and IFT25/IFT27^{WT} and for the second Aurora B kinase activity assay. This batch was frozen at -80°C. The uncleaved batch would be used for the first Aurora B kinase activity assay and pull-down assay between Aurora B$^{60-360}$ and IFT25/IFT27^{WT}

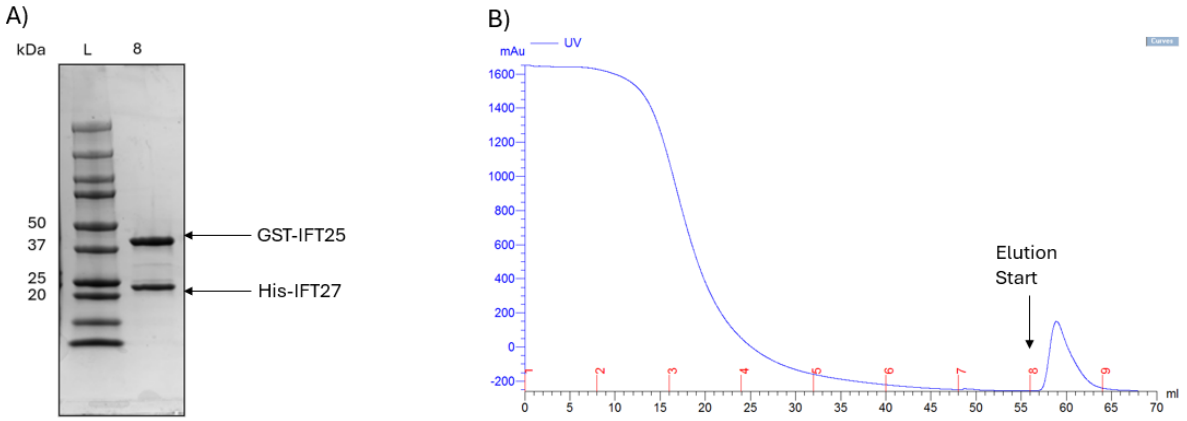

Figure 4.1.6.1: A) Shows the SDS-PAGE gel from purification of GST-IFT25/His-IFT27^{WT} left to right: Ladder and fractions 8 from GST column. B) Shows the GST purification of GST-3C-IFT25 and His-TEV-IFT27

His purification (figure 4.1.6.2 B) was successful in determining that HIS-IFT27 was indeed expressed. If the lower band around 25 kDa was only free GST (figure 4.1.6.2 A), the absence of a His tag would prevent the protein complex from attaching to the column and no protein would be visible in the elution. The protein complex was determined to be pure enough, so there was no need to run SEC. Both IFT25 and IFT27 WT was successfully expressed and purified with 1.4 mg of pure final protein.

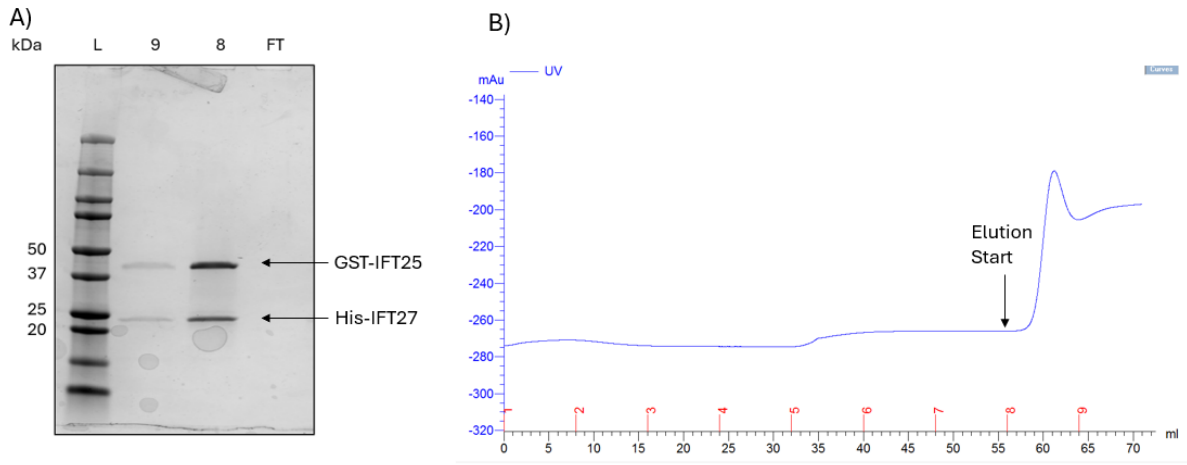

Figure 4.1.6.2: A) Shows the SDS-PAGE gel from purification of GST-IFT25/His-IFT27^{WT} left to right: Ladder, fractions 9 and 8 from Ni^{+} column. B) Shows the Ni-affinity purification of His-TEV-IFT27 and GST-3C-IFT25.

4.1.7 Expression and Purification of GST-IFT25/His-IFT27^{Y35C} heterodimer

GST-IFT25 and His-IFT27 Y35C was expressed in Rosetta 2 cells and purified in the same manner as IFT25/IFT27^{WT} (figure 4.1.7.1 and 4.1.7.2). We concluded that IFT27^{Y35C} expresses and purifies in the same manner as the WT.

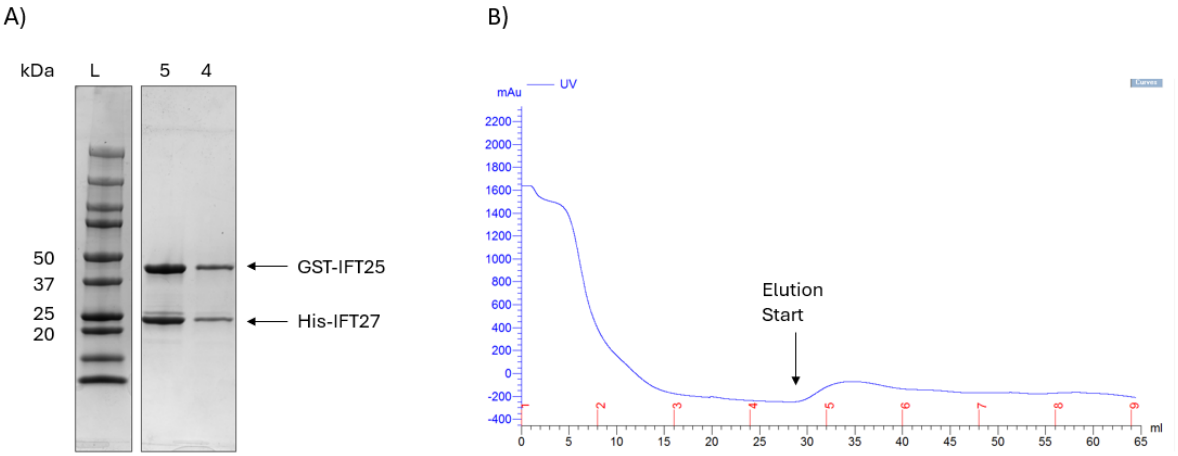

Figure 4.1.7.1: A) Shows the SDS-PAGE gel from purification of GST-IFT25/His-IFT27^{Y35C}. From left to right: Ladder, fractions 5 and 4 from GST column B) Shows the GST purification of GST-3C-IFT25 and His-TEV-IFT27^{Y35C}

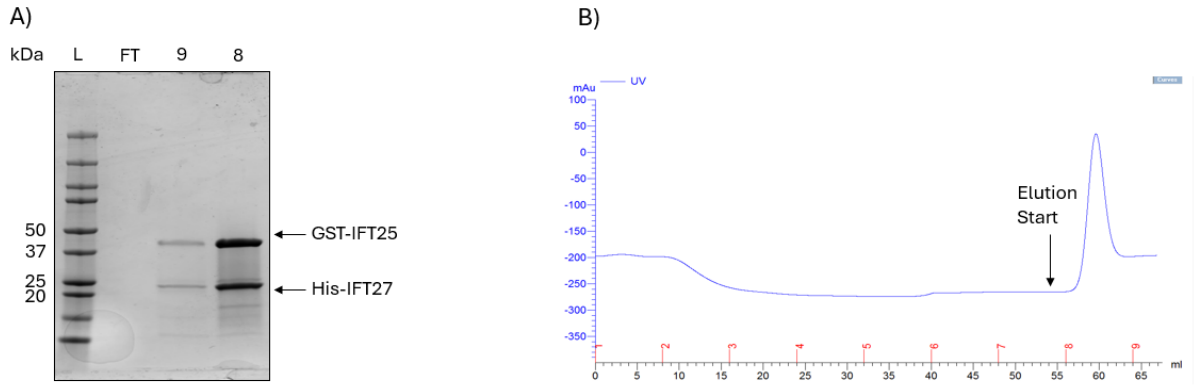

Figure 4.1.7.2: A) Shows the SDS-PAGE gel from purification of GST-IFT25/His-IFT27^{Y35C}. From left to right: Ladder, flowthrough, fractions 9 and 8 from Ni^{+} column. B) Shows the Ni-affinity purification of GST-3C-IFT25 and His-TEV-IFT27^{Y35C}.

4.1.8 SEC to determine possible difference in folding between IFT25/IFT27^{WT} and IFT25/IFT27^{Y35C}

Although IFT25/His-IFT27^{Y35C} is purified in the same way as the WT complex during GST and Ni-Affinity purification, we still wanted to test if this mutant is as compact as the WT complex. Because both size and shape affect how proteins move through SEC, we compared the elution times of the IFT25/His-IFT27^{WT} and IFT25/His-IFT27^{Y35C}. Running SEC will also determine if IFT25/His-IFT27^{Y35C} is aggregated, as it will then elute in the void volume, much earlier than the IFT25/His-IFT27^{WT}. We loaded each of the complexes on a HiLoad 16/600 Superdex 75 pg and observed that they elute at almost the exact volume (figure 4.1.8.1), with the mutant eluting slightly earlier. The difference in elution was so small (3.224 mL), that it can be explained by an inherent margin of error each injection has, as the column has a volume of 120 mL. Therefore, we concluded that IFT25/His-IFT27^{Y35C} has the same fold as IFT25/His-IFT27^{WT}, so mutation did not result in the misfolded protein. Both IFT25/His-IFT27 complexes have expected MW at 37.1 kDa and should therefore elute around 67.1 mL according to the calibration curve of the column. This is calculated from globular proteins, and IFT25/His-IFT27 is not globular. This explains why both complexes elutes before they are theoretically expected to.

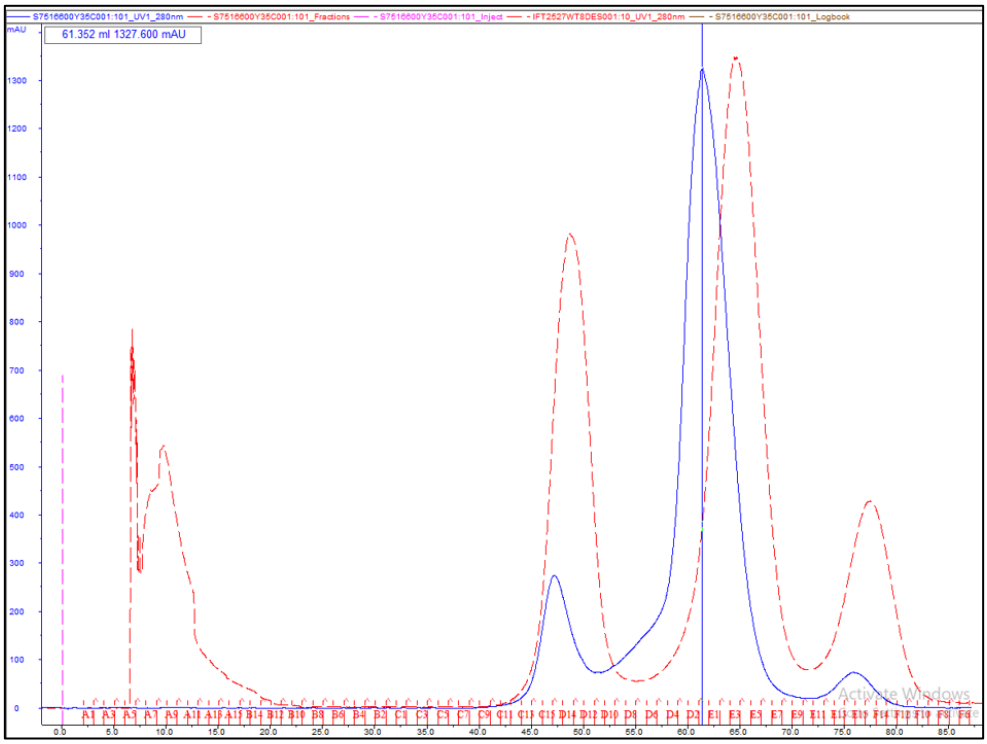

Figure 4.1.8.1: A) Shows the overlayed SEC of IFT25/His-IFT27^{WT} (red stitches) and IFT25/2727^{Y35C} (blue). Both protein complexes elute almost at the same volume, with the mutant eluting at 61.352 mL and the WT at 64.576 mL, a difference of 3.224 mL

4.1.9 Expression and Purification of GST-IFT25/His-IFT27^{C99Y} heterodimer

IFT25 and IFT27^{C99Y} was expressed in Rosetta 2 cells overnight at 18ºC. Cells were harvested, lysed with sonication and the cell debris spun down at 40000 x G. The supernatant was injected on a GST-column. The first purification to be conducted was GST purification (Figure 4.1.9.1 B). The protein was eluted with 10 mM imidazole in fraction number 8, 9 and 10, and the content was run on a SDS-PAGE gel (Figure 4.1.9.1 A). We could observe two bands, a thicker band slightly lower than 50 kDa that is in agreement with the expected MW for GST-IFT25 (expected MW 41.7 kDa) and a fainter band between 20 and 25 kDa in agreement with MW for free GST (expected MW 25 kDa) and His-IFT27^{C99Y} (expected MW 23 kDa), fractions 8-12 were pooled, 3C protease added to cleave GST off and dialyzed overnight to remove glutathione.

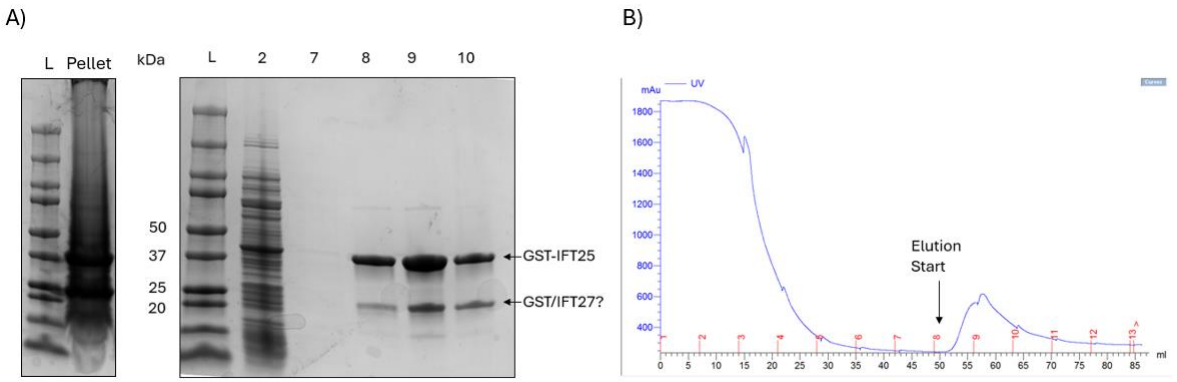

Figure 4.1.9.1: A) Shows the SDS-PAGE gel from purification of GST-IFT25/His-IFT27^{C99Y} From left to right: Ladder, Pellet, Ladder, fractions 2, 7, 8, 9 and 10 from GST column. B) Shows the GST purification of GST-3C-IFT25 and His-TEV-IFT27^{C99Y}

We proceeded with Ni-affinity chromatography (Figure 4.1.9.2 B) so that only IFT25/His-IFT27^{C99Y} complex (and potentially uncut GST-IFT25/His-IFT27^{C99Y}) will bind the column and free GST would be washed off. Column was loaded, washed with several CVs of buffer and eluted with 300 mM imidazole. We concluded that GST-IFT25 was successfully cleaved but we could not see His-IFT27^{C99Y} and thus the complex was never formed. The bands in figure 4.1.9.2 A elute around 25 kDa and between 15 kDa and 20 kDa. The upper band agrees with expected MW for His-IFT27^{C99Y} (23 kDa) and GST (25 kDa), and the lower band is in agreement with MW of IFT25, so from here we conclude that GST-IFT25 was successfully cleaved. Furthermore, the band above 37 kDa that was present after elution from the GST column is very faint in our elution samples. Also, wash fraction shows band ˜25 kDa which agrees with MW of GST, but interestingly nothing eluted from the column, indicating the absence of His-IFT27^{C99Y}. Figure 4.1.9.1 A includes the pellet, where a band around 25 kDa might be visible, suggesting that all of IFT27^{C99Y} ended up in inclusion bodies. From here we concluded that His-IFT27^{C99Y} was insoluble.

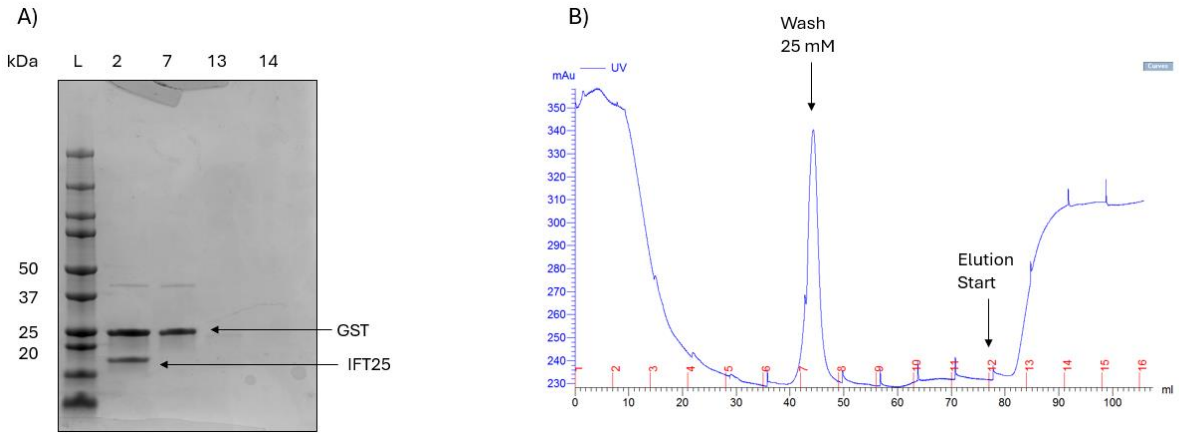

Figure 4.1.9.2: A). Shows the SDS-PAGE gel from purification of GST-IFT25/His-IFT27^{C99Y}. From left to right: Ladder, fractions 2, 7, 13 and 14 from Ni^{+} column B) Shows the Ni-affinity purification of His-TEV-IFT27^{C99Y} and GST-3C-IFT25.

The expression and purification were repeated with new sets of columns to assure that negative results were not due to technical issues, but this yielded the same results. We have also tried to favour protein expression by growing over night at 18 °C, but this was without success.

To understand how this mutation could affect protein stability we analysed the predicted structure (Figure 4.1.8.3). The IFT27^{C99Y} mutation is at the surface of the protein but it fits tightly with the surrounding residues. When this residue is mutated to a much bulkier and hydrophobic tyrosine, it is possible that there are sterical clashes with the surrounding residues that could destabilize the fold of the protein and also induce aggregation.

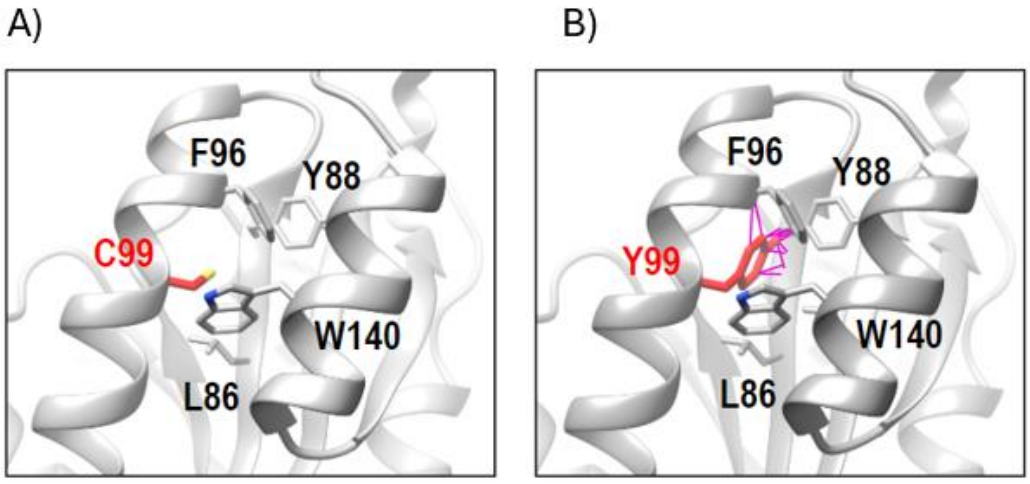

Figure 4.1.9.3: A) Shows cystine (red) in IFT27^{WT} B) Shows the tyrosine in the C99Y mutant (red) in IFT27^{C99Y}. All possible rotamers of tyrosine clashes with the labelled residues. Figure created in Chimera

4.1.10 Expression and Purification of MBP-CENP-J$^{412-897}$

His-MBP-TEV-CENP-J$^{412-897}$ was expressed in Rosetta 2 cells overnight at 18°C. Cells were harvested, lysed with sonication and the cell debris spun down at 40000 x G. The supernatant was injected Ni-affinity chromatography (Figure 4.1.10.1 B). The column was washed with 25 and 50 mM imidazole and eluted with 300 mM imidazole and fractions were run on SDS-PAGE gel (figure 4.1.10.1 A). His-MBP-TEV-CENP-J$^{412-897}$ has expected MW of 107.7 kDa and the band around that size is enriched in the final elution. Since we see the same band is also present in the elution, we have saved those fractions too for possible further processing. The elution fractions 23-25 were pooled and dialyzed overnight to remove imidazole. We have decided to not cleave of the MBP-tag, so that the protein could be used as bait in pull down assays, but proceeded to SEC to further purify the eluted protein.

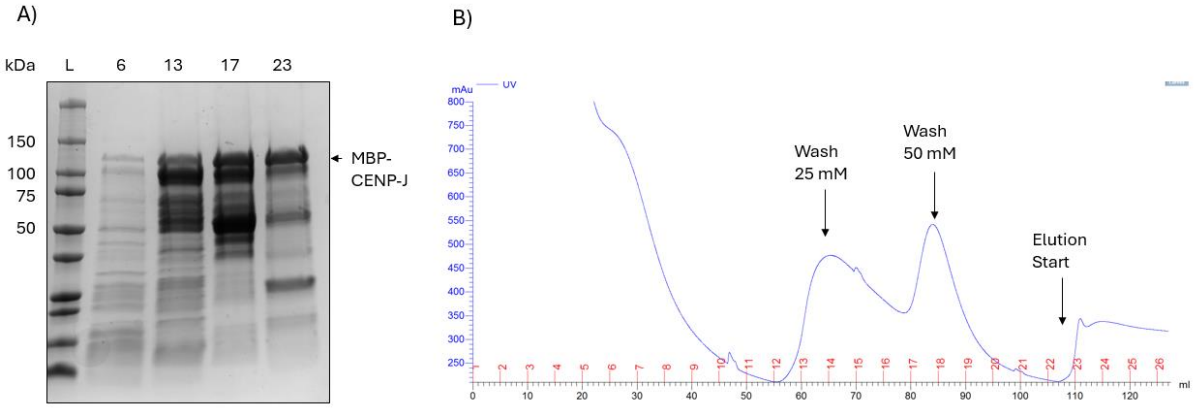

Figure 4.1.10.1: A) Shows the SDS-PAGE gel from His-MBP-CENP-J$^{412-897}$. From left to right: Ladder, fractions 3, 5, 9, 12 and 13 from Ni^{+} column. B) Shows the Ni-affinity purification of His-MBP-TEV-CENP-J$^{412-897}$

The elution from SEC using HiLoad 16/600 Superdex 200 pg (figure 4.1.10.2 B) showed three major peaks and fractions were run on SDS-PAGE (figure 4.1.10.2 A). The gel revealed that the first peak (fraction 19 and 20) contains mostly MBP-CENP-J$^{412-897}$ (107.7 kDa) with some minor contaminants. Thus fractions 17-21 were collected and the protein supplemented with, 20% glycerol, flash frozen and stored at -80 °C for function experiments.

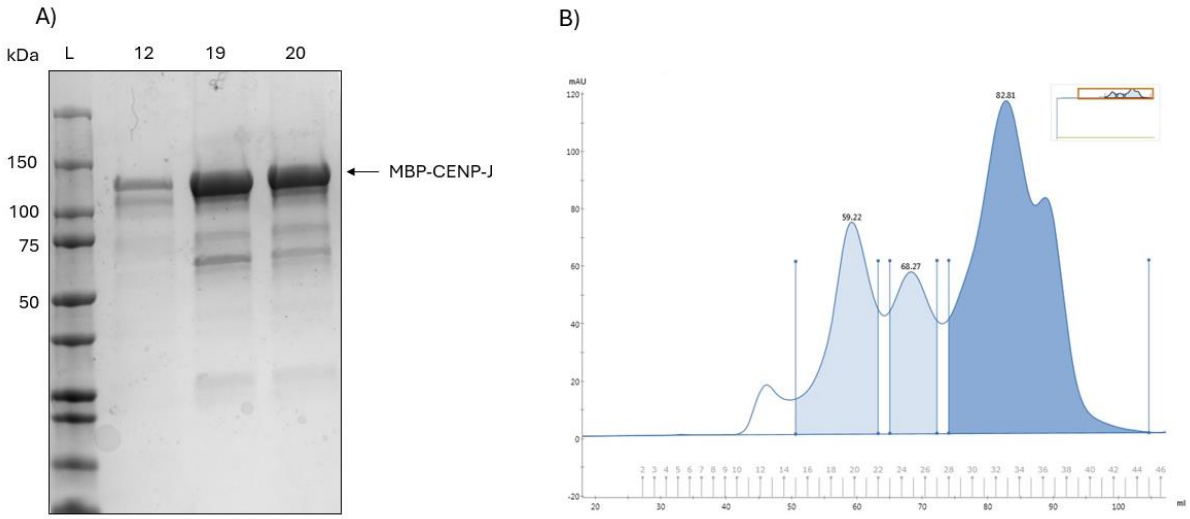

Figure 4.1.10.2: A) Shows the SDS-PAGE gel run from His-MBP-CENP-J$^{412-897}$ SEC purification from left to right: ladder, fraction 12, fraction 19 and fraction 20. Fraction 12 is in peak 1, fraction 19-20 is in the second peak (59.22). B) Shows the SEC purification of His-MBP-TEV-CENP-J$^{412-897}$using HiLoad 16/600 Superdex 200 pg

4.1.11 Expression and Purification of Aurora B$^{60-360}$/INCENP$^{790-858}$

Aurora B$^{60-361}$ and INCENP$^{790-858}$ were co-expressed in Rosetta 2 cells. Aurora B$^{60-360}$ is expressed with a 6x His tag and a GB1 solubility tag, and therefore purified with a His-column (figure 4.1.11.1 B) After induction with IPTG, cells were grown over night at 18^{o}C, cells were harvested, lysed with sonication and the cell debris spun down at 40000 x G. The supernatant was injected on Ni-affinity column. The column was washed with 25 and 50 mM imidazole buffers and protein eluted with 500 mM imidazole. Fractions eluted during the wash and elution were analysed with SDS-PAGE (figure 4.1.11.1 A). In the eluted fraction we could observe enrichment in bands corresponding to His-GB1-Aurora B$^{60-360}$ (expected MW 43.1 kDa) and INCENP$^{790-858}$ (expected MW 9.0 kDa). Fractions 18-21 were pooled and dialyzed overnight in the presence of TEV, to cleave His-GB1tag from Aurora B$^{60-360}$.

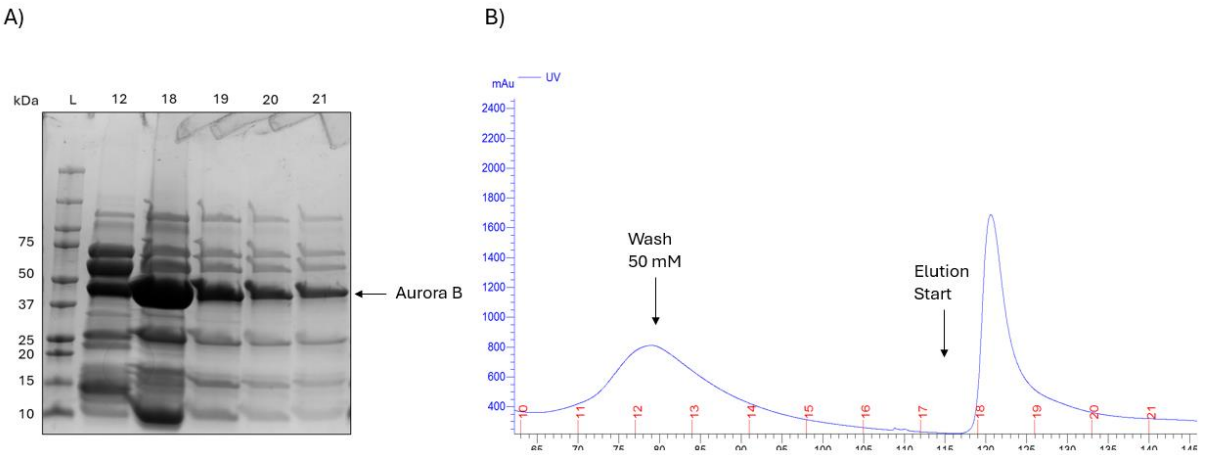

Figure 4.1.11.1: A) Shows the SDS-PAGE gel from His-GB1-Aurora B^{60-360}. From left to right: Ladder, fractions 3, 5, 9, 12 and 13 from Ni^{+} column. B) Shows the Ni-affinity purification of His-GB1-AuroraB^{60-360} and $INCENP^{790-858}$.

To further purify the complex and remove cleaved tags, the sample was subjected to SEC (figure 4.1.11.2 B). Fractions containing Aurora B^{60-360} and $INCENP^{790-858}$ (D5-E4) were pooled together with a final amount of 4.9 mg of protein. 20% glycerol was added to the sample before, flash freezing and was stored at -80 °C.

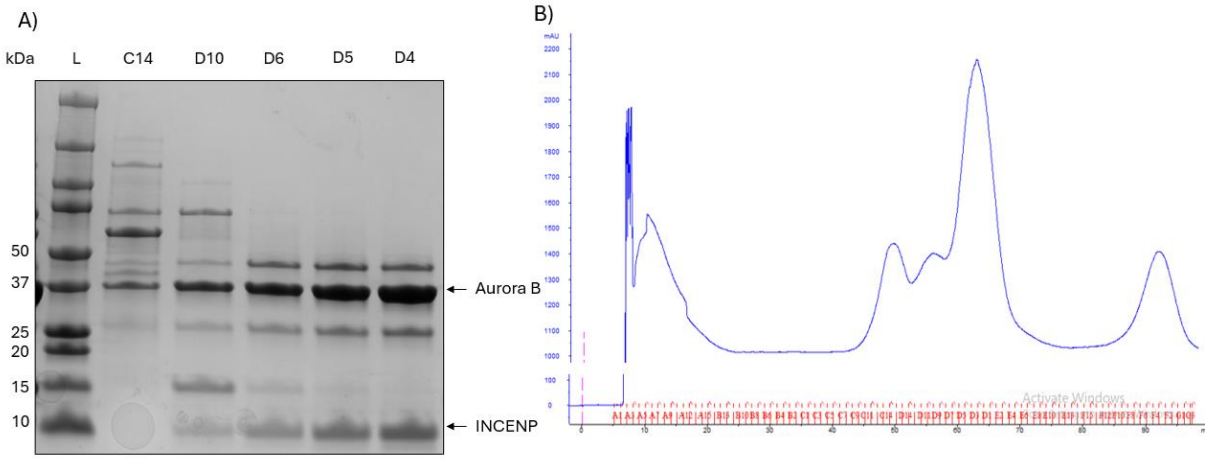

Figure 4.1.11.2: A) Shows the SDS-PAGE gel run after SEC purification of His-GB1-Aurora B^{60-360}. From left to right: ladder, fraction C14, fraction D10, fraction D5 and fraction D4. Fractions D6-D4 are in the largest peak. B) Shows the SEC purification of His-GB1-AuroraB^{60-360} and $INCENP^{790-858}$ using HiLoad 16/600 Superdex 75 pg.

4.2 GTPase test to determine if His-IFT27 is folded

Although association with binding partner IFT25 and expected elution volume from SEC are all indication that we have purified functional IFT27, we went further and tested if our purified protein complexes have GTPase activity.

The GTPase test is performed as established by (Borg Distefano et al. 2018) (see materials and method). Along with our samples (GST-IFT25/His-IFT27^{WT} and GST-IFT25/His-IFT27^{Y35C}) in the presence of GTP, we also measured the absorbance of sodium phosphate solution at the same concentration of GST-IFT25/His-IFT27 (positive control). The phosphate sample should give a theoretical maximum signal, assuming that one IFT27 molecule can hydrolyse only one GTP molecule in the absence of the guanine nucleotide exchange factor (GEF), responsible for the GDP removal from the active site by destabilizing the Mg^{2+} ion and GDP binding to the GTPase (Uejima et al. 2010) In addition, GST-IFT25/His-IFT27^{WT} and GST-IFT25/His-IFT27^{Y35C} samples without GTP and a sample containing only GTP were included, as negative controls. Results are presented in (table 4.2.1) and in a graph bar (figure 4.2.1)

Table 4.2.1: Shows the GTPase test, with the positive and negative controls

Phosphate	**GST-IFT25/His-IFT27^{WT} + GTP**	**GST-IFT25/His-IFT27^{Y35C} + GTP**	**GST-IFT25/His-IFT27^{WT} alone**	**GST-IFT25/His-IFT27^{Y35C} alone**	**GTP alone**
0.3668	1.2153	0.6062	0.0212	0.0009	0.0567

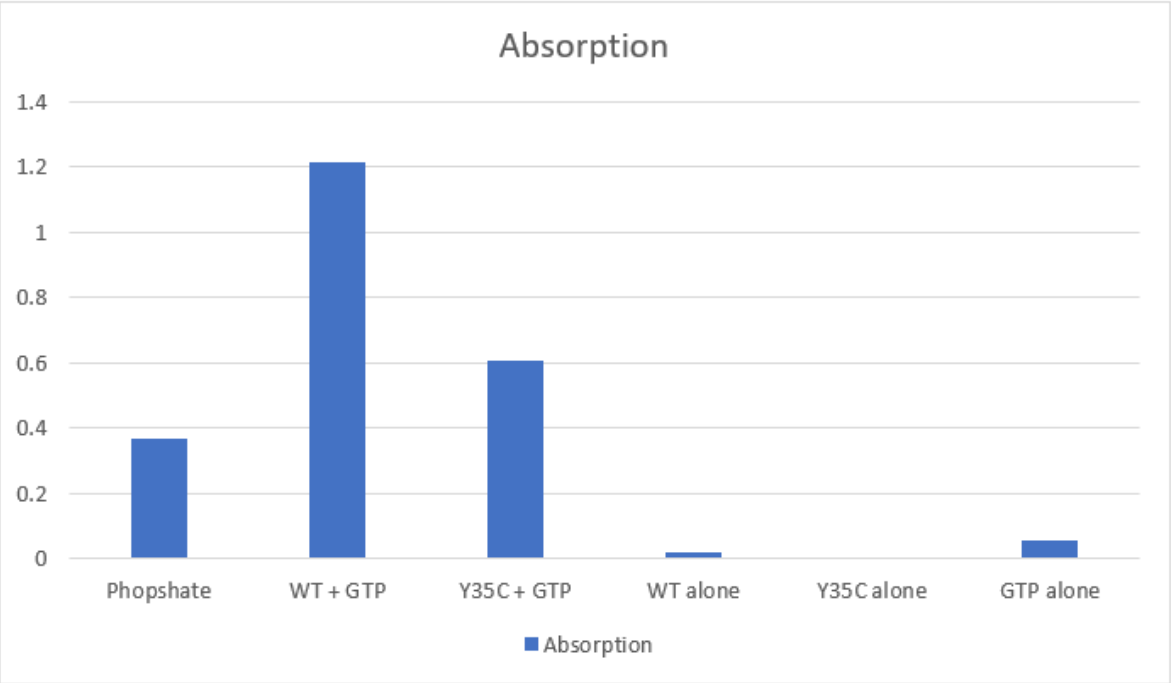

Figure 4.2.1: A) Shows the results of the GTPase activity test, the Y-axis is the measured absorbance. Samples from left to right: 12 µM phosphate, 12 µM GST-IFT25/His-IFT27^{WT} and 1 mM GTP, 12 µM GST-IFT25/His-IFT27^{Y35C} and 1 mM GTP, GST-IFT25/His-IFT27^{WT} alone, GST-IFT25/His-IFT27^{Y35C} alone and 1 mM of GTP alone

Both GST-IFT25/His-IFT27^{WT} and GST-IFT25/His-IFT27^{Y35C} with GTP samples precipitated after adding solution II and III. We believe this to be caused by the large amounts of phosphate generated by both IFT27s causing $(NH_4)_3PMo_{12}O_{40}$ to precipitate due to high concentration of the molecule.

Usually, GEF proteins are present together with small GTPases to remove the GDP remaining in the active site, before another GTP can bind to IFT27. But much higher concentration of GTP might outcompete IFT27-bound GDP and bind to the active site of IFT27. In this case, one IFT27 molecule might perform multiple GTP hydrolysis reactions, which might explain why the absorbance is higher than the theoretical maximum. Thus, we determined that GST-IFT25/His-IFT27^{WT} and GST-IFT25/His-IFT27^{Y35C} both have high GTPase activity, and therefore are properly folded.

4.3 Exploring interaction between IFT25/IFT27^{WT} and IFT25/IFT27^{Y35C} and CENP-J$^{412-897}$

Pull down assays are used to determine if there is any direct interaction between two proteins. The MBP-CENP-J was chosen as the bait protein as the MBP-tag will bind the amylose beads and IFT25/His-IFT27^{WT} serves as the prey. Since IFT25/His-IFT27^{WT} was not expressed with an MBP-tag it should not bind the amylose beads by itself.

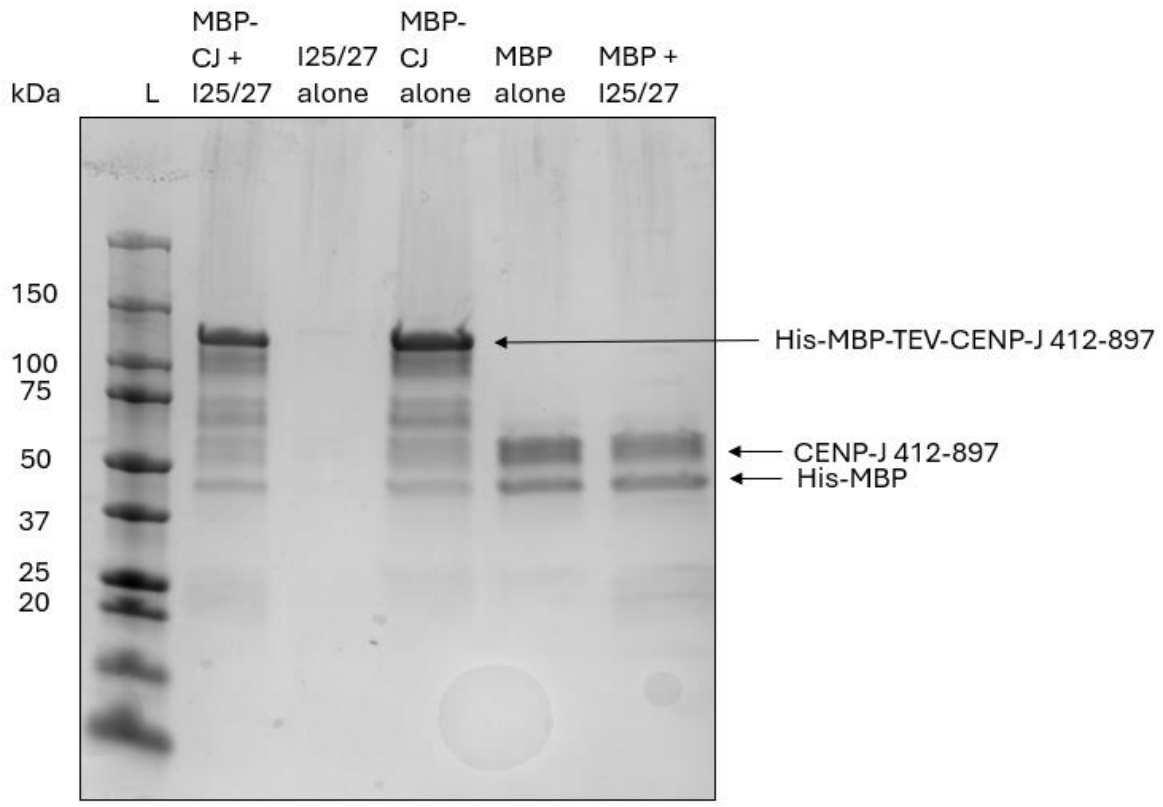

Figure 4.3.1: This figure shows the result of the pull-down assay with IFT25/His-IFT27^{WT} and MBP-CENP-J$^{412-897}$. From left to right: ladder, MBP-CENP-J$^{412-897}$ and IFT25/His-IFT27^{WT}, IFT25/IFT27^{WT} alone, MBP-CENP-J$^{412-897}$ alone, MBP alone and MBP and IFT25/His-IFT27^{WT}

The samples where amylose beads are incubated with IFT25/His-IFT27^{WT} without MBP-CENP-J$^{412-897}$ show no bound proteins indicating that indeed IFT25/His-IFT27^{WT} by itself does not bind the resin (Figure 4.3.1, second lane; negative control.) This is in difference to amylose beads incubated with MBP-CENP-J$^{412-897}$ that show nice binding of MBP-CENP-J$^{412-897}$ (Figure 4.3.1 fourth lane; positive control) as it should. And finally, if IFT25/His-IFT27^{WT} would bind directly to MBP, it would suggest that the bait binds MBP instead, (Figure 4.3.1, fifth lane; negative control) and fortunately it does not. When we now analyse the sample where MBP-CENP-J$^{412-897}$ was incubated with IFT25/His-IFT27^{WT}

(figure 4.3.1, first lane; experiment) we see only bands corresponding to MBP-CENP-J$^{412-897}$ we can conclude that IFT25/His-IFT27^{WT} does not interact with MBP-CENP-J$^{412-897}$.

The same experiment was repeated with IFT25/His-IFT27^{Y35C} and we observe exactly the same result (Figure 4.3.2) From here, we conclude that both WT and mutant does not directly bind CENP-J$^{412-897}$. This does not rule out the possibility of indirect interaction, as they may need another binding partner to associate with. Aurora B has been shown to localize with both IFT27 and CENP-J, and they could interact if all three are present. Also, CENP-J have many post translational modifications (PTMs) and maybe need those to bind IFT27.

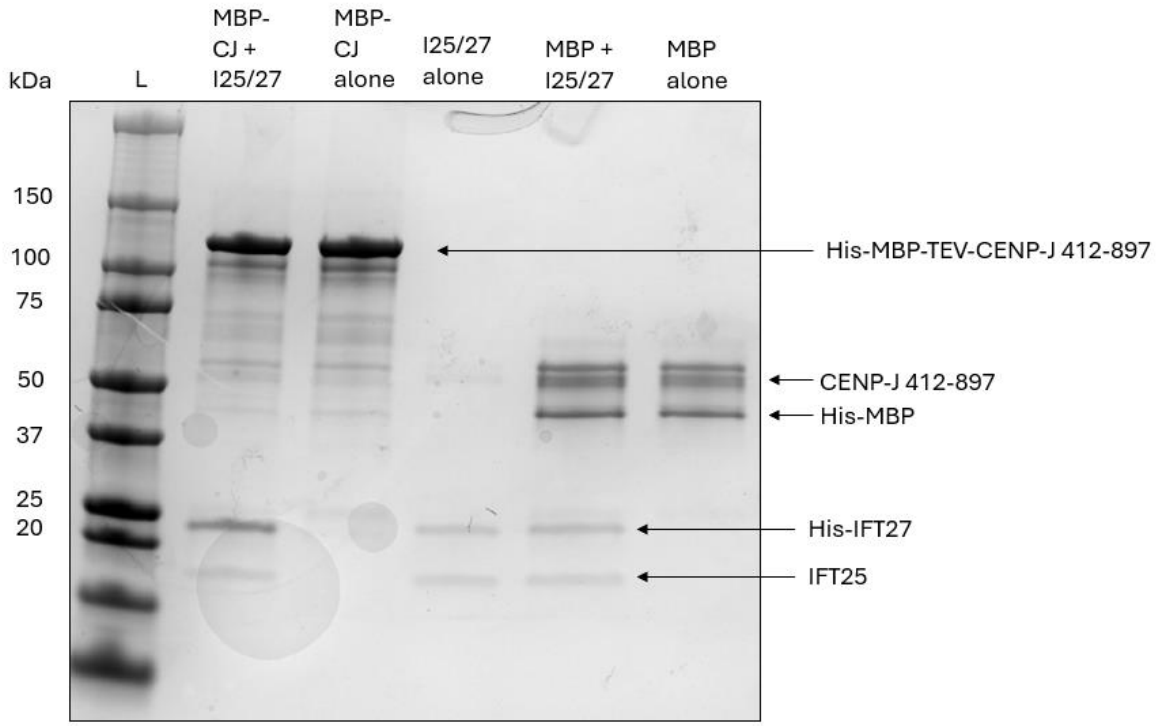

Figure 4.3.2: This figure shows the result of the pull-down assay with IFT25/His-IFT27^{Y35C} and MBP-CENP-J$^{412-897}$. From left to right: ladder, MBP-CENP-J$^{412-897}$ and IFT25/His-IFT27^{Y35C}, MBP-CENP-J$^{412-897}$ alone, IFT25/His-IFT27^{Y35C} alone, MBP and IFT25/His-IFT27^{Y35C} and MBP alone

4.4 Exploring interaction between IFT25/IFT27 (and mutants) and Aurora B

To check for interaction between IFT25/IFT27 and Aurora B^{60-360}, GST-IFT25/His-IFT27 was used as the bait protein as the GST-tag will bind the glutathione beads and Aurora B kinase serves as the prey. Since Aurora B^{60-360} was not expressed with a GST-tag it should not bind the glutathione beads by itself.

In a similar manner, we have incubated beads with Aurora B^{60-360} alone (Figure 4.4.1 third line, negative control) to see if Aurora B^{60-360} could bind glutathione beads and indeed, we see a faint band indicating some level of non-specific binding. Next, when GST-IFT25/$IFT27^{WT}$ is incubated with beads, we see good binding (Figure 4.4.1 second line, positive control). Finally, when we incubate beads with both, GST-IFT25/$IFT27^{WT}$ and Aurora B^{60-360} we see that both GST-IFT25/$IFT27^{WT}$ and Aurora B^{60-360} elute from beads (Figure 4.4.1 first lane, experiment) indicating that GST-IFT25/$IFT27^{WT}$ directly interacts with Aurora B^{60-360}. Note that this band is much more prominent than the one corresponding to Aurora B^{60-360} non-specifically bound to glutathione beads (Figure 4.4.1 third line, negative control). To eliminate the possibility of Aurora B^{60-360} interacting with GST tag rather than IFT25/$IFT27^{WT}$ we have incubated beads with only GST (Figure 4.4.1., right gel, first line; positive control) and then with both GST and Aurora B^{60-360} (Figure 4.5.1 right gel, first line; negative control). Here we see that GST binds beads but it does not pull-down Aurora B^{60-360}. In summary, we conclude that IFT25/$IFT27^{WT}$ directly interacts with Aurora B^{60-360}.

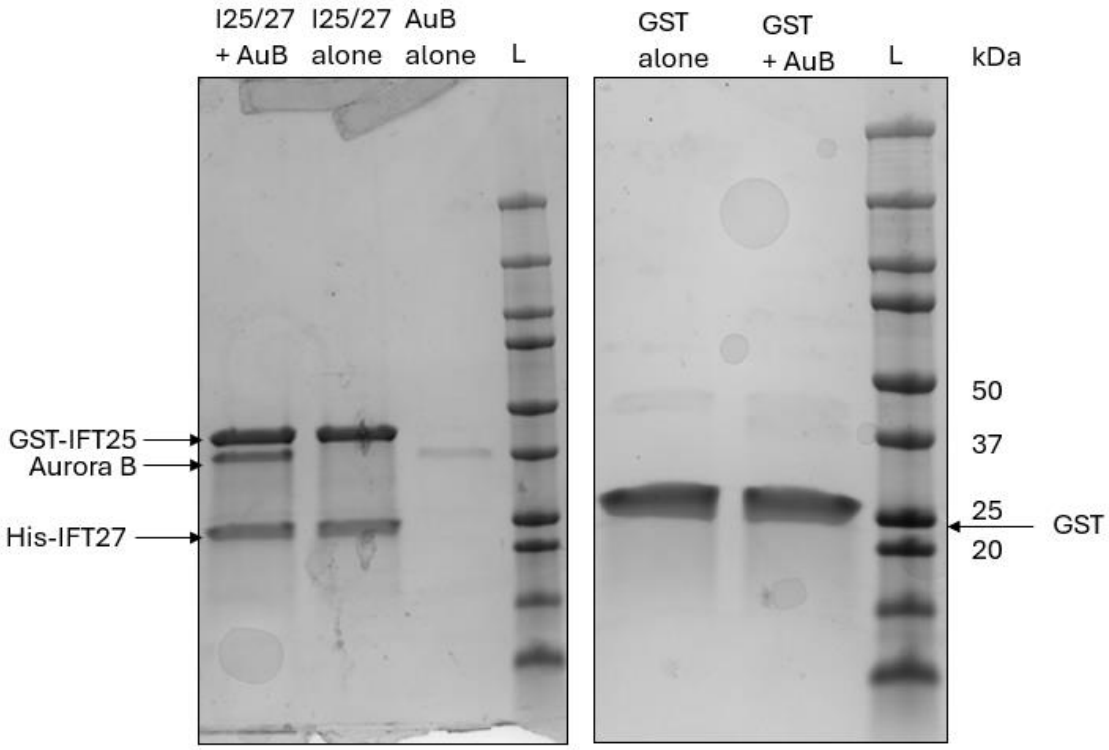

Figure 4.4.1: This figure shows the result of the pull-down assay with Aurora B^{60-360} and IFT25/$IFT27^{WT}$. From left to right: GST-IFT25/$IFT27^{WT}$ and Aurora B^{60-360}, GST-IFT25/$IFT27^{WT}$ alone, Aurora B^{60-360} alone, ladder, GST and Aurora B^{60-360} and GST alone. Both GST controls were run on a sperate gel, that is included on the right

The experiment was repeated with GST-IFT25/His-$IFT27^{Y35C}$ and we observe exactly the same result (figure 4.4.2) So, we conclude that both WT and mutant directly bind Aurora B^{60-360}.

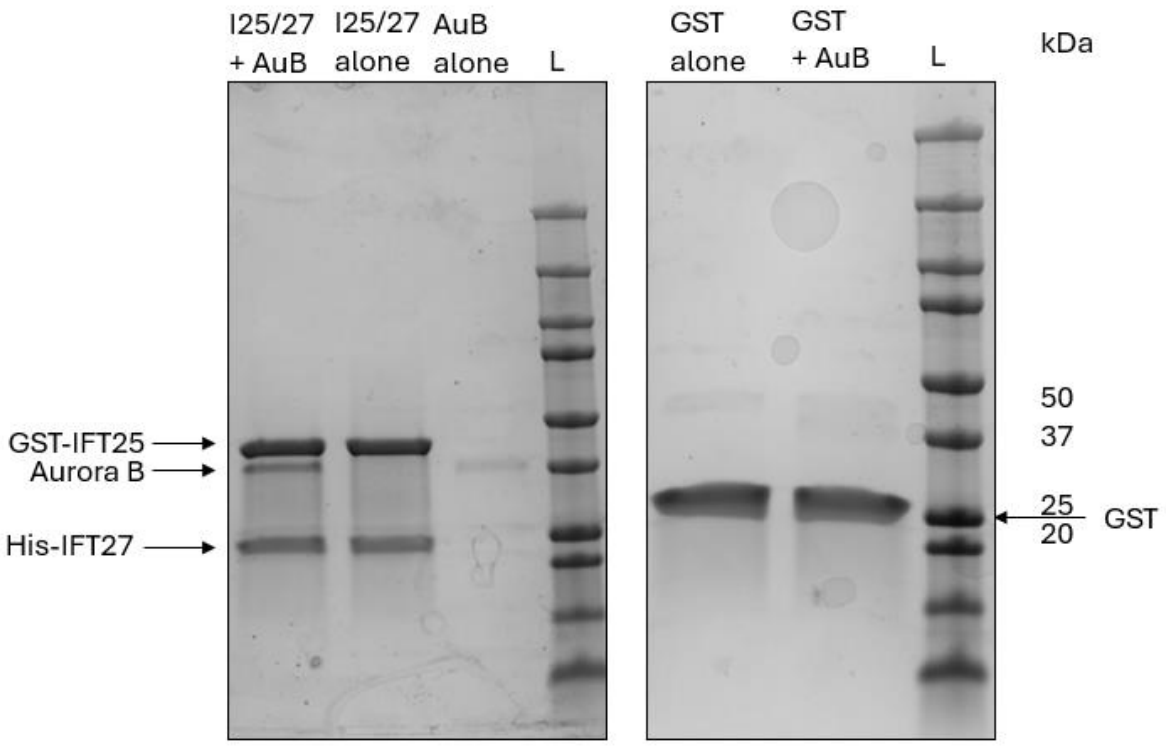

Figure 4.4.2: This figure shows the result of the pull-down assay with Aurora B^{60-360} and GST-IFT25/$IFT27^{Y35C}$. From left to right: GST-IFT25/$IFT27^{Y35C}$ and Aurora B^{60-360}, GST-IFT25/$IFT27^{Y35C}$ alone, Aurora B^{60-360} alone, ladder, GST and Aurora B^{60-360} and GST alone.

4.5 Testing if IFT25/$IFT27^{WT}$ and IFT25/$IFT27^{Y35C}$ affect Aurora B activity

Because IFT25/$IFT27^{WT}$ directly interact with Aurora B^{60-360}, we wanted to test if IFT25/$IFT27^{WT}$ and the IFT25/$IFT27^{Y35C}$ mutant affect the phosphorylation activity of Aurora B kinase. The kinetic assay for Aurora B that uses helper enzymes pyruvate kinase (PK) and lactate dehydrogenase (LDH) to relate amount of generated ADP in kinase reaction to the amount of consumed NADH (that is followed spectrophotometrically at 340 nm) is already established in the Sekulic lab (see materials and method 3.12) All components are mixed in a cuvette and reaction is triggered with the addition of Aurora B kinase and decrease in absorbance is measured continually. The slope of the cure is proportional to the velocity of Aurora B kinase phosphorylation of substrate peptide.

I have performed this experiment twice using slightly different construct of IFT25/IFT27 First, I used GST-IFT25/His-$IFT27^{WT}$ and GST-IFT25/His-$IFT27^{Y35C}$. The results for this experiment are shown in figure 4.5.1.

First, we tested activity of Aurora B^{60-360} /$INCENP^{790-858}$ alone to establish a benchmark for the samples. We measured a velocity of 50 µM/min formation of NAD.

Since we don't know the dissociation constant between IFT25/IFT27 and Aurora B, we decide to test two different ratios of GST-IFT25/His-$IFT27^{WT}$: Aurora B^{60-360}. We tested activity in 1:1 ratio and in 1:4 ratio.

The GST-IFT25/His-$IFT27^{WT}$ was incubated with Aurora B^{60-360} in 1:1 and 1:4 ratio and the mixture added to the cuvette we saw a steeper decline in absorbance, corresponding to a average velocity of 69 µM/min for the 1:1 ratio, and 67 µM/min for 1:4. This could suggest that GST-IFT25/His-$IFT27^{WT}$ might be an activator of Aurora B, boosting its activity when proteins are in complex.

In difference, when GST-IFT25/His-$IFT27^{Y35C}$ was tested in the same way we saw roughly the same velocities as Aurora B^{60-360} by itself. The 1:1 sample averaged 51 µM/min and the 1:4 sample averaged 52 µM/min.

Two control samples were run to make sure that GST-IFT25/His-$IFT27^{WT}$ or mutant was not exhibiting any kinase activity. No meaningful activity was detected and it was determined that both GST-IFT25/His-$IFT27^{WT}$ and GST-IFT25/His-$IFT27^{Y35C}$, does not exhibit any kinase activity by themselves.

Although these results are exciting, upon closer examination of the original kinetic slopes we noticed they start flat and gradually gain inclination, indicating that Aurora B^{60-360} was most likely not completely active at the beginning of the experiment, so the Aurora B^{60-360} autoactivation was happening in parallel with the experiment making the correct interpretation of slopes difficult. Therefore, this test was repeated with another batch of Aurora B^{60-360} kinase, kindly provided by another member of the lab.

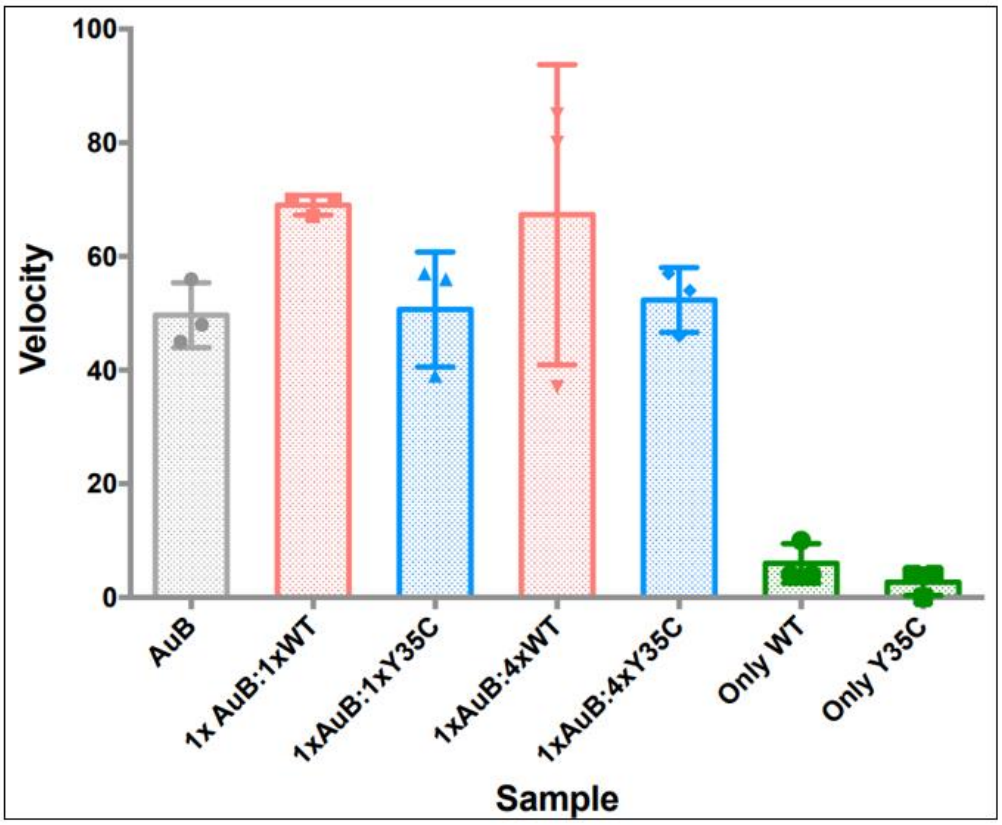

Figure 4.5.1: This figure shows the results from the first Aurora B^{60-360} kinase activity test. The negative slopes are measured on the Y-axis, with higher negative slopes indicating higher activity. There are three replicates of each sample, from left to right: Aurora B^{60-360} alone, 1:1 Aurora B^{60-360} and GST-IFT25/His-$IFT27^{WT}$, Aurora B^{60-360} 1:1 GST-IFT25/His-$IFT27^{Y35C}$, 1:4 Aurora B^{60-360} and GST-IFT25/His-$IFT27^{WT}$, 1:4 Aurora B^{60-360} and GST-IFT25/His-$IFT27^{Y35C}$, only GST-IFT25/His-$IFT27^{WT}$ and only GST-IFT25/HIS-$IFT27^{Y35C}$

This time, to avoid possible influence of the GST tag, I have used IFT25/His-$IFT27^{WT}$ and IFT25/His-$IFT27^{Y35C}$, but proteins were stored for over 3 weeks at -80°C before activity experiment took place.

It became clear immediately that the activity of this batch of Aurora B^{60-360} was much better reaching average velocity of 304 µM/min (Figure 4.5.2) However, the velocity did not change significantly in the presence of IFT25/His-$IFT27^{WT}$ and IFT25/His-$IFT27^{Y35C}$. This could be due to long shelf time of the proteins, and it would be worthwhile repeating the experiment with freshly purified proteins but I did not due that due to time constrains.

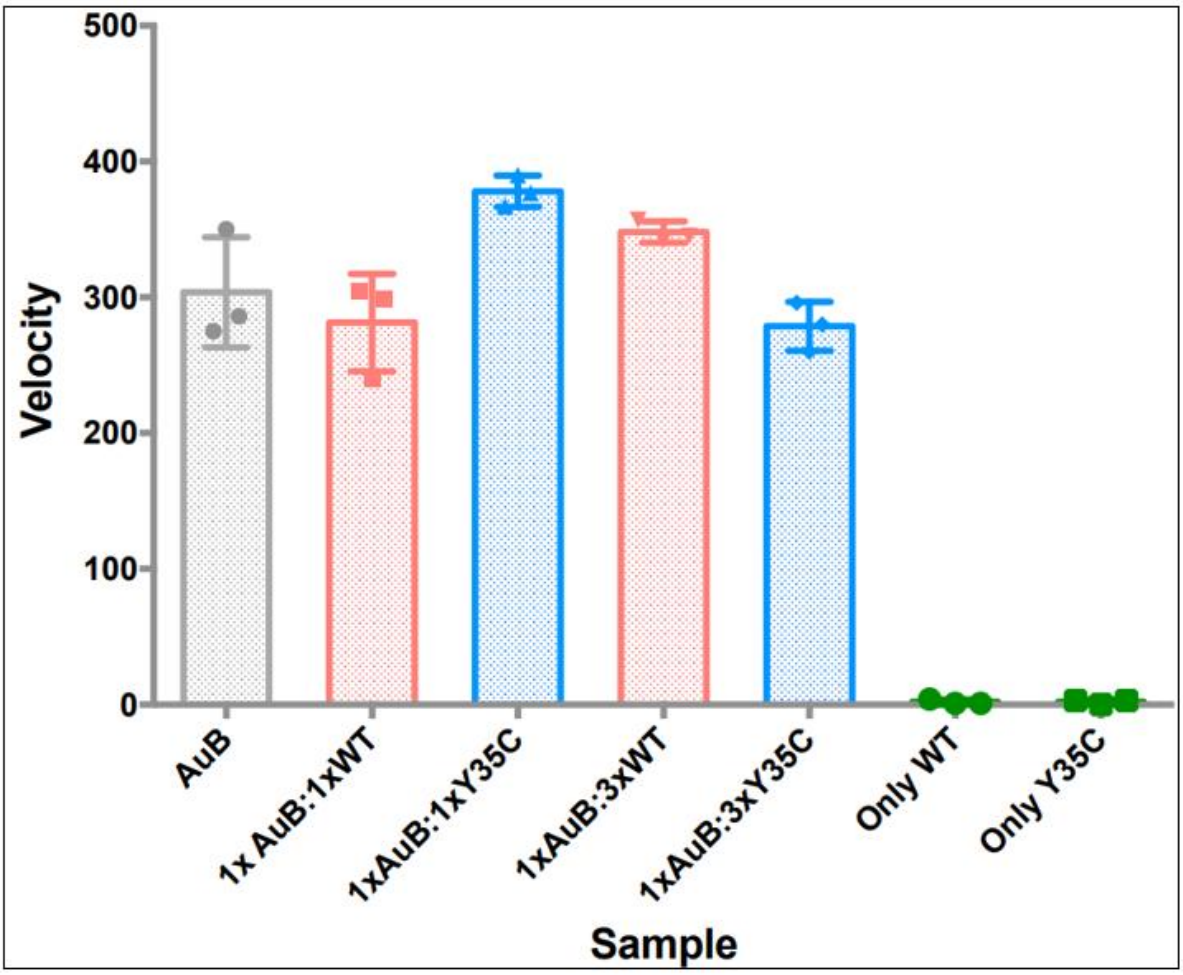

Figure 4.5.2: This figure shows the results from the second Aurora B^{60-360} kinase activity test. The negative slopes are measured on the Y-axis, with higher negative slopes indicating higher activity. There are three replicates of each sample, from left to right: Aurora B^{60-360} alone, 1:1 Aurora B^{60-360} and IFT25/His-$IFT27^{WT}$, Aurora B^{60-360} 1:1 IFT25/His-$IFT27^{Y35C}$, 1:3 Aurora B^{60-360} and IFT25/His-$IFT27^{WT}$, 1:4 Aurora B^{60-360} and IFT25/His-$IFT27^{Y35C}$, only IFT25/His-$IFT27^{WT}$ and only IFT25/His-$IFT27^{Y35C}$

5. Conclusion and Future Perspectives

This thesis focused on the study of Intraflagellar Transport Protein IFT27 and mutations associated with Bardet-Beidl Syndrome (BBS) and cell division. By performing in vitro biochemical studies, I have showed that human IFT27, as previously reported in *Chlamydomonas* (Bhogaraju et al. 2011), is not soluble by itself and needs to form a hetero-dimer with IFT25. The mutations of C99Y and Y35C reported in BBS showed different impacts on IFT27. The C99Y mutation completely knocked down IFT27 that could not be expressed in *E. coli,* even in the presence of IFT25, which might be caused by steric clashes with surrounding residues, and its subsequent effect on the protein fold. IFT27^{Y35C} on the other hand was possible to obtain. Using SEC and GTPase activity we showed the overall fold and activity of the mutated protein complex is comparable to WT. Both IFT25/IFT27^{WT} and IFT25/IFT27^{Y35C} did not show any binding to CENP-J$^{412-897}$ expressed in *E. coli*. This could be due to the absence of PTMs that are heavily present on CENP-J or maybe they need another binding partner to associate together. Interestingly, GST-IFT25/IFT27^{WT} and its GST-IFT25/IFT27^{Y35C} mutant showed direct binding to Aurora B$^{60-360}$-INCENP$^{790-858}$ complex in vitro. This direct binding also potentially affects Aurora B kinase activity, boosting it only in the presence of IFT25/IFT27^{WT} but not with the mutant. These experiments are a good first step but should be further investigated with freshly made protein to confirm the results.

If the capacity of IFT27^{WT} to boost Aurora B activity is confirmed, this would suggest that the mutations reported in BBS have indirect effect on decreasing Aurora B activity, either by completely knocking down IFT27 in the case of the C99Y mutation, or by decreasing the effect of IFT27 on Aurora B activity in the case of the Y35C mutations. These results, even though incomplete, might explain the previous findings of the Progida lab, that indicates that IFT27^{Y35C} increase the length of abscission, simply because Aurora B does not obtain its boost of activity found in cells expressing WT IFT27. Hopefully this work will inspire further experiments towards elucidating the molecular mechanisms behind Bardet-Beidl Syndrome.

6. References

Aldahmesh, M. A., Y. Li, A. Alhashem, S. Anazi, H. Alkuraya, M. Hashem, A. A. Awaji, S. Sogaty, A. Alkharashi, S. Alzahrani, S. A. Al Hazzaa, Y. Xiong, S. Kong, Z. Sun, and F. S. Alkuraya. 2014. 'IFT27, Encoding a Small GTPase Component of IFT Particles, Is Mutated in a Consanguineous Family with Bardet-Biedl Syndrome'. *Human Molecular Genetics* 23(12):3307–15. doi: 10.1093/hmg/ddu044.

Alvarez-Cabrera, Ana L., Sandra Delgado, David Gil-Carton, Gulnahar B. Mortuza, Guillermo Montoya, Carlos O. S. Sorzano, Tang K. Tang, and Jose M. Carazo. 2017. 'Electron Microscopy Structural Insights into CPAP Oligomeric Behavior: A Plausible Assembly Process of a Supramolecular Scaffold of the Centrosome'. *Frontiers in Molecular Biosciences* 4. doi: 10.3389/fmolb.2017.00017.

Anvarian, Zeinab, Kirk Mykytyn, Saikat Mukhopadhyay, Lotte Bang Pedersen, and Søren Tvorup Christensen. 2019. 'Cellular Signalling by Primary Cilia in Development, Organ Function and Disease'. *Nature Reviews Nephrology* 15(4):199–219. doi: 10.1038/s41581-019-0116-9.

Basten, Sander G., and Rachel H. Giles. 2013. 'Functional Aspects of Primary Cilia in Signaling, Cell Cycle and Tumorigenesis'. *Cilia* 2(1):6. doi: 10.1186/2046-2530-2-6.

Beales, P. L., N. Elcioglu, A. S. Woolf, D. Parker, and F. A. Flinter. 1999. 'New Criteria for Improved Diagnosis of Bardet-Biedl Syndrome: Results of a Population Survey'. *Journal of Medical Genetics* 36(6):437–46.

Bhogaraju, Sagar, Michael Taschner, Michaela Morawetz, Claire Basquin, and Esben Lorentzen. 2011. 'Crystal Structure of the Intraflagellar Transport Complex 25/27'. *The EMBO Journal* 30(10):1907–18. doi: 10.1038/emboj.2011.110.

Borg Distefano, Marita, Linda Hofstad Haugen, Yan Wang, Harmonie Perdreau-Dahl, Ingrid Kjos, Da Jia, Jens Preben Morth, Jacques Neefjes, Oddmund Bakke, and Cinzia Progida. 2018. 'TBC1D5 Controls the GTPase Cycle of Rab7b'. *Journal of Cell Science* jcs.216630. doi: 10.1242/jcs.216630.

Breslow, David K., and Andrew J. Holland. 2019. 'Mechanism and Regulation of Centriole and Cilium Biogenesis'. *Annual Review of Biochemistry* 88(1):691–724. doi: 10.1146/annurev-biochem-013118-111153.

Chou, En-Ju, Liang-Yi Hung, Chieh-Ju C. Tang, Wen-Bin Hsu, Hsin-Yi Wu, Pao-Chi Liao, and Tang K. Tang. 2016. 'Phosphorylation of CPAP by Aurora-A Maintains Spindle Pole Integrity during Mitosis'. *Cell Reports* 14(12):2975–87. doi: 10.1016/j.celrep.2016.02.085.

Dunker, A. Keith, Marc S. Cortese, Pedro Romero, Lilia M. Iakoucheva, and Vladimir N. Uversky. 2005. 'Flexible Nets: The Roles of Intrinsic Disorder in Protein Interaction Networks'. *The FEBS Journal* 272(20):5129–48. doi: 10.1111/j.1742-4658.2005.04948.x.

Eggenschwiler, Jonathan T., and Kathryn V. Anderson. 2007. 'Cilia and Developmental Signaling'. *Annual Review of Cell and Developmental Biology* 23(1):345–73. doi: 10.1146/annurev.cellbio.23.090506.123249.

Elawad, Omer Ali Mohamed Ahmed, Mumen Abdalazim Dafallah, Mohammed Mahgoub Mirghani Ahmed, Ahmed Abdalazim Dafallah Albashir, Sahar Mohammed Abbas Abdalla, Habiballa Hago Mohamed Yousif, Anwar Ali Elamin Daw Elbait, Moawia Elbalal Mohammed, Hassan Ismail Hassan Ali, Mohamed Mutasim Mohamed Ahmed, Najla Fouad Nassir Mohammed, Fadwa Hashim Mohamed Osman, Mussab Alnazeer Yousif Mohammed, and Ejlal Ahmed Ebrahim Abu Shama. 2022. 'Bardet–Biedl Syndrome: A Case Series'. *Journal of Medical Case Reports* 16(1):169. doi: 10.1186/s13256-022-03396-6.

Forsythe, E., K. Sparks, B. E. Hoskins, E. Bagkeris, B. M. McGowan, P. V. Carroll, M. S. B. Huda, S. Mujahid, C. Peters, T. Barrett, S. Mohammed, and P. L. Beales. 2015. 'Genetic Predictors of Cardiovascular Morbidity in Bardet–Biedl Syndrome'. *Clinical Genetics* 87(4):343–49. doi: 10.1111/cge.12373.

Gabriel, Elke, Arpit Wason, Anand Ramani, Li Ming Gooi, Patrick Keller, Andrei Pozniakovsky, Ina Poser, Florian Noack, Narasimha Swamy Telugu, Federico Calegari, Tomo Šarić, Jürgen Hescheler, Anthony A. Hyman, Marco Gottardo, Giuliano Callaini, Fowzan Sami Alkuraya, and Jay Gopalakrishnan. 2016. 'CPAP Promotes Timely Cilium Disassembly to Maintain Neural Progenitor Pool'. *The EMBO Journal* 35(8):803–19. doi: 10.15252/embj.201593679.

Hatzopoulos, Georgios N., Michèle C. Erat, Erin Cutts, Kacper B. Rogala, Leanne M. Slater, Philip J. Stansfeld, and Ioannis Vakonakis. 2013. 'Structural

Analysis of the G-Box Domain of the Microcephaly Protein CPAP Suggests a Role in Centriole Architecture'. *Structure* 21(11):2069–77. doi: 10.1016/j.str.2013.08.019.

Hildebrandt, Friedhelm, and Edgar Otto. 2005. 'Cilia and Centrosomes: A Unifying Pathogenic Concept for Cystic Kidney Disease?' *Nature Reviews Genetics* 6(12):928–40. doi: 10.1038/nrg1727.

Honda, Reiko, Roman Körner, and Erich A. Nigg. 2003. 'Exploring the Functional Interactions between Aurora B, INCENP, and Survivin in Mitosis'. *Molecular Biology of the Cell* 14(8):3325–41. doi: 10.1091/mbc.e02-11-0769.

Huet, Diego, Thierry Blisnick, Sylvie Perrot, and Philippe Bastin. 2014. 'The GTPase IFT27 Is Involved in Both Anterograde and Retrograde Intraflagellar Transport'. *eLife* 3:e02419. doi: 10.7554/eLife.02419.

Hunt, Tim, Kim Nasmyth, and Béla Novák. 2011. 'The Cell Cycle'. *Philosophical Transactions of the Royal Society of London. Series B, Biological Sciences* 366(1584):3494–97. doi: 10.1098/rstb.2011.0274.

Kleylein-Sohn, Julia, Jens Westendorf, Mikael Le Clech, Robert Habedanck, York-Dieter Stierhof, and Erich A. Nigg. 2007. 'Plk4-Induced Centriole Biogenesis in Human Cells'. *Developmental Cell* 13(2):190–202. doi: 10.1016/j.devcel.2007.07.002.

Kvam, M (24 May 2022) *Bardet Beidl Syndrome*
https://nhi.no/sykdommer/sjeldne-tilstander/b/bardet-biedl-syndrom

Lawo, Steffen, Monica Hasegan, Gagan D. Gupta, and Laurence Pelletier. 2012. 'Subdiffraction Imaging of Centrosomes Reveals Higher-Order Organizational Features of Pericentriolar Material'. *Nature Cell Biology* 14(11):1148–58. doi: 10.1038/ncb2591.

Lechtreck, Karl F., Julie C. Van De Weghe, James Aaron Harris, and Peiwei Liu. 2017. 'Protein Transport in Growing and Steady-State Cilia'. *Traffic (Copenhagen, Denmark)* 18(5):277–86. doi: 10.1111/tra.12474.

Liew, Gerald M., Fan Ye, Andrew R. Nager, J. Patrick Murphy, Jaclyn S. Lee, Mike Aguiar, David K. Breslow, Steven P. Gygi, and Maxence V. Nachury. 2014. 'The Intraflagellar Transport Protein IFT27 Promotes BBSome Exit from Cilia through the GTPase ARL6/BBS3'. *Developmental Cell* 31(3):265–78. doi: 10.1016/j.devcel.2014.09.004.

Mallampalli, Rama K., Jennifer R. Glasser, Tiffany A. Coon, and Bill B. Chen. 2013. 'Calmodulin Protects Aurora B on the Midbody to Regulate the Fidelity of Cytokinesis'. *Cell Cycle (Georgetown, Tex.)* 12(4):663–73. doi: 10.4161/cc.23586.

Mo, Fei, Xiaoxuan Zhuang, Xing Liu, Phil Y. Yao, Bo Qin, Zeqi Su, Jianye Zang, Zhiyong Wang, Jiancun Zhang, Zhen Dou, Changlin Tian, Maikun Teng, Liwen Niu, Donald L. Hill, Guowei Fang, Xia Ding, Chuanhai Fu, and Xuebiao Yao. 2016. 'Acetylation of Aurora B by TIP60 Ensures Accurate Chromosomal Segregation'. *Nature Chemical Biology* 12(4):226–32. doi: 10.1038/nchembio.2017.

Nakayama, Kazuhisa, and Yohei Katoh. 2020. 'Architecture of the IFT Ciliary Trafficking Machinery and Interplay between Its Components'. *Critical Reviews in Biochemistry and Molecular Biology* 55(2):179–96. doi: 10.1080/10409238.2020.1768206.

Nicastro, Daniela, Cindi Schwartz, Jason Pierson, Richard Gaudette, Mary E. Porter, and J. Richard McIntosh. 2006. 'The Molecular Architecture of Axonemes Revealed by Cryoelectron Tomography'. *Science (New York, N.Y.)* 313(5789):944–48. doi: 10.1126/science.1128618.

Nigg, Erich A., and Tim Stearns. 2011. 'The Centrosome Cycle: Centriole Biogenesis, Duplication and Inherent Asymmetries'. *Nature Cell Biology* 13(10):1154–60. doi: 10.1038/ncb2345.

Nonaka, Shigenori, Yosuke Tanaka, Yasushi Okada, Sen Takeda, Akihiro Harada, Yoshimitsu Kanai, Mizuho Kido, and Nobutaka Hirokawa. 1998. 'Randomization of Left–Right Asymmetry Due to Loss of Nodal Cilia Generating Leftward Flow of Extraembryonic Fluid in Mice Lacking KIF3B Motor Protein'. *Cell* 95(6):829–37. doi: 10.1016/S0092-8674(00)81705-5.

Pan, Junmin, and William Snell. 2007. 'The Primary Cilium: Keeper of the Key to Cell Division'. *Cell* 129(7):1255–57. doi: 10.1016/j.cell.2007.06.018.

Plotnikova, Olga V., Elena N. Pugacheva, and Erica A. Golemis. 2009. 'Primary Cilia and the Cell Cycle'. Pp. 137–60 in *Methods in Cell Biology*. Vol. 94. Elsevier.

Pomeroy, Jeremy, Kelsi-Marie Offenwanger, and Tammi Timmler. 2023. 'Diabetes Mellitus in Bardet Biedl Syndrome'. *Current Opinion in Endocrinology, Diabetes & Obesity* 30(1):27–31. doi: 10.1097/MED.0000000000000788.

Qin, Hongmin, Zhaohui Wang, Dennis Diener, and Joel Rosenbaum. 2007. 'Intraflagellar Transport Protein 27 Is a Small G Protein Involved in Cell-Cycle Control'. *Current Biology: CB* 17(3):193–202. doi: 10.1016/j.cub.2006.12.040.

Schaefer, Elise, Clarisse Delvallée, Laura Mary, Corinne Stoetzel, Véronique Geoffroy, Caroline Marks-Delesalle, Muriel Holder-Espinasse, Jamal Ghoumid, Hélène Dollfus, and Jean Muller. 2019. 'Identification and Characterization of Known Biallelic Mutations in the IFT27 (BBS19) Gene in a Novel Family With Bardet-Biedl Syndrome'. *Frontiers in Genetics* 10:21. doi: 10.3389/fgene.2019.00021.

Segura-Peña, Dario, Oda Hovet, Hemanga Gogoi, Jennine Dawicki-McKenna, Stine Malene Hansen Wøien, Manuel Carrer, Ben E. Black, Michele Cascella, and Nikolina Sekulic. 2023. 'The Structural Basis of the Multi-Step Allosteric Activation of Aurora B Kinase'. *eLife* 12:e85328. doi: 10.7554/eLife.85328.

Taulet, Nicolas, Benjamin Vitre, Christelle Anguille, Audrey Douanier, Murielle Rocancourt, Michael Taschner, Esben Lorentzen, Arnaud Echard, and Benedicte Delaval. 2017. 'IFT Proteins Spatially Control the Geometry of Cleavage Furrow Ingression and Lumen Positioning'. *Nature Communications* 8(1):1928. doi: 10.1038/s41467-017-01479-3.

Taylor, Stephen, and Jan-Michael Peters. 2008. 'Polo and Aurora Kinases—Lessons Derived from Chemical Biology'. *Current Opinion in Cell Biology* 20(1):77–84. doi: 10.1016/j.ceb.2007.11.008.

Uejima, Tamami, Kentaro Ihara, Tatsuaki Goh, Emi Ito, Mariko Sunada, Takashi Ueda, Akihiko Nakano, and Soichi Wakatsuki. 2010. 'GDP-Bound and Nucleotide-Free Intermediates of the Guanine Nucleotide Exchange in the Rab5·Vps9 System'. *Journal of Biological Chemistry* 285(47):36689–97. doi: 10.1074/jbc.M110.152132.

Wang, Liang, Xin Wen, Zhengmao Wang, Zaisheng Lin, Chunhong Li, Huilin Zhou, Huimin Yu, Yuhan Li, Yifei Cheng, Yuling Chen, Geer Lou, Junmin Pan, and Muqing Cao. 2022. 'Ciliary Transition Zone Proteins Coordinate Ciliary Protein Composition and Ectosome Shedding'. *Nature Communications* 13(1):3997. doi: 10.1038/s41467-022-31751-0.

Wang, Weiping, Tao Wu, and Marc W. Kirschner. 2014. 'The Master Cell Cycle Regulator APC-Cdc20 Regulates Ciliary Length and Disassembly of the Primary Cilium'. *eLife* 3:e03083. doi: 10.7554/eLife.03083.

Wang, Zhaohui, Zhen-Chuan Fan, Shana M. Williamson, and Hongmin Qin. 2009. 'Intraflagellar Transport (IFT) Protein IFT25 Is a Phosphoprotein Component of IFT Complex B and Physically Interacts with IFT27 in Chlamydomonas' edited by D.-Y. Jin. *PLoS ONE* 4(5):e5384. doi: 10.1371/journal.pone.0005384.

Wheatley, S. P., A. Carvalho, P. Vagnarelli, and W. C. Earnshaw. 2001. 'INCENP Is Required for Proper Targeting of Survivin to the Centromeres and the Anaphase Spindle during Mitosis'. *Current Biology: CB* 11(11):886–90. doi: 10.1016/s0960-9822(01)00238-x.

Wingfield, Jenna L., Karl-Ferdinand Lechtreck, and Esben Lorentzen. 2018. 'Trafficking of Ciliary Membrane Proteins by the Intraflagellar Transport/BBSome Machinery'. *Essays in Biochemistry* 62(6):753–63. doi: 10.1042/EBC20180030.

Yasui, Yoshihiro, Takeshi Urano, Aie Kawajiri, Koh-ichi Nagata, Masaaki Tatsuka, Hideyuki Saya, Koichi Furukawa, Toshitada Takahashi, Ichiro Izawa, and Masaki Inagaki. 2004. 'Autophosphorylation of a Newly Identified Site of Aurora-B Is Indispensable for Cytokinesis'. *The Journal of Biological Chemistry* 279(13):12997–3. doi: 10.1074/jbc.M311128200.

Zheng, Xiangdong, Li Ming Gooi, Arpit Wason, Elke Gabriel, Narges Zare Mehrjardi, Qian Yang, Xingrun Zhang, Alain Debec, Marcus L. Basiri, Tomer Avidor-Reiss, Andrei Pozniakovsky, Ina Poser, Tomo Saric, Anthony A. Hyman, Haitao Li, and Jay Gopalakrishnan. 2014. 'Conserved TCP Domain of Sas-4/CPAP Is Essential for Pericentriolar Material Tethering during Centrosome Biogenesis'. *Proceedings of the National Academy of Sciences of the United States of America* 111(3):E354-363. doi: 10.1073/pnas.1317535111.

Zhou, Zhuang, Hantian Qiu, Roiner-Francisco Castro-Araya, Ryota Takei, Kazuhisa Nakayama, and Yohei Katoh. 2022. 'Impaired Cooperation between IFT74/BBS22-IFT81 and IFT25-IFT27/BBS19 Causes Bardet-Biedl Syndrome'. *Human Molecular Genetics* 31(10):1681–93. doi: 10.1093/hmg/ddab354.

7. Appendix

Part 1: Chemicals

Table 7.1.1: Chemicals used in alphabetical order

Chemicals	Supplier
2-Mercaptoethanol	Sigma Aldrich
Agarose	Bio-Rad
Ammonium Molybdate	Sigma Aldrich
Ammonium Phosphate	EMSURE
Ammonium Sulphate	Sigma-Aldrich
Ampicillin	Fisher BioReagents
Asorbic Acid	Sigma Aldrich
BamHI High Fidelity	New England Biolabs
Bismuth Citrate	Sigma Aldrich
Brij 35	Thermo Scientific
Calcium Chloride	Sigma Aldrich
Chloroamphenicol	Sigma Aldrich
Deoxynucleotide triphosphate	Thermo Scientific
DNA loading dye 6X	Thermo Scientific
Dithiothreitol	Thermo Scientific
Etylenediaminetetraacetic acid tetrasodium dihydrate	Sigma Aldrich
Egtazic Acid	Sigma Aldrich
Ethanol	Antibac
GelRed Nucleic Acid Stain 50k x	Biotium
GeneRuler 1 kb Plus DNA	Thermo Scientific
GeneRuler 100 bp Plus DNA	Thermo Scientific
Glutathione	Sigma Aldrich

Glycine	Bio-Rad
Glycerol	Fisher BioReagents
HindIII High Fidelity	New England Biolabs
Hydrochloric acid	Sigma Aldrich
Imidazole	Sigma Aldrich
In-Fusion Snap Assembely Master Mix	Takara Bio
InstantBlue Coomassie Stain	Abcam
Invitrogen AccuPrime Pfx DNA polymerase	Fisher Scientific
Isopropyl β-D-1-thiogalactopyranoside	Fisher Scientific
Kanamycin	Fisher BioReagents
KLD Enzyme Mix 10X	New England Biolabs
KLD Reaction Buffer 2X	New England Biolabs
L-Lactate Dehydrogenase	Sigma Aldrich
Magnesium Chloride	EMSURE
Magnesium Sulphate	Sigma Aldrich
Mini Protean TGX Gels	Bio-Rad
NcoI High Fidelity	Bio-Rad
Nicotineamide adenine dinucleotide	Sigma Aldrich
NotI	New England Biolabs
Phosphoenolpyruvic acid	Sigma Aldrich
PacI High Fidelity	New England Biolabs
Phenylmethylsulfonyl fluoride	Sigma Aldrich
Potassium Chloride	EMSURE
Precision Plus Protein Dual Standards	Bio-Rad
Pyruvate Kinase	Sigma Aldrich
PstI	New England Biolabs
Q5 High Fidelity DNA Polymerase	New England Biolabs
Q5 High Fidelity GC Enhancer	New England Biolabs
Q5 Reaction Buffer	New England Biolabs
Sodium Acetate	Fisher Scientific
Sodium Chloride	Fisher Scientific

Sodium Citrate	Sigma Aldrich
Sodium Dodecyl Sulphate	VWR
T4 DNA Ligase Reaction Buffer (10X)	New England Biolabs
T4 DNA Ligase	New England Biolabs
Tris(hydroxymethyl)aminomethane	Sigma Aldrich
TurboNuclease *Serratia Marcesens*	Sigma Aldrich
Tween 20%	Sigma Aldrich
Tryptone	Oxoid
XhoI	New England Biolabs
Yeast Extract	Thermo Fisher

Part 2: Consumables

Table 7.2.1: Consumables used in alphabetical order

Consumables	**Supplier**
AmiCon Ultra-15 Centrifugal Filter Units 10000 MWCO	Sigma Aldrich
AmiCon Ultra-0.5 Centrifugal Filter Units 10000 MWCO	Sigma Aldrich
Eppendorf Tube 1.5 mL	Sarstedt
Eppendorf Tube 2.0 mL	Sarstedt
Falcon Tube 15 mL	Sarstedt
Falcon Tube 50 mL	Sarstedt
Mini-PROTEAN TGX Precast Gels	BioRad
Multiply Pro 0.2 mL	Sarstedt
Petridish	Sarstedt
Pipette tip gray	Sarstedt
Pipette tip yellow	Sarstedt
Pipette tip blue	Sarstedt
SnakeSkin Dialysis tubing 10000 MWCO	Thermo Scientific

Syringe	Henke-Ject
UV-Cuvettes 0.5 mL	Brand GMBH
UV-Cuvette 1.5 mL	Brand GMBH

Part 3: Kits

Table 7.3.1: Kits used in alphabetical order

Kit	**Supplier**
Gel Extraction Kit (QIAquick Gel Extraction Kit)	Qiagen
QIAprep Spin Miniprep Kit	Qiagen
QIA PCR purification kit	Qiagen

Part 4: Columns and loops

Table 7.4.1: Columns and loops used in alphabetical order

Columns/Loops	**Supplier**
GSTrap 4B 5mL	GE Healthcare
HiLoad 10/300 Superdex 75 pg	GE Healthcare
HiLoad 16/600 Superdex 75 pg	GE Healthcare
HiLoad 16/600 Superdex 200 pg	GE Healthcare
HisTrap HP 5 mL	Cytiva
Sample loop 10 mL	Cytiva
Sample loop 2 mL	Cytiva
Sample loop 0.5 mL	Cytiva

Part 5: Instruments

Table 7.5.1: Instruments used in alphabetical order

Instruments	**Supplier**
3510 pH-meter	Fisher Scientific
Akta Prime Plus	GE Healthcare
Akta Pure	GE Healthcare
Akta Purifier	GE Healthcare
Avanti J-26 XP Centrifuge	Beckman Coulter
Branson 550 Sonifier	Branson
Capsulefuge TOMY PMC-060	VWR
Cary 60 UV-Vis Spectrophotometer	Agilent Technology
ChemiDoc MP Imaging System	Bio-Rad
Corning LSE Digital Dry Bath	Corning
AccuSpin Micro 17	Fisher Scientific
Infors HT Multitron Triple Incubator	VWR
JA-25.50 Rotor	Beckman Coulter
JLA-8.1 Rotor	Beckman Coulter
KelvitronT Incubator	Thermo Scientific
Millipore Direct Q5	Millipore
Mini Orbital Shaker SSM1	VWR
PowerPac Basic Power Supply	Bio-Rad
Sartorius Quintix	Brand GMBH
Sorvall Legend X1R Centrifuge	Thermo Scientific
Thermorister	VWR
Uno96 Thermal Cycler	VWR
Precision GP 05 Bead bath	Thermo Scientific

Part 6: Software

Table 7.6.1: Software used in alphabetical order

Softwares	**Supplies**
Chimera	RBVI
InkScape	Inkscape
Excel	Microsoft
PowerPoint	Microsoft
ProtParam	ExPasy
PyMol	PyMol
SnapGene	Domatics

Part 7: Cells and Plasmids

Table 7.7.1: Cells and Plasmids used in alphabetical order

Cells/Plasmids	**Supplier** **All cells and plasmids are made in house**
E. coli BL21 (DE3) PLyS cells	
E. coli Rosetta (DE3) cells	
pET16b	
pGEX-6P plasmid	
pMAL-c6T plasmid	
XL 10 Ultra Competent cells	

Part 8: Solutions and Buffers used in Expression

Table 7.8.1: Ampicillin 50 mg/mL 25 mL

Chemical	**Volume/Amount**
MilliQ water	25 mL

Ampicillin	1.05 g

Table 7.8.2: Kanamycin 50 mg/mL 25 mL

Chemical	**Volume/Amount**
MilliQ water	25 mL
Kanamycin	1.315 g

Table 7.8.3: Chloroamphenicol 34 mg/mL 25 mL

Chemical	**Volume/Amount**
MilliQ water	25 mL
Chloroamphenicol	0.85 mg

Table 7.8.4 Isopropyl β-D-1thiogalactopyranoside 1 Molar 20 mL

Chemical	**Volume/Amount**
MilliQ water	20 mL
Isopropyl β-D-1thiogalactopyranoside	4.766 g

Table 7.8.5: 2 x YT media 5 L

Chemical	**Volume/Amount**
Yeast Extract	50 g
Sodium Chloride	25 g
Tryptone	80 g
MilliQ water	5 L

Table 7.8.6: Lysis buffer A for His-TEV-IFT27 alone, His-FaX-IFT27, His-MBP-TEV-IFT27, IFT27-TEV-His-MBP, His-MBP-TEV-IFT27 extra linker, MBP-CENP-J$^{412-897}$ 1 L

Chemical	**Final Concentration**
MilliQ Water	
Tris HCl pH 8 1 M	50 mM

Sodium Chloride 5 M	500 mM
Magnesium Chloride	8 mM
BME 14.3 M	5 mM
Glyserol	5%

Table 7.8.7: Lysis buffer B for GST-3C-IFT25 and His-TEV-IFT27 1 L

Chemical	**Final Concentration**
MilliQ Water	
Tris HCl pH 8 1 M	50 mM
Sodium Chloride 5 M	150 mM
Calcium Chloride	1 mM
Magnesium Chloride	5 mM

Table 7.8.8 Lysis C buffer for His-GB1-AuB and INBox 1 L

Chemical	**Final Concentration**
MilliQ Water	
Tris HCl pH 7.5 1 M	25 mM
Sodium Chloride 5 M	300 mM
Phenylmethylsulfonyl Fluoride	1 mM
Imidazole 1 M	50 mM

Part 9: Solution and Buffers used in Purification

Table 7.9.1: Wash buffer A for HIS purification His-TEV-IFT27 alone, His-FaX-IFT27, His-MBP-TEV-IFT27, IFT27-TEV-His-MBP, His-MBP-TEV-IFT27 extra linker, MBP-CENP-J$^{412-897}$ 1 L

Chemical	**Final Concentration**
MilliQ Water	
Tris HCl pH 8 1 M	50 mM

Sodium Chloride 5 M	500 mM
Glyserol	5%
BME	5 mM
Imidazole 1 M	0, 25 or 50 mM

Table 7.9.2 Wash buffer B for HIS and GST purification GST-3C-IFT25 and His-TEV-IFT27 1 L

Chemical	**Final Concentration**
MilliQ Water	
Tris HCl pH 7.5 1 M	50 mM
Sodium Chloride 5 M	300 mM
Imidazole 1 M	0, 25 or 50 mM (0 for GST purification)

Table 7.9.3 Wash buffer C for HIS purification His-GB1-AuB and INBox 1 L

Chemical	**Final Concentration**
MilliQ Water	
Tris HCl pH 7.5 1 M	25 mM
Sodium Chloride 5 M	300 mM
Imidazole 1 M	0, 25 or 50 mM

Table 7.9.4: Elution buffer A for HIS purification His-TEV-IFT27 alone, His-FaX-IFT27, His-MBP-TEV-IFT27, IFT27-TEV-His-MBP, His-MBP-TEV-IFT27 extra linker, MBP-CENP-J$^{412-897}$ 1 L

Chemical	**Final Concentration**
MilliQ Water	
Tris HCl pH 8 1 M	50 mM
Sodium Chloride 5 M	500 mM
Glyserol	5%
BME	5 mM
Imidazole 1 M	500 mM

Table 7.9.5: Elution buffer B for HIS purification GST-3C-IFT25 and His-TEV-IFT27 1 L

Chemical	Final Concentration
MilliQ Water	
Tris HCl pH 7.5 1 M	50 mM
Sodium Chloride 5 M	150 mM
Imidazole 1 M	300 mM

Table 7.9.6 Elution buffer C for HIS purification His-GB1-AuB and INBox 1 L

Chemical	Final Concentration
MilliQ Water	
Tris HCl pH 7.5 1 M	25 mM
Sodium Chloride 5 M	150 mM
Imidazole 1 M	500 mM

Table 7.9.7 Elution buffer D for GST purification GST-3C-IFT25 and His-TEV-IFT27 1 L

Chemical	Final Concentration
MilliQ Water	
Tris HCl pH 7.5 1 M	50 mM
Sodium Chloride 5 M	150 mM
Glutathione	10 mM

Table 7.9.8 SEC buffer A for SEC purification His-TEV-IFT27 alone, His-FaX-IFT27, His-MBP-TEV-IFT27, IFT27-TEV-His-MBP, His-MBP-TEV-IFT27 extra linker, MBP-CENP-J$^{412\text{-}897}$ 1 L

Chemical	Final Concentration
MilliQ Water	
Tris HCl pH 8 1 M	50 mM
Sodium Chloride 5 M	300 mM

Glyserol	5%
BME	5 mM

Table 7.9.9: SEC buffer B for SEC purification GST-3C-IFT25 and His-TEV-IFT27 1 L

Chemical	**Final Concentration**
MilliQ Water	
Tris HCl pH 7.5 1 M	10 mM
Sodium Chloride 5 M	150 mM
Dithiothreitol 1 M	1 mM

Table 7.9.10: SEC buffer C for SEC purification His-GB1-AuB and INBox 1 L

Chemical	**Final Concentration**
MilliQ Water	
Tris HCl pH 7.5 1 M	25 mM
Sodium Chloride 5 M	150 mM
Dithiothreitol 1 M	2 mM

Part 10: Solutions and Buffers used in GTPase test

Table 7.10.1: Solution I

Chemicals	**Amount/Volume**
Ammonium Molybdate	10% v/w
MilliQ Water	10 mL

Table 7.10.2: Solution II

Chemicals	**Stock**	**Working Concentration**	**Amount/Volume**
Solution I		0.162 M	166 µL
Asorbic Acid		0.162 M	100 mg

SDS	20%	2.86%	500 µL
Hydrogen Chloride	1 M	0.47 M	1.66 mL
MilliQ Water			1.16 mL

The final volume is 3.5 mL

Solution II is made by dissolving 0.1 g of Asorbic Acid in 1.16 mL of MilliQ water, then adding 1.66 mL of HCl and cooling to 0 ^{o}C. 0.166 mL of Solution I was added, then 0.5 mL of SDS under rapid stirring. The tube was wrapped in aluminium foil as the buffer is light sensitive.

Table 7.10.3: Solution III

Chemicals	**Stock**	**Working Concentration**	**Amount/Volume**
Bismuth Citrate		88 mM	175 mg
Sodium Citrate		135 mM	175 mg
Hydrogen Chloride	1 M	1 M	5 mL

Part 11: Solutions and Buffers used in Aurora B Kinase Activity

Table 7.11.1: Kmg-100 solution for Aurora B Kinase Activity Test

Chemicals	**Final Concentration**
Potassium Chloride	100 mM
Magnesium Chloride	2 mM
Egtazic acid	1 mM
Dithiothreitol	2 mM
Tris HCl pH 7.4	25 mM
Brij 35	0.01%
MilliQ Water	<50 mL>

Table 7.11.2: 5 x Cocktail Solution for Aurora B Kinase Activity Test

Chemicals	Stock	Working Concentration	Amount Added
Kmg-100			526 µL
Phosphoenolpyruvic acid	40 mM	2.5 mM	41 µL
Pyruvate Kinase	2000 u/mL	100 u/mL	33 µL
L-Lactase Dehydrogenase	2750 u/mL	100 u/mL	24 µL
Nicotineamide adenine dinucleotide	50 mM	0.8 mM	10.4 µL

Final volume is 650 µL

Table 7.11.3: Kinase Assay Buffer Solution for Aurora B Kinase Activity Test

Chemicals	Stock	Working Concentration	Amount Added
Kmg100			828.6 µL
5 x Cocktail			216 µL
Adenosine Triphosphate	70 mM	1 mM	15.4 µL
Peptide	8.6 mM	200 µM	25 µL

Final volume is 1080 µL

Part 12: Supplementary Buffers and Solution

Table 7.12.1: 10X SDS Running Buffer used for SDS-PAGE gels

Chemicals	Amount/Volume
20% SDS stock solution	100 mL
Tris(hydroxymethyl)aminomethane	60.57 g
Glycine	288.27 g
MilliQ Water	<2L>

Table 7.12.2: 4X SDS Loading Buffer used for SDS-PAGE gels

Chemicals	Amount/Volume
20% SDS Stock	1 mL
BME 14.3 M	0.4 mL
Bromphenol Blue	A dash
Glycerol	4 mL
EDTA 0.5 M	1 mL
Tris HCl pH 6.8	4 mL
MilliQ water	<10 mL>

Table 7.12.3: Dithiothreitol 1 M

Chemicals	Amont/Volume
Dithiothreitol	3.09 g
Sodium Acetate pH 5.2 0.01 M	20 mL

Table 7.12.4: TAE Buffer 50 x 1L

Chemicals	Amount/Volume
EDTA	7.43 g
Acetic Acid	57.1 mL
Tris(hydroxymethyl)aminomethane	242 g
MilliQ Water	<1L>

The agarose gel itself was made using 100 mL of 1 x TAE buffer, mixed with 1 g of agarose, heated in the microwave until the all the agarose was dissolved. The solution was then cooled until it reached a temperature where it could be held with hurting. 1 x GelRed was added, mixed carefully and poured into a mold where it solidified.

Part 13: Solutions and Buffers used in Cloning

Table 7.13.1: PCR reaction using Q5 polymerase

Chemicals	**Concentration**
Fwd Primer	500 nM
Rev Primer	500 nM
Template	20 ng
dNTP	200 µM
Q5 Reaction Buffer	1 x
Q5 Enhancer	1 x
Q5 High Fidelity DNA Polymerase	1 x
MilliQ Water	<50µ>

Table 7.13.2: Infusion reaction using In-Fusion

Chemicals	**Concentration**	**Amount/Volume**
In-Fusion Mix 5x	1 x	1 µL
Fragment Insert		3 x molar compared to plasmid
Linearized Plasmid	30 ng	
MilliQ Water	<5µL>	

Incubated for 15 minutes at 50°C

Table 7.13.3: Linearization of plasmids

Chemicals	**Concentration**	**Amount/Volume**
Plasmid	2 µg	
Restriction enzyme 1	5 units	1.5 µL
Restriction enzyme 2	5 unites	1.5 µL
NEB buffer 3.1 (10X)	1 x	10 µL
MilliQ Water	<50µL>	

Incubated for 3 hours at 37°C

Table 7.13.4: KLD reaction

Chemicals	Concentration	Amount/Volume
PCR Product		1 µL
KLD Reaction Buffer 2 x	1 x	5 µL
KLD Enzyme mix 10 x	1 x	1 µL
MilliQ Water		3 µL

Incubated for 5 minutes at room temperature

Chemicals	Concentration	Amount/Volume
T4 DNA Ligase (10x)	1 x	2 µL
T4 DNA Ligase Buffer (10x)	1 x	2 µL
Insert	3 x Molar	
Plasmid	1 x Molar	
MilliQ Water		< 20 µL>

The reaction proceeded for 10 minutes at room temperature, before deactivation of the ligase at 65 ^{o}C for 15 minutes.

Part 14: Primers

Table 7.14.1: Primers used to make His-MBP-TEV-IFT27 plasmid

Primer	Sequence
Fwd AA392	CTGTACTTCCAGGGATCCATGGTGAAGCTGGCA
Rev AA391	TGCCAAGCTTGCCTGCAGTTATGCCAGGGCCCG

Table 7.14.2: Primers used to make IFT27-TEV-His-MBP plasmid

Primer	Sequence
Fwd AA395	AGGAGATATACCATGGGCGTGAAGCTGGCAGCC

Rev AA396	TCCCTGGAAGTACAGGTTTTCCCCTGCCAGGGCCCG

Table 7.14.3: Primers used to make His-MBP-TEV-IFT27 extra linker plasmid

Primer	**Sequence**
Fwd AA397	TCCGGAGGAGGAGGTACCATGGTGAAGCTGGCA
Rev AA398	TCCTCCTCCGGAGGATCCGGATCCCTGGAAGTACAG

Table 7.14.4: Primers used to extract IFT25 from non-expressive vector for insertion into *pGEX* vector

Primer	**Sequence**
Fwd AA416	CAGGGGCCCCTGGGATCCATGAGAAAAATTGATCTCTGTCTG
Rev AA415	GCCGCTCGAGTTAATTAATTATGAGGAAAGATTTGAGACTAC

Table 7.14.5: Primers used make His-TEV-IFT27 fragment for insertion into *pGEX* vector

Primer	**Sequence**
Fwd AA417	AGTCGTATTATTAATTAATTATGAGGAAAGATTTGAGACTAC
Rev AA418	CAGTCACGATGCGGCCGCCAAAAACCCCTCAAGAC

Table 7.14.6: Primers used make MBP-CENP-J$^{412\text{-}897}$ fragment for insertion into *pMAL* vector

Primer	**Sequence**

Fwd AA284	CTGTACTTCCAGGGATCCCTGTTTAAAATGGATAGACAGCAACTC
Rev AA390	TGCCAAGCTTGCCTGCAGTCATAGCTTCCTCATCTCCTCCTT

Part 15: Protein Constructs

Table 7.15.1: Protein parameters calculated by ProtParam

Parameter	**His-TEV-IFT27**	**His-FaX-IFT27**	**His-MBP-TEV-IFT27**	**IFT27-TEV-HIS-MBP**	**His-MBP-TEV-IFT27 extra linker**	**GST-3C-IFT25 and His-TEV-IFT27**	**MBP-CENP-J$^{412-897}$**	**Aurora B$^{60-360}$ and INCENP$^{790-858}$**
MW Da	23438	23001	64600	63509	65418	66542	107720	44341
Theoretical pI	6.09	6.29	5.36	5.42	5.36	5.62	5.88	9.45
Abs 0.1%	0.958	0.912	1.375	1.398	1.358	1.192	0.876	1.124

Table 7.15.2: Protein parameters calculated by ProtParam

Protein	**Sequence**
His-TEV-IFT27	MSPILGYWKIKGLVQPTRLLLEYLEEKYEEHLYERDEG DKWRNKKFELGLEFPNLPYYIDGDVKLTQSMAIIRYI ADKHNMLGGCPKERAEISMLEGAVLDIRYGVSRIAY SKDFETLKVDFLSKLPEMLKMFEDRLCHKTYLNGDH VTHPDFMLYDALDVVLYMDPMCLDAFPKLVCFKKRI EAIPQIDKYLKSSKYIAWPLQGWQATFGGGDHPPKS DLEVLFQGPLGSMRKIDLCLSSEGSEVILATSSDEKHP

	PENIIDGNPETFWTTTGMFPQEFIICFHKHVRIERLVI QSYFVQTLKIEKSTSKEPVDFEQWIEKDLVHTEGQLQ NEEIVAHDGSATYLRFIIVSAFDHFASVHSVSAEGTVV SNLSS
His-FaX-IFT27	MGHHHHHHHHHHSSGHIEGRHMVKLAAKCILAGD PAVGKTALAQIFRSDGAHFQKSYTLTTGMDLVVKTV PVPDTGDSVELFIFDSAGKELFSEMLDKLWESPNVLC LVYDVTNEESFNNCSKWLEKARSQAPGISLPGVLVG NKTDLAGRRAVDSAEARAWALGQGLECFETSVKEM ENFEAPFHCLAKQFHQLYREKVEVFRALA
His-MBP-TEV-IFT27	MGSSHHHHHHSGSGKIEEGKLVIWINGDKGYNGLA EVGKKFEKDTGIKVTVEHPDKLEEKFPQVAATGDGP DIIFWAHDRFGGYAQSGLLAEITPDKAFQDKLYPFT WDAVRYNGKLIAYPIAVEALSLIYNKDLLPNPPKTWE EIPALDKELKAKGKSALMFNLQEPYFTWPLIAADGGY AFKYENGKYDIKDVGVDNAGAKAGLTFLVDLIKNKH MNADTDYSIAEAAFNKGETAMTINGPWAWSNIDTS KVNYGVTVLPTFKGQPSKPFVGVLSAGINAASPNKE LAKEFLENYLLTDEGLEAVNKDKPLGAVALKSYEEELA KDPRIAATMENAQKGEIMPNIPQMSAFWYAVRTAV INAASGRQTVDEALKDAQTNSSSNNNNNNNNNNE NLYFQGSMVKLAAKCILAGDPAVGKTALAQIFRSDG AHFQKSYTLTTGMDLVVKTVPVPDTGDSVELFIFDSA GKELFSEMLDKLWESPNVLCLVYDVTNEESFNNCSK WLEKARSQAPGISLPGVLVGNKTDLAGRRAVDSAEA RAWALGQGLECFETSVKEMENFEAPFHCLAKQFHQ LYREKVEVFRALA

IFT27-TEV-HIS-MBP	MGVKLAAKCILAGDPAVGKTALAQIFRSDGAHFQKS YTLTTGMDLVVKTVPVPDTGDSVELFIFDSAGKELFS EMLDKLWESPNVLCLVYDVTNEESFNNCSKWLEKA RSQAPGISLPGVLVGNKTDLAGRRAVDSAEARAWAL GQGLECFETSVKEMENFEAPFHCLAKQFHQLYREKV EVFRALAGENLYFQGKLGSSHHHHHHSGSGKIEEGK LVIWINGDKGYNGLAEVGKKFEKDTGIKVTVEHPDK LEEKFPQVAATGDGPDIIFWAHDRFGGYAQSGLLAEI TPDKAFQDKLYPFTWDAVRYNGKLIAYPIAVEALSLIY NKDLLPNPPKTWEEIPALDKELKAKGKSALMFNLQE PYFTWPLIAADGGYAFKYENGKYDIKDVGVDNAGA KAGLTFLVDLIKNKHMNADTDYSIAEAAFNKGETAM TINGPWAWSNIDTSKVNYGVTVLPTFKGQPSKPFVG VLSAGINAASPNKELAKEFLENYLLTDEGLEAVNKDK PLGAVALKSYEEELAKDPRIAATMENAQKGEIMPNIP QMSAFWYAVRTAVINAASGRQTVDEALKDAQTNSS
His-MBP-TEV-IFT27 extra linker	MGSSHHHHHHSGSGKIEEGKLVIWINGDKGYNGLA EVGKKFEKDTGIKVTVEHPDKLEEKFPQVAATGDGP DIIFWAHDRFGGYAQSGLLAEITPDKAFQDKLYPFT WDAVRYNGKLIAYPIAVEALSLIYNKDLLPNPPKTWE EIPALDKELKAKGKSALMFNLQEPYFTWPLIAADGGY AFKYENGKYDIKDVGVDNAGAKAGLTFLVDLIKNKH MNADTDYSIAEAAFNKGETAMTINGPWAWSNIDTS KVNYGVTVLPTFKGQPSKPFVGVLSAGINAASPNKE LAKEFLENYLLTDEGLEAVNKDKPLGAVALKSYEEELA KDPRIAATMENAQKGEIMPNIPQMSAFWYAVRTAV INAASGRQTVDEALKDAQTNSSSNNNNNNNNNNE

	NLYFQGSGSSGGGSGGGGTMVKLAAKCILAGDPAV GKTALAQIFRSDGAHFQKSYTLTTGMDLVVKTVPVP DTGDSVELFIFDSAGKELFSEMLDKLWESPNVLCLVY DVTNEESFNNCSKWLEKARSQAPGISLPGVLVGNKT DLAGRRAVDSAEARAWALGQGLECFETSVKEMENF EAPFHCLAKQFHQLYREKVEVFRALA
GST-3C-IFT25 and His-TEV-IFT27	MSPILGYWKIKGLVQPTRLLLEYLEEKYEEHLYERDEG DKWRNKKFELGLEFPNLPYYIDGDVKLTQSMAIIRYI ADKHNMLGGCPKERAEISMLEGAVLDIRYGVSRIAY SKDFETLKVDFLSKLPEMLKMFEDRLCHKTYLNGDH VTHPDFMLYDALDVVLYMDPMCLDAFPKLVCFKKRI EAIPQIDKYLKSSKYIAWPLQGWQATFGGGDHPPKS DLEVLFQGPLGSMRKIDLCLSSEGSEVILATSSDEKHP PENIIDGNPETFWTTTGMFPQEFIICFHKHVRIERLVI QSYFVQTLKIEKSTSKEPVDFEQWIEKDLVHTEGQLQ NEEIVAHDGSATYLRFIIVSAFDHFASVHSVSAEGTVV SNLSS MGHHHHHHHHHHSSGGGGGENLYFQGSMVKLA AKCILAGDPAVGKTALAQIFRSDGAHFQKSYTLTTGM DLVVKTVPVPDTGDSVELFIFDSAGKELFSEMLDKLW ESPNVLCLVYDVTNEESFNNCSKWLEKARSQAPGISL PGVLVGNKTDLAGRRAVDSAEARAWALGQGLECFE TSVKEMENFEAPFHCLAKQFHQLYREKVEVFRALA
His-MBP-CENP-J$^{412-897}$	MGSSHHHHHHSGSGKIEEGKLVIWINGDKGYNGLA EVGKKFEKDTGIKVTVEHPDKLEEKFPQVAATGDGP DIIFWAHDRFGGYAQSGLLAEITPDKAFQDKLYPFT

	WDAVRYNGKLIAYPIAVEALSLIYNKDLLPNPPKTWE EIPALDKELKAKGKSALMFNLQEPYFTWPLIAADGGY AFKYENGKYDIKDVGVDNAGAKAGLTFLVDLIKNKH MNADTDYSIAEAAFNKGETAMTINGPWAWSNIDTS KVNYGVTVLPTFKGQPSKPFVGVLSAGINAASPNKE LAKEFLENYLLTDEGLEAVNKDKPLGAVALKSYEEELA KDPRIAATMENAQKGEIMPNIPQMSAFWYAVRTAV INAASGRQTVDEALKDAQTNSSSNNNNNNNNNNE NLYFQGSLFKMDRQQLQRKTALKNKELCADNPILKK DSKARTKSGSVTLSQKPKMLKCSNRKSLSPSGLKIQT GKKCDGQFRDQIKFENKVTSNNKENVTECPKPCDT GCTGWNKTQGKDRLPLSTGPASRLAAKSPIRETMKE SESSLDVSLQKKLETWEREKEKENLELDEFLFLEQAA DEISFSSNSSFVLKILERDQQICKGHRMSSTPVKAVP QKTNPADPISHCNRSEDLDHTAREKESECEVAPKQL HSLSSADELREQPCKIRKAVQKSTSENQTEWNARDD EGVPNSDSSTDSEEQLDVTIKPSTEDRERGISSREDSP QVCDDKGPFKDTRTQEDKRRDVDLDLSDKDYSSDES IMESIKHKVSEPSRSSSLSLSKMDFDDERTWTDLEEN LCNHDVVLGNESTYGTPQTCYPNNEIGILDKTIKRKIA PVKRGEDLSKSRRSRSPPTSELMMKFFPSLKPKPKSD SHLGNELKLNISQDQPPGDNARSQVLREKIIELETEIE KFKAENASLAKLRIERESALEKLRKEIADFEQQKAKEL ARIEEFKKEEMRKL
His-GB1-Aurora B kinase$^{60\text{-}360}$ and INCENP$^{790\text{-}858}$	MHHHHHHQYKLALNGKTLKGETTTEAVDAATAEKV FKQYANDNGVDGEWTYDDATKTFTVTEENLYFQGS

	SSSVPGRVAVSTEMPSQNTALAEMPKRKFTIDDFDI GRPLGKGKFGNVYLAREKQNKFIMALKVLFKSQLEK EGVEHQLRREIEIQSHLRHPNILRMYNYFHDRKRIYL MLEFAPRGELYKELQKHGRFDEQRSATFMEELADAL HYCHERKVIHRDIKPENLLMGYKGELKIADFGWSVH APSLRRRTMCGTLDYLPPEMIEGKTHDEKVDLWCA GVLCYEFLVGMPPFDSPSHTETHRRIVNVDLKFPPFL SDGSKDLISKLLRYHPPQRLPLKGVMEHPWVKANSR RVLPPVYQSTQSK MDESQPRKPIPAWASGNLLTQAIRQQYYKPIDVDR MYGTIDSPKLEELFNKSKPRYFKRTSSAVWHSPPLHH HHHH

Part 16: Aurora B kinase activity tests

The following figures contain the chromatograms measured in first Aurora B kinase activity tests:

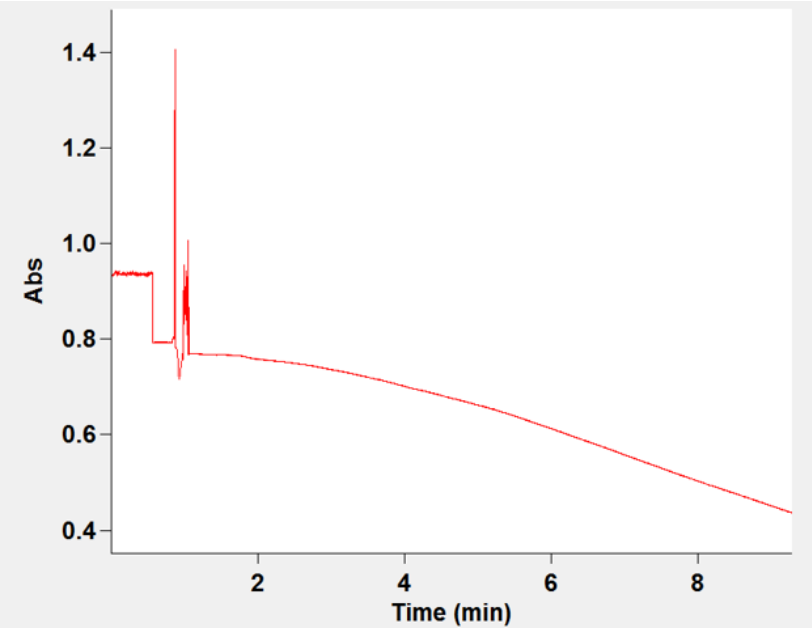

Figure 7.16.1: Shows the chromatogram obtained when measuring Aurora B alone replicate 1. Measured between 4-6 minutes.

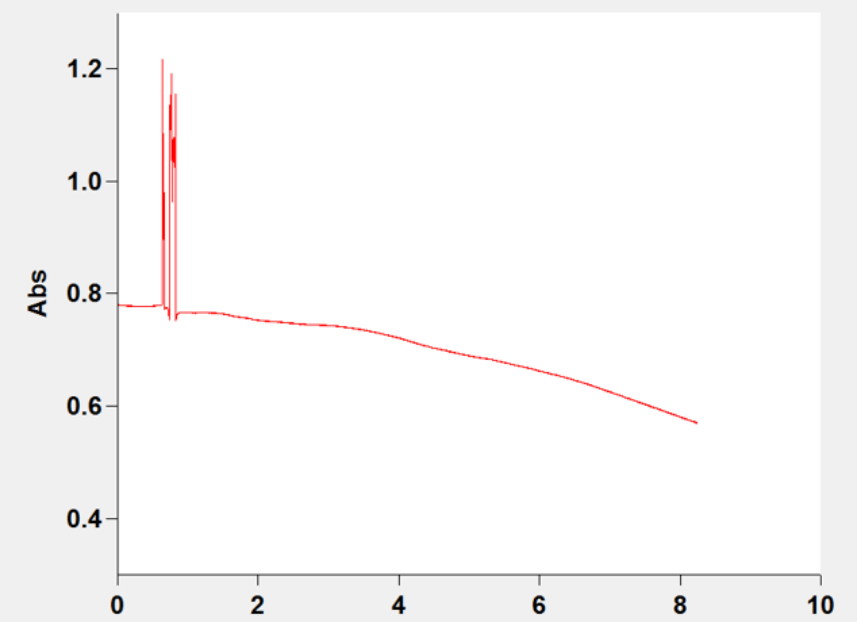

Figure 7.16.2: Shows the chromatogram obtained when measuring Aurora B alone replicate 2. Measured between 4.5-6.5 minutes.

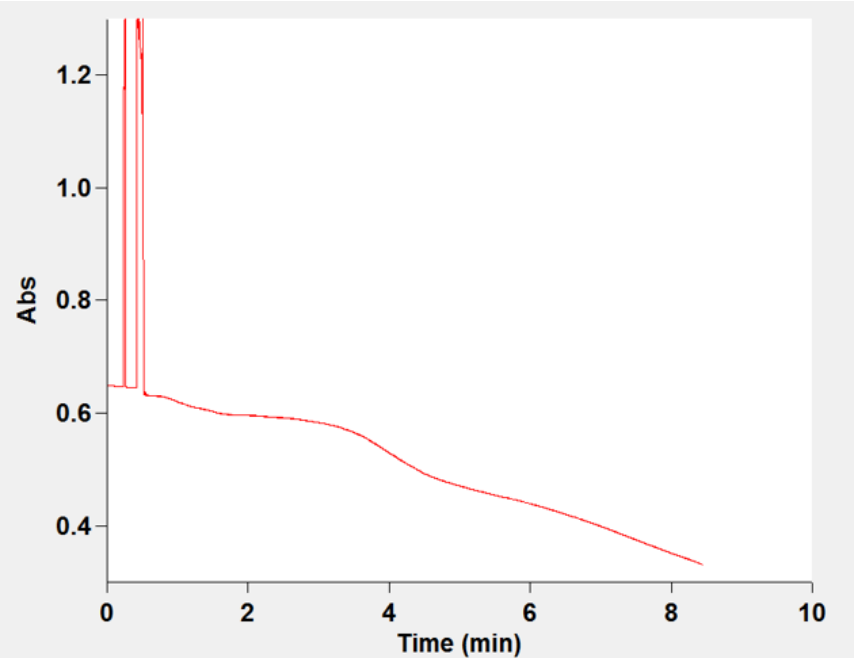

Figure 7.16.3: Shows the chromatogram obtained when measuring Aurora B alone replicate 3. Measured between 4-6 minutes.

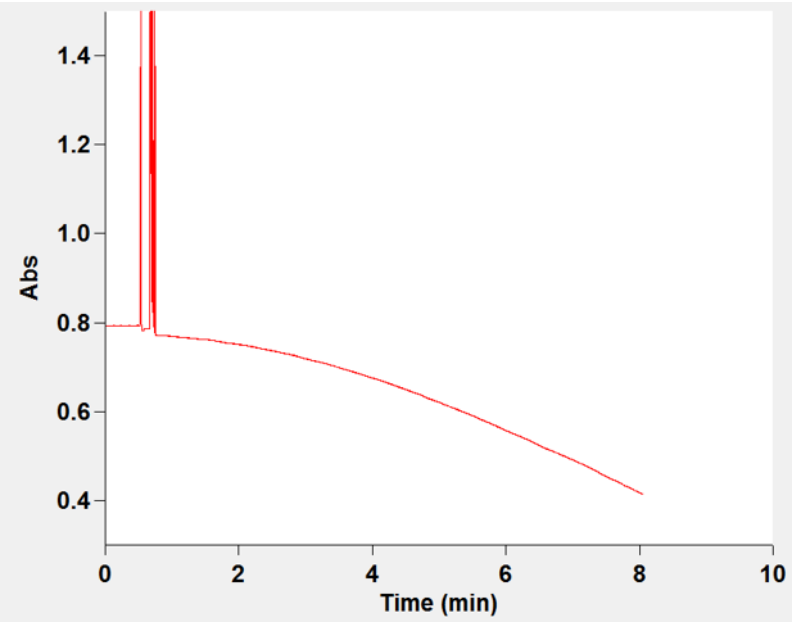

Figure 7.16.4: Shows the chromatogram obtained when measuring IFT25/27^{WT} 1:1 replicate 1. Measured between 5-7 minutes.

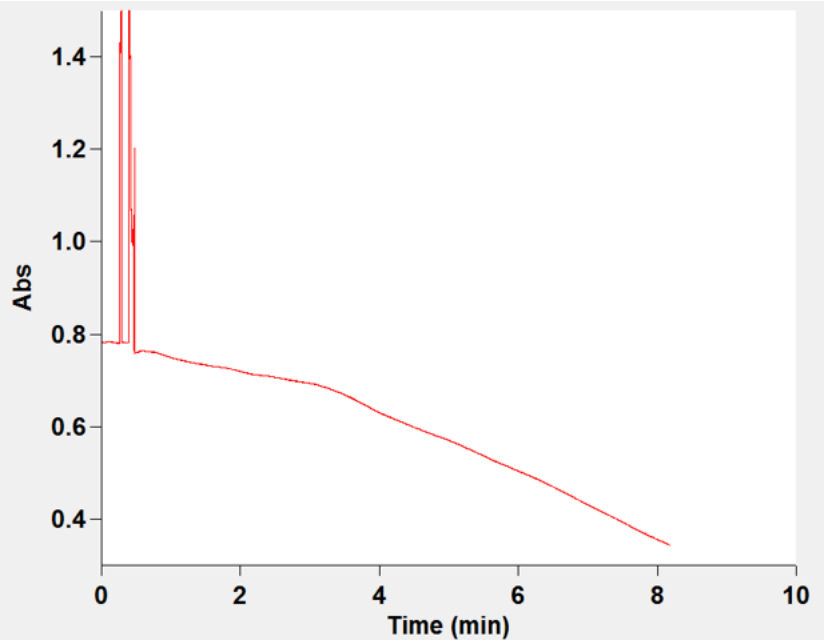

Figure 7.16.5: Shows the chromatogram obtained when measuring IFT25/27^{WT} 1:1 replicate 2. Measured between 4-6 minutes.

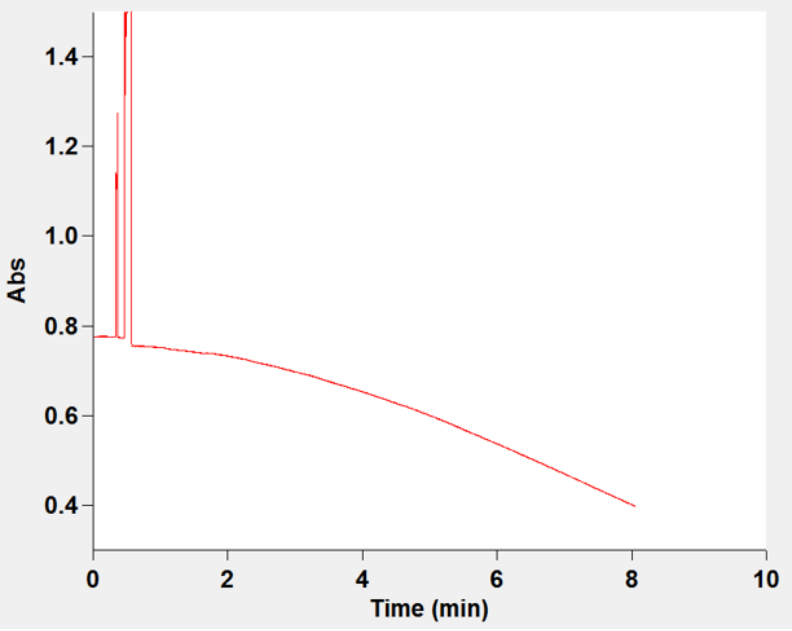

Figure 7.16.6: Shows the chromatogram obtained when measuring IFT25/27^{WT} 1:1 replicate 3. Measured between 5-7 minutes.

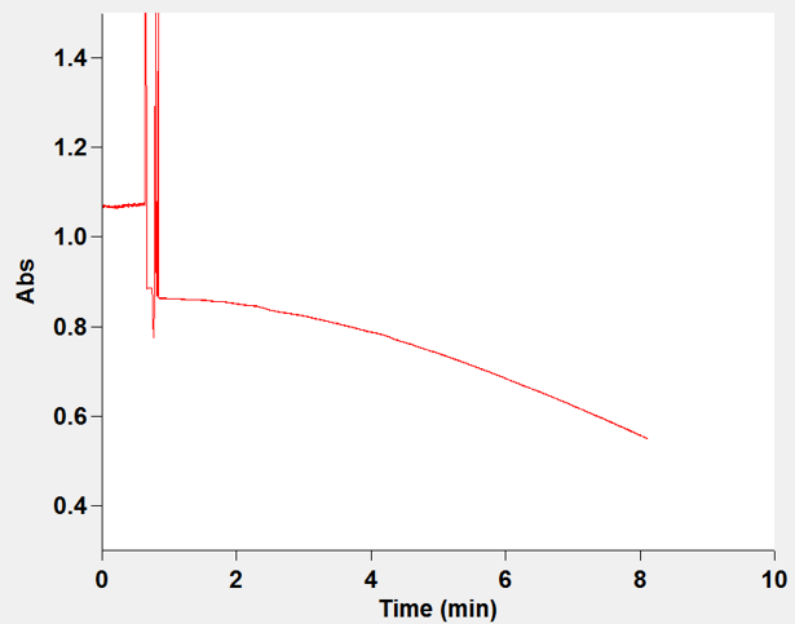

Figure 7.16.7: Shows the chromatogram obtained when measuring IFT25/27^{Y35C} 1:1 replicate 1. Measured between 4-6 minutes.

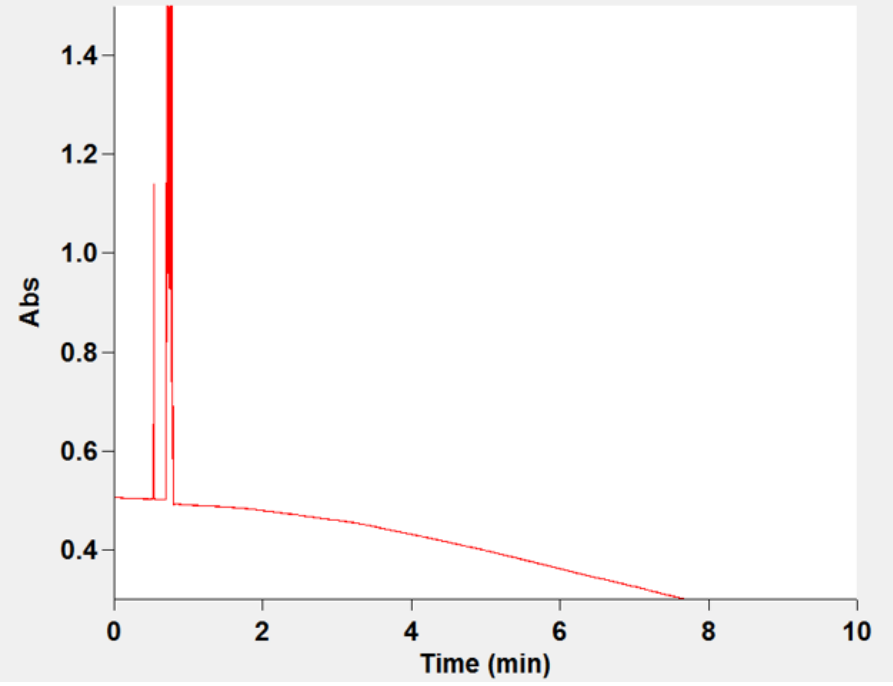

Figure 7.16.8: Shows the chromatogram obtained when measuring IFT25/27^{Y35C} 1:1 replicate 2. Measured between 5-7 minutes.

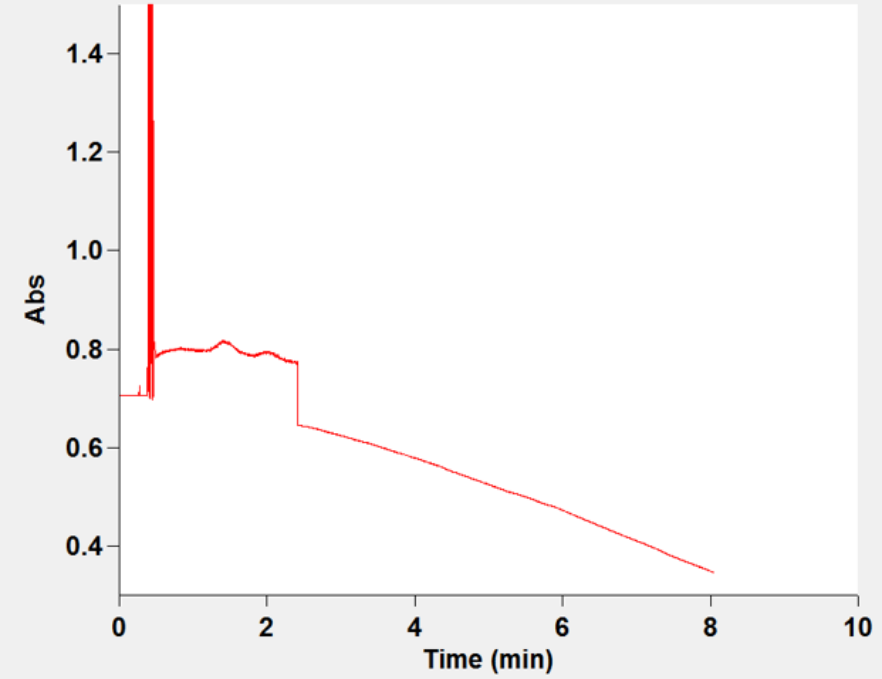

Figure 7.16.9: Shows the chromatogram obtained when measuring IFT25/27^{Y35C} 1:1 replicate 3. Measured between 4-6 minutes.

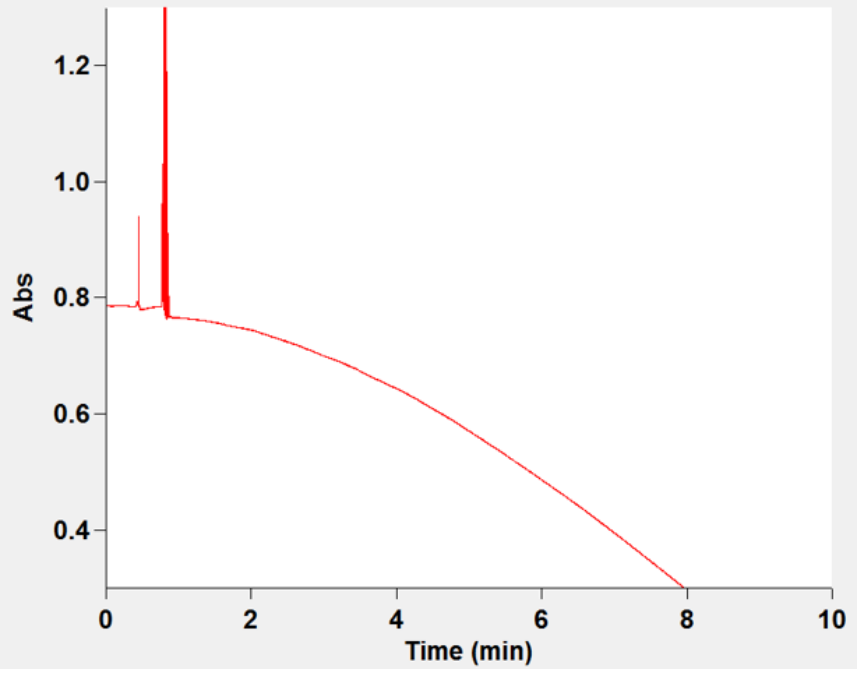

Figure 7.16.10: Shows the chromatogram obtained when measuring IFT25/27^{WT} 1:4 replicate 1. Measured between 4.5-6.5 minutes

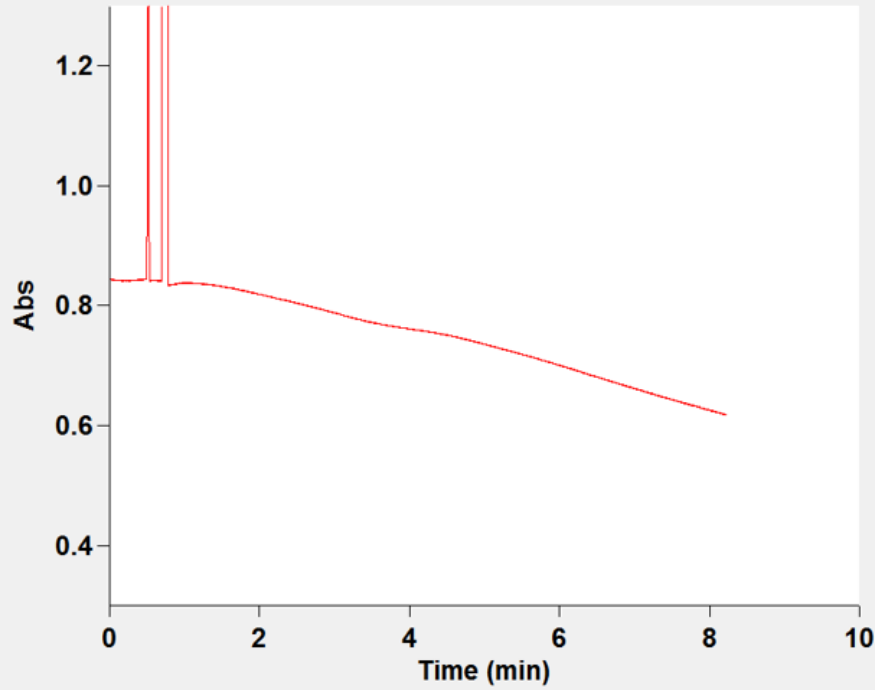

Figure 7.16.11: Shows the chromatogram obtained when measuring IFT25/27^{WT} 1:4 replicate 2. Measured between 4.5-6.5 minutes

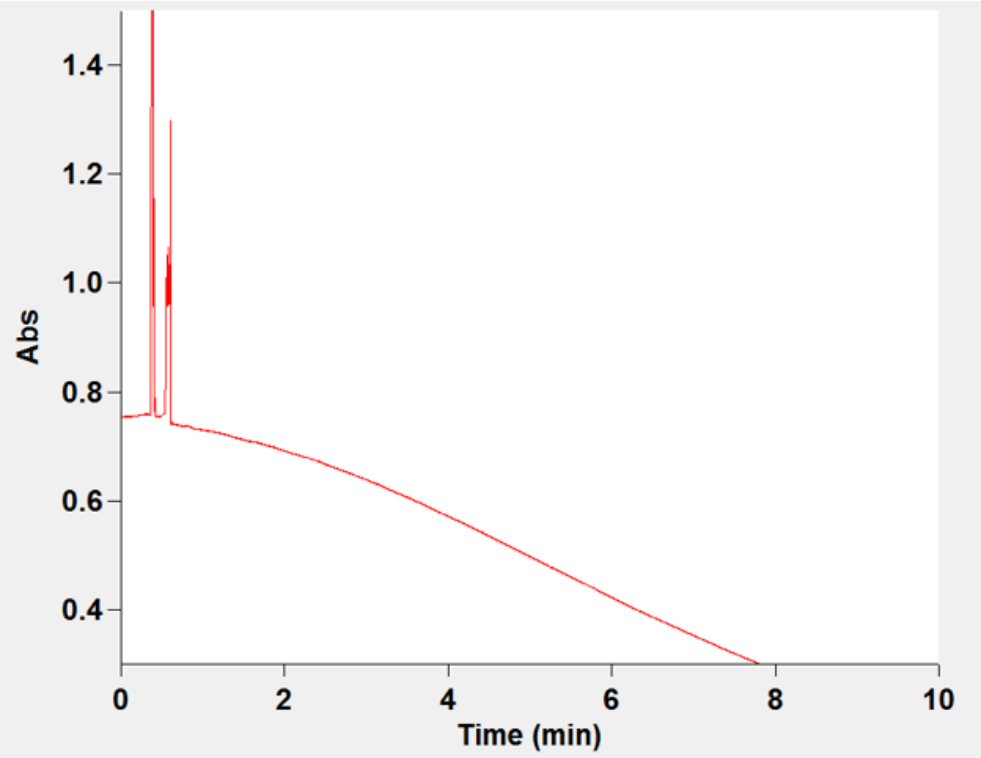

Figure 7.16.12: Shows the chromatogram obtained when measuring IFT25/27^{WT} 1:4 replicate 3. Measured between 4-6 minutes

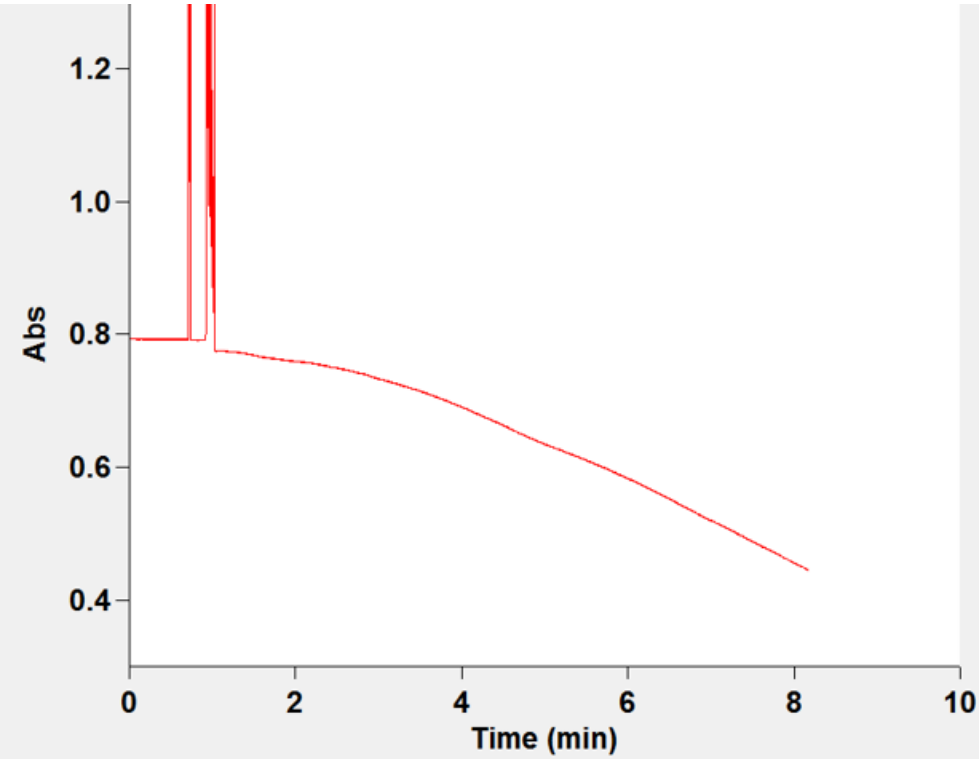

Figure 7.16.13: Shows the chromatogram obtained when measuring IFT25/27^{Y35C} 1:4 replicate 1. Measured between 5-7 minutes

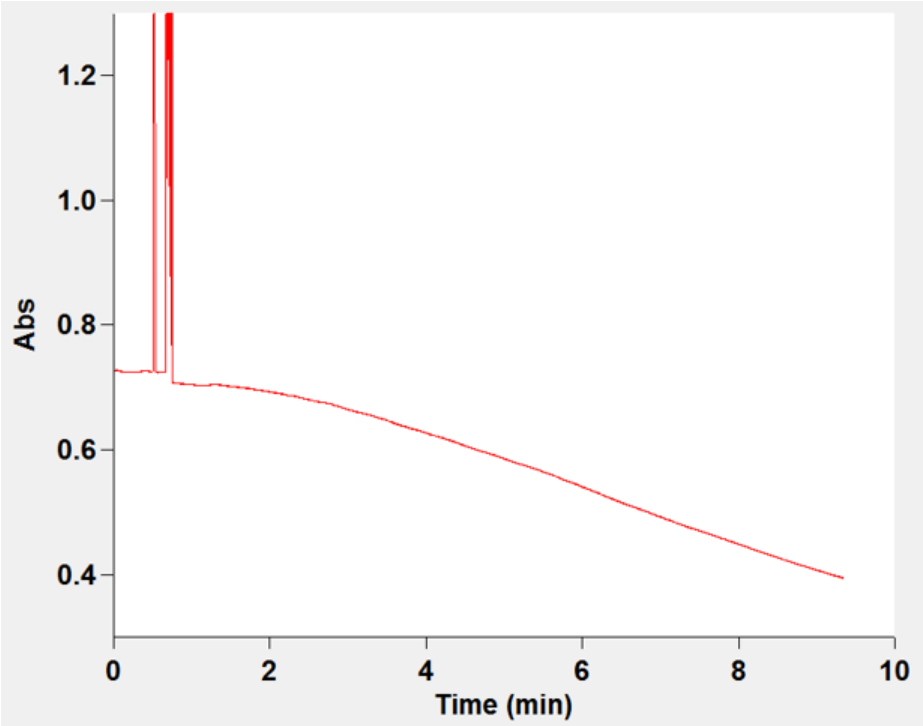

Figure 7.16.14: Shows the chromatogram obtained when measuring IFT25/27^{Y35C} 1:4 replicate 2. Measured between 4-6 minutes

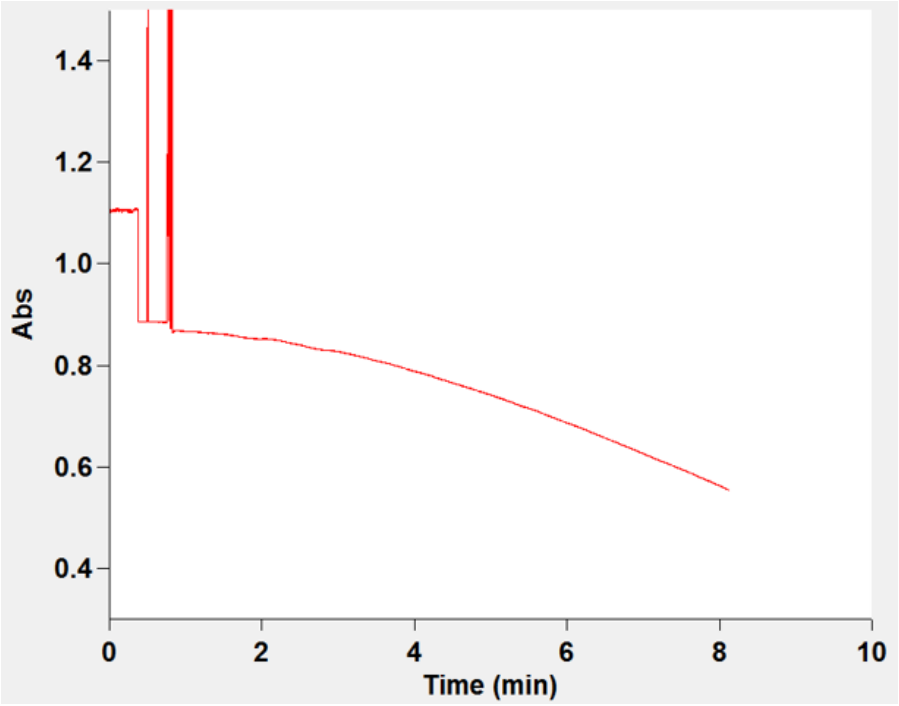

Figure 7.16.15: Shows the chromatogram obtained when measuring IFT25/27^{Y35C} 1:4 replicate 3. Measured between 4-6 minutes

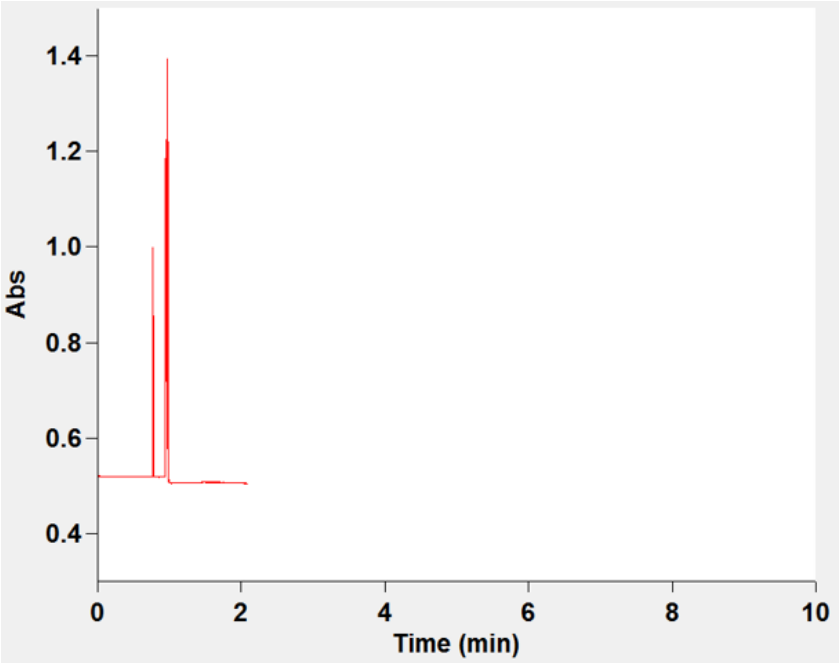

Figure 7.16.16: Shows the chromatogram obtained when measuring IFT25/27^{WT} 0:4 replicate 1.

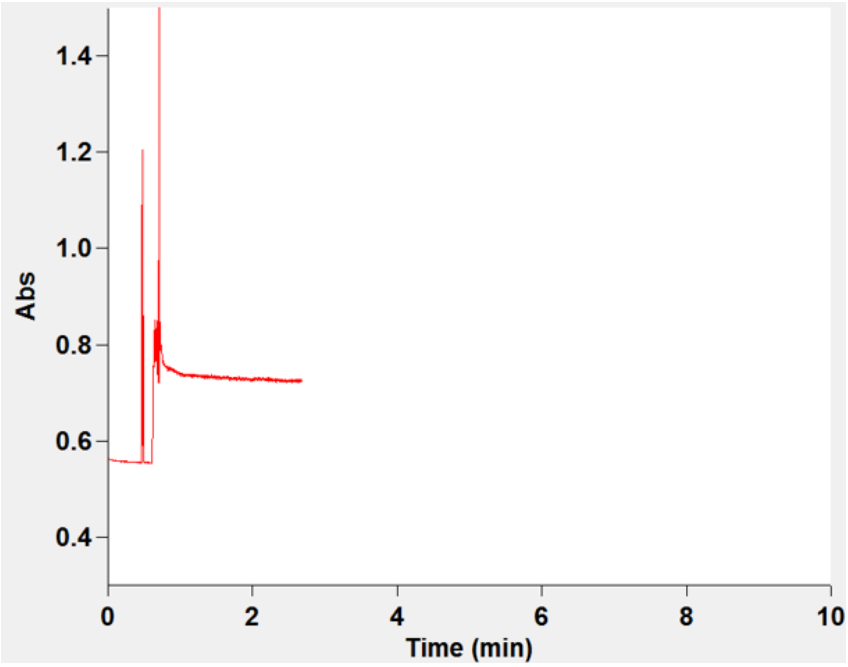

Figure 7.16.17: Shows the chromatogram obtained when measuring IFT25/27^{WT} 0:4 replicate 2.

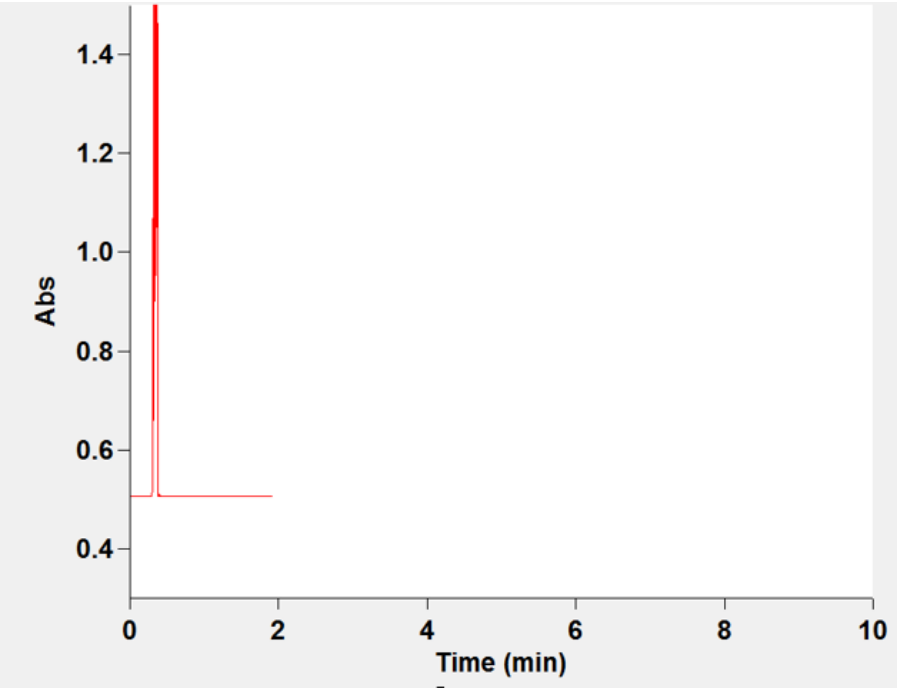

Figure 7.16.18: Shows the chromatogram obtained when measuring IFT25/27^{WT} 0:4 replicate 3.

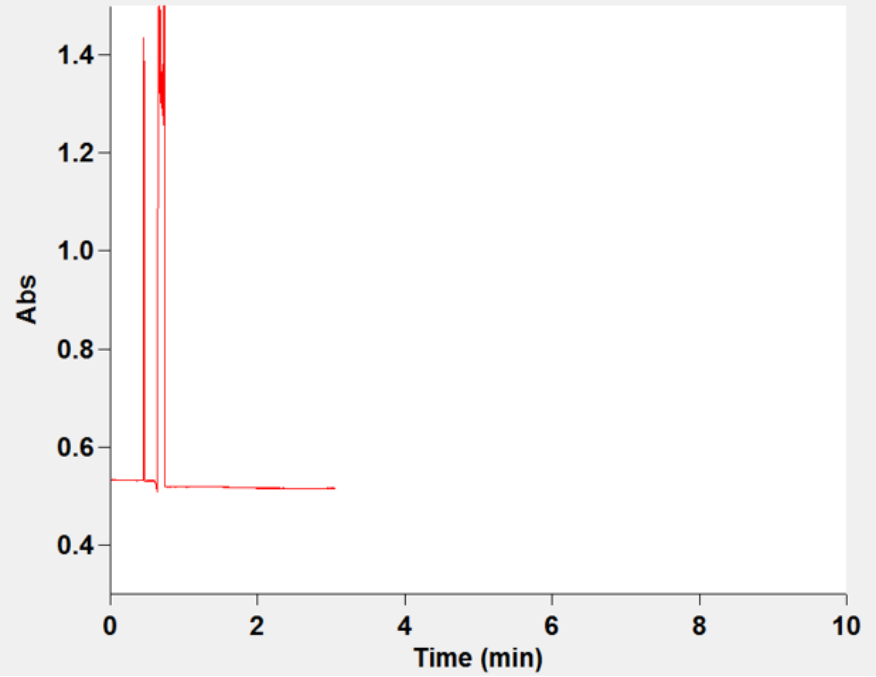

Figure 7.16.19: Shows the chromatogram obtained when measuring IFT25/27^{Y35C} 0:4 replicate 1.

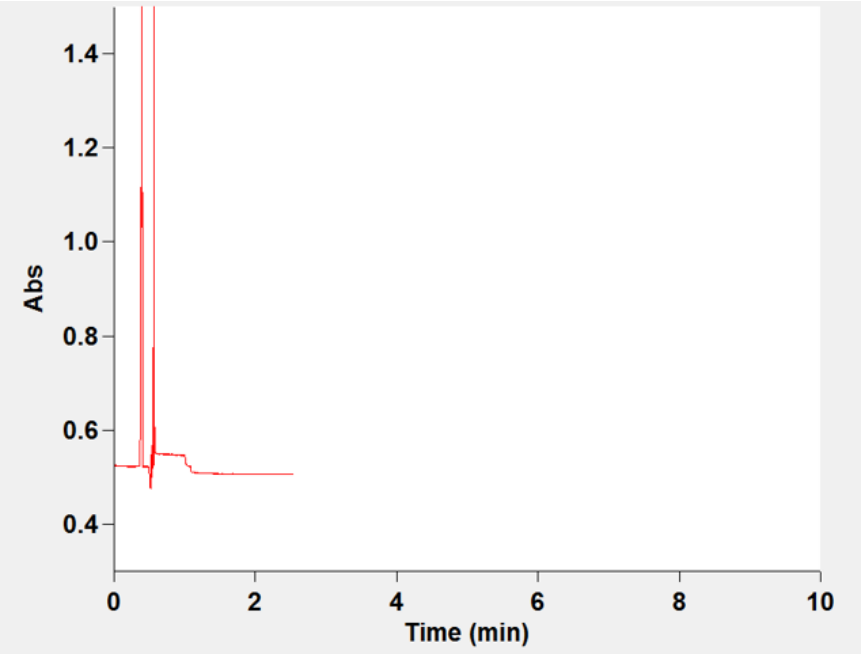

Figure 7.16.20: Shows the chromatogram obtained when measuring IFT25/27^{Y35C} 0:4 replicate 2.

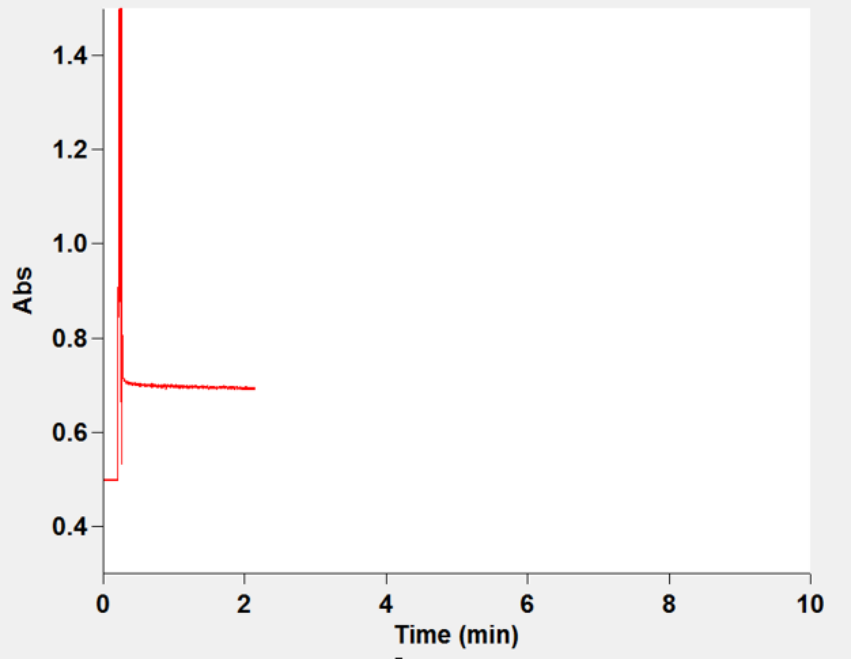

Figure 7.16.21: Shows the chromatogram obtained when measuring IFT25/27^{Y35C} 0:4 replicate 3.

The following figures contain the chromatograms measured in the second Aurora B kinase activity tests:

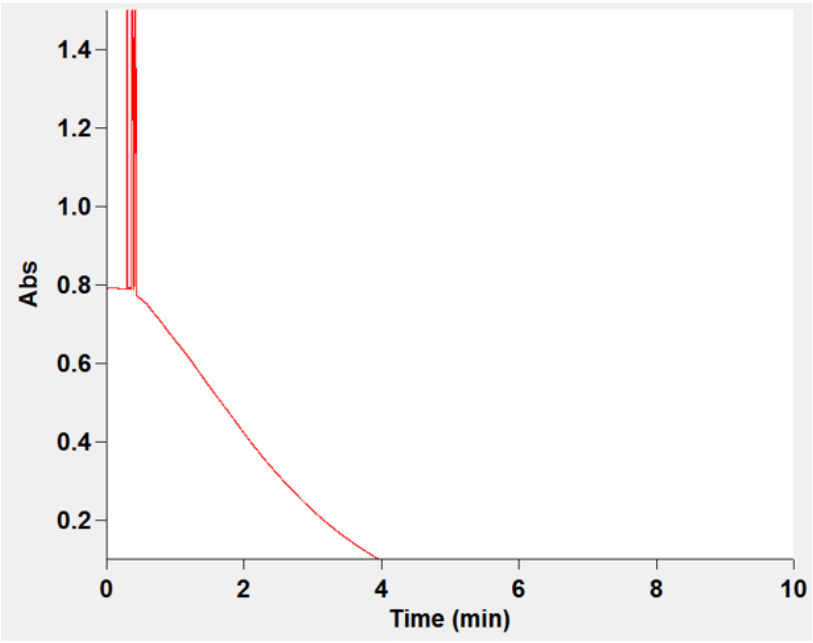

Figure 7.16.22: Shows the chromatogram obtained when measuring Aurora B alone replicate 1. Measured between 1-2 minutes.

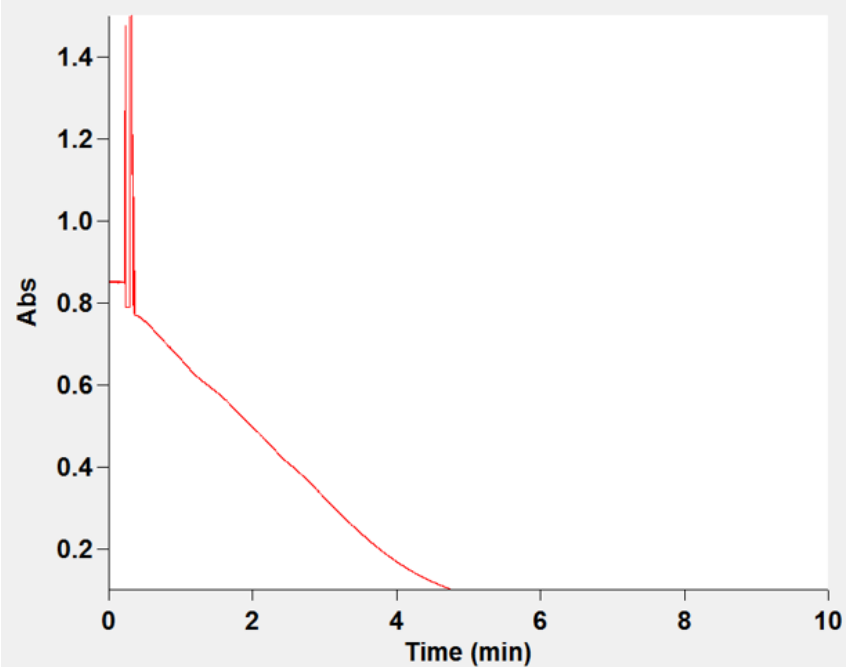

Figure 7.16.23: Shows the chromatogram obtained when measuring Aurora B alone replicate 2. Measured between 0.5-1.5 minutes.

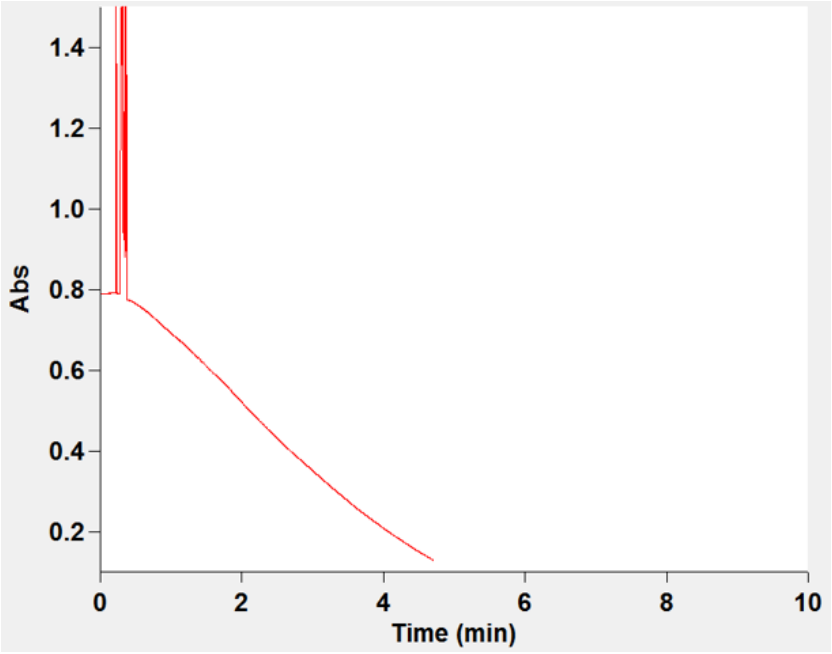

Figure 7.16.24: Shows the chromatogram obtained when measuring Aurora B alone replicate 3. Measured between 1-2 minutes.

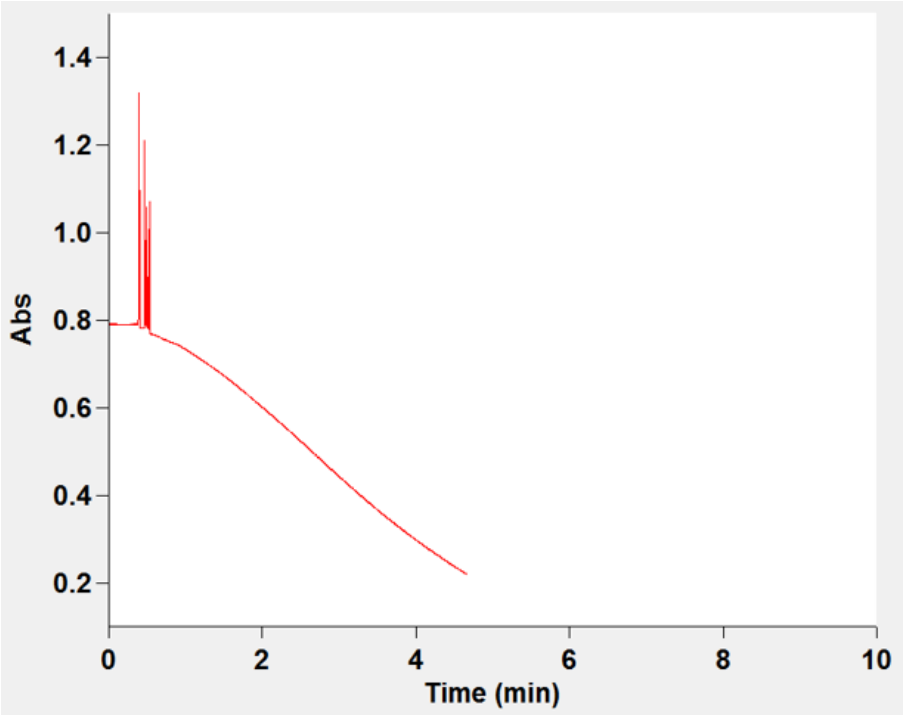

Figure 7.16.25: Shows the chromatogram obtained when measuring IFT25/27^{WT} 1:1 replicate 2. Measured between 1-2 minutes

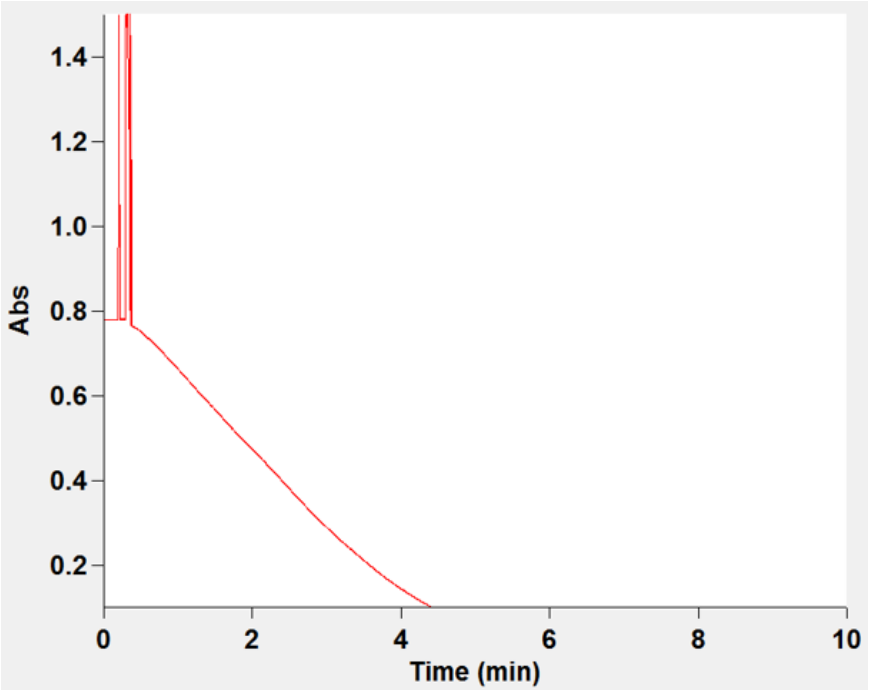

Figure 7.16.26: Shows the chromatogram obtained when measuring IFT25/27^{WT} 1:1 replicate 3. Measured between 0.8-2 minutes

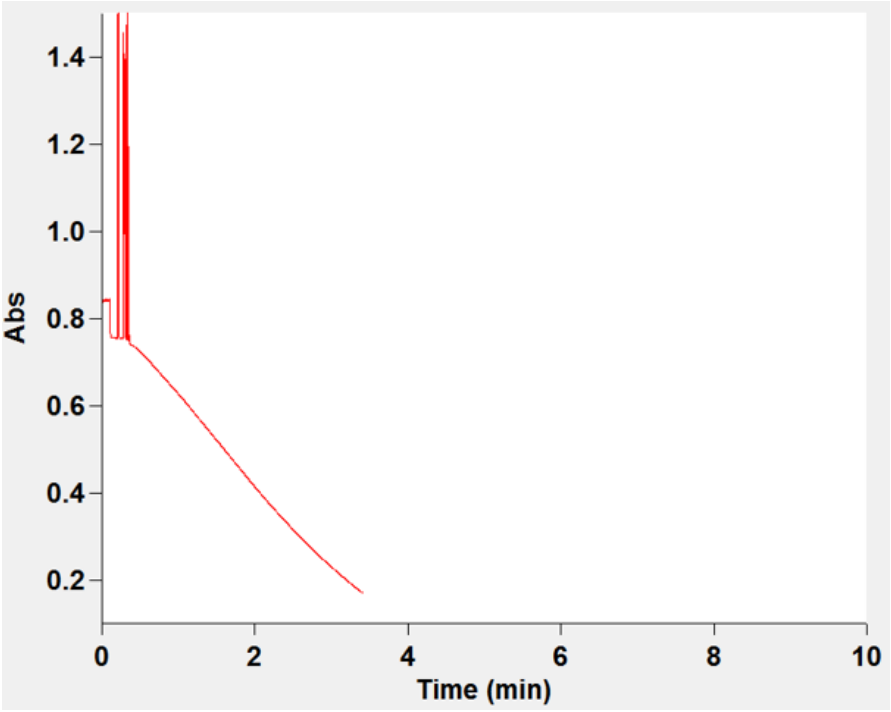

Figure 7.16.27: Shows the chromatogram obtained when measuring IFT25/27^{WT} 1:3 replicate 1. Measured between 1-2 minutes

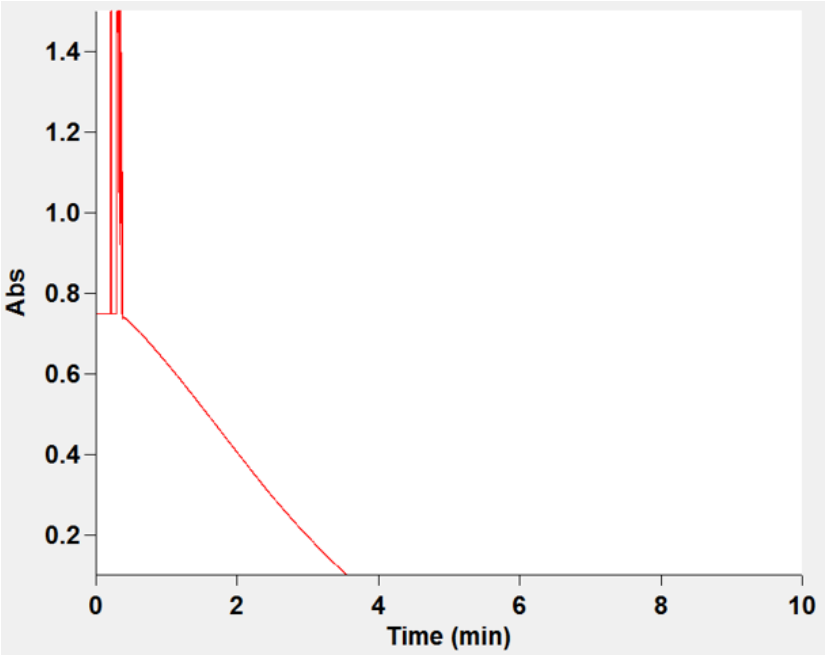

Figure 7.16.28: Shows the chromatogram obtained when measuring IFT25/27^{WT} 1:3 replicate 2. Measured between 1-2 minutes

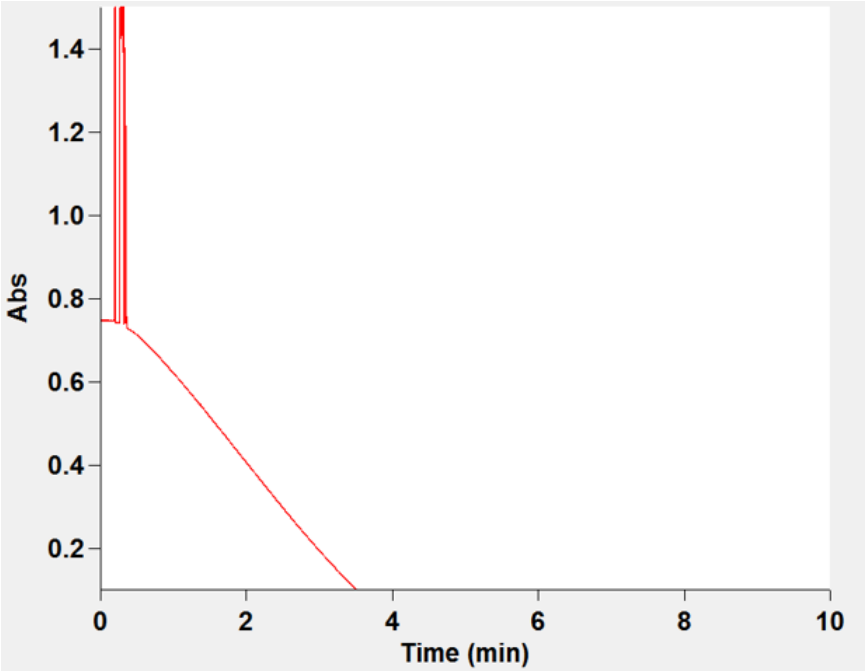

Figure 7.16.29: Shows the chromatogram obtained when measuring IFT25/27^{WT} 1:3 replicate 3. Measured between 1-2 minutes

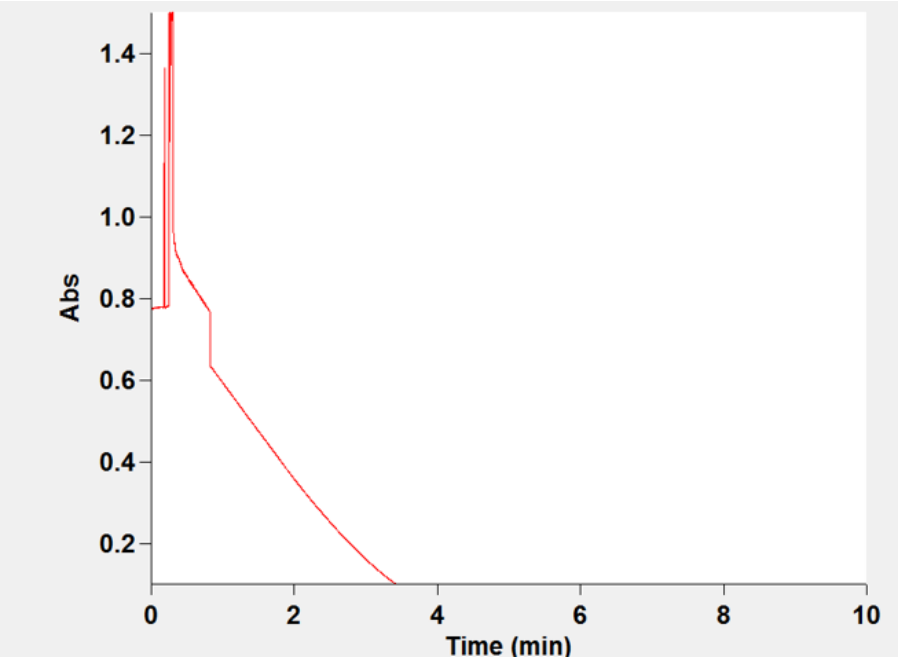

Figure 7.16.30: Shows the chromatogram obtained when measuring IFT25/27^{Y35C} 1:1 replicate 1. Measured between 1-2 minutes

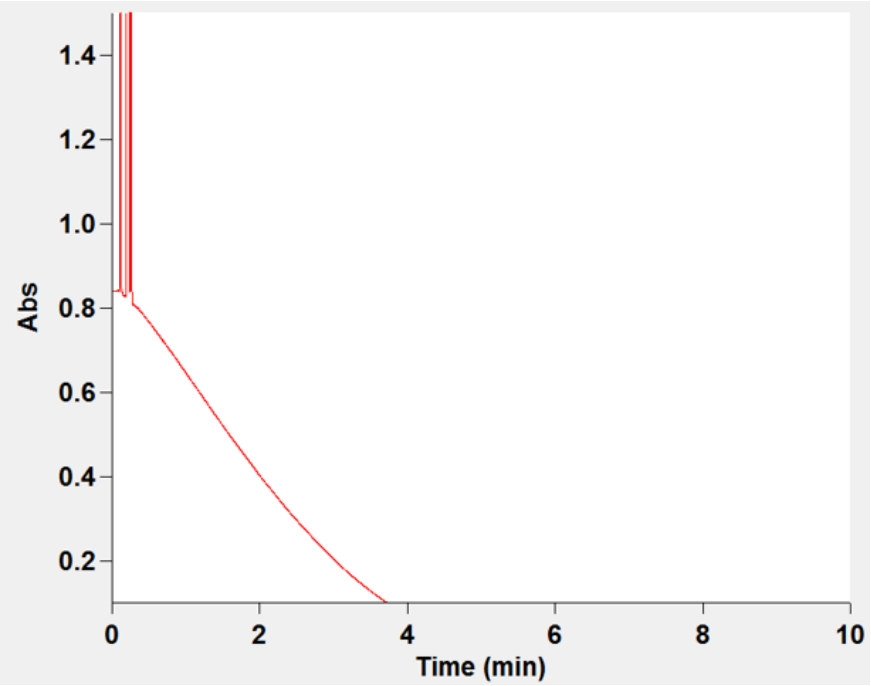

Figure 7.16.31: Shows the chromatogram obtained when measuring IFT25/27^{Y35C} 1:1 replicate 2. Measured between 1-2 minutes

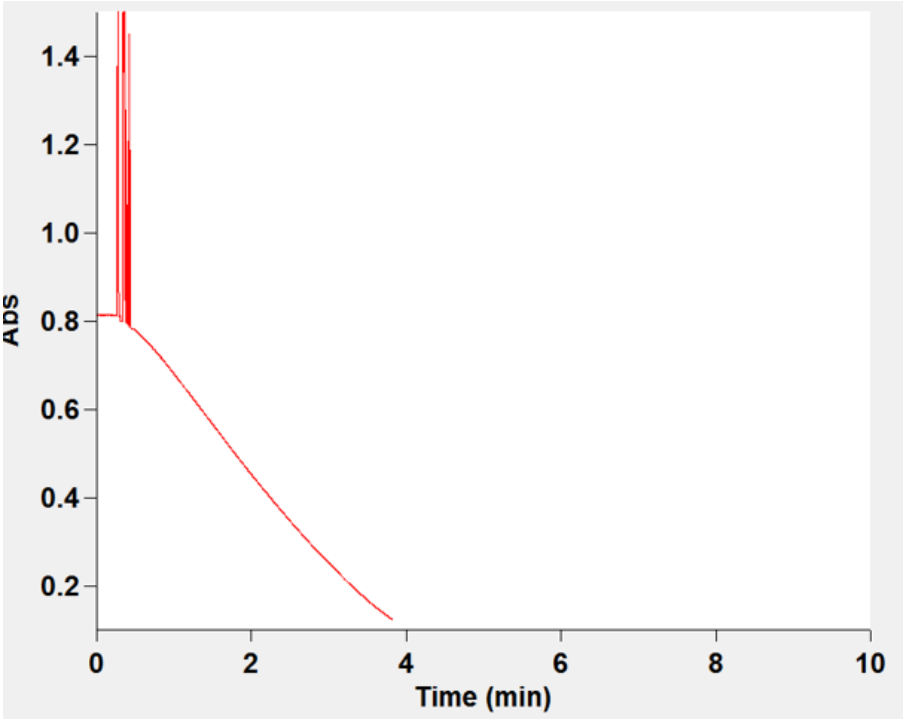

Figure 7.16.32: Shows the chromatogram obtained when measuring IFT25/27^{Y35C} 1:1 replicate 3. Measured between 1-2 minutes

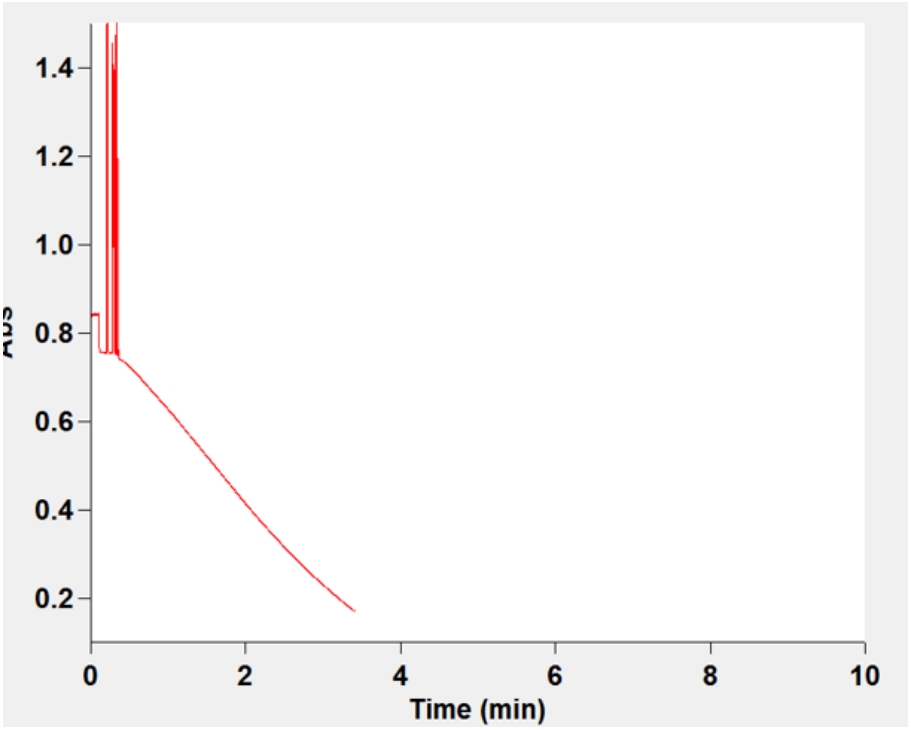

Figure 7.16.33: Shows the chromatogram obtained when measuring IFT25/27^{Y35C} 1:3 replicate 1. Measured between 1-2 minutes

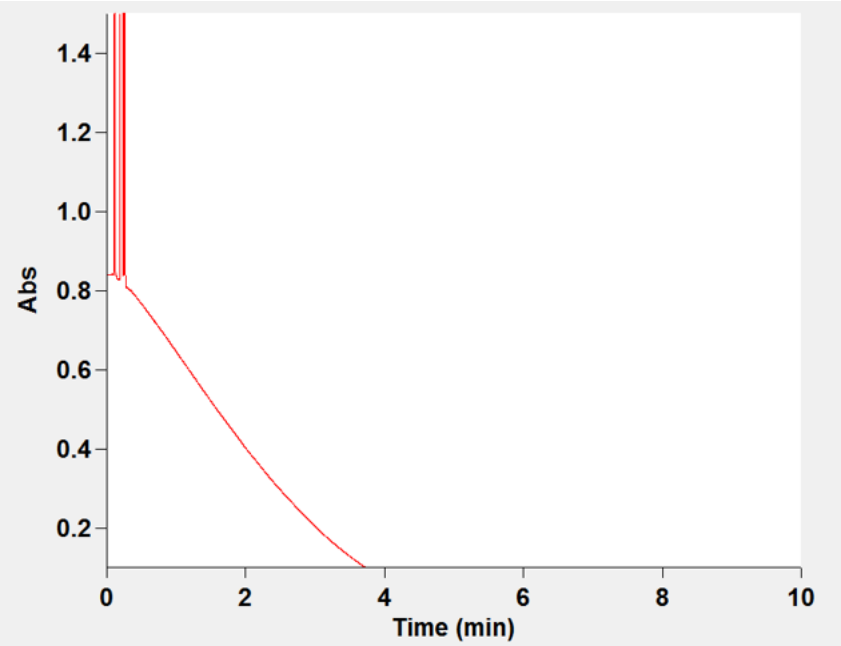

Figure 7.16.34: Shows the chromatogram obtained when measuring IFT25/27^{Y35C} 1:3 replicate 2. Measured between 1-2 minutes

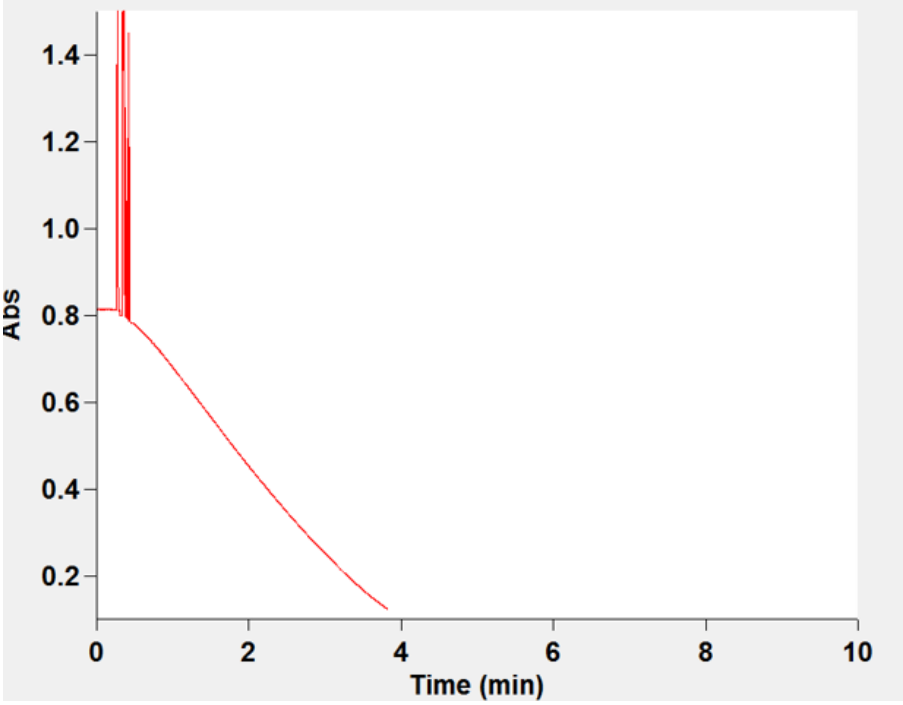

Figure 7.16.35: Shows the chromatogram obtained when measuring IFT25/27^{Y35C} 1:3 replicate 3. Measured between 1-2 minutes

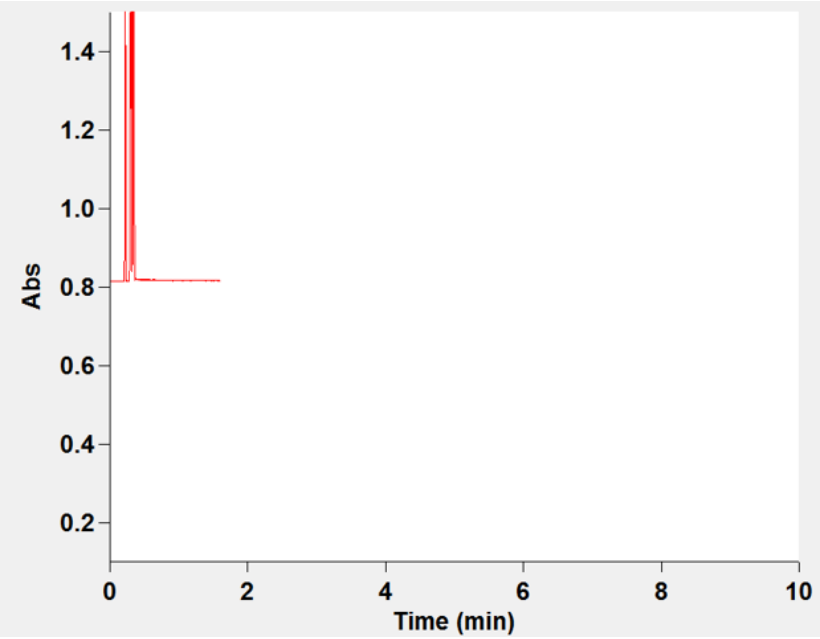

Figure 7.16.36: Shows the chromatogram obtained when measuring IFT25/27^{WT} 0:3 replicate 1. Measured between 1-2 minutes

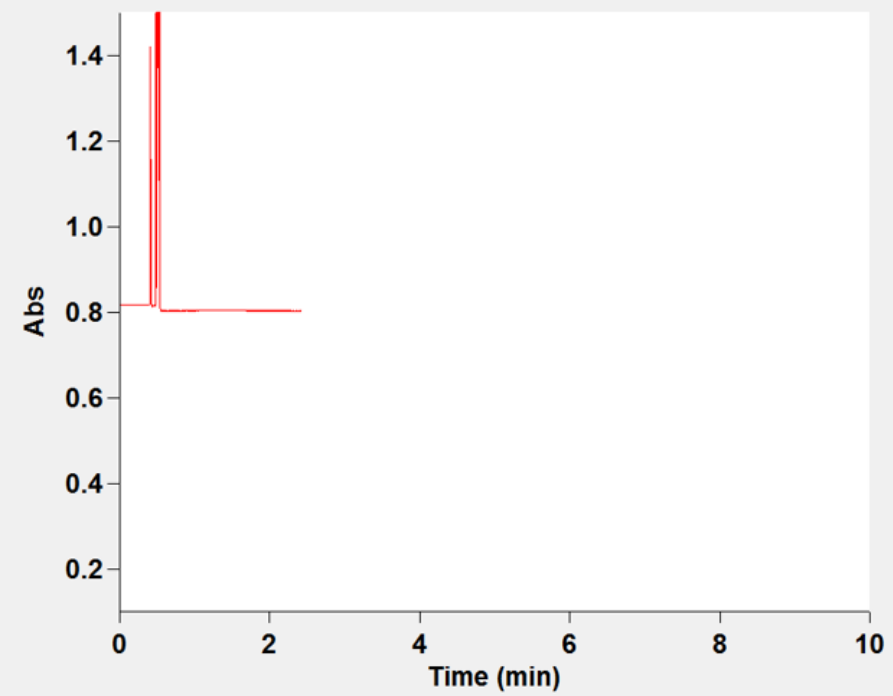

Figure 7.16.37: Shows the chromatogram obtained when measuring IFT25/27^{WT} 0:3 replicate 2. Measured between 1-2 minutes

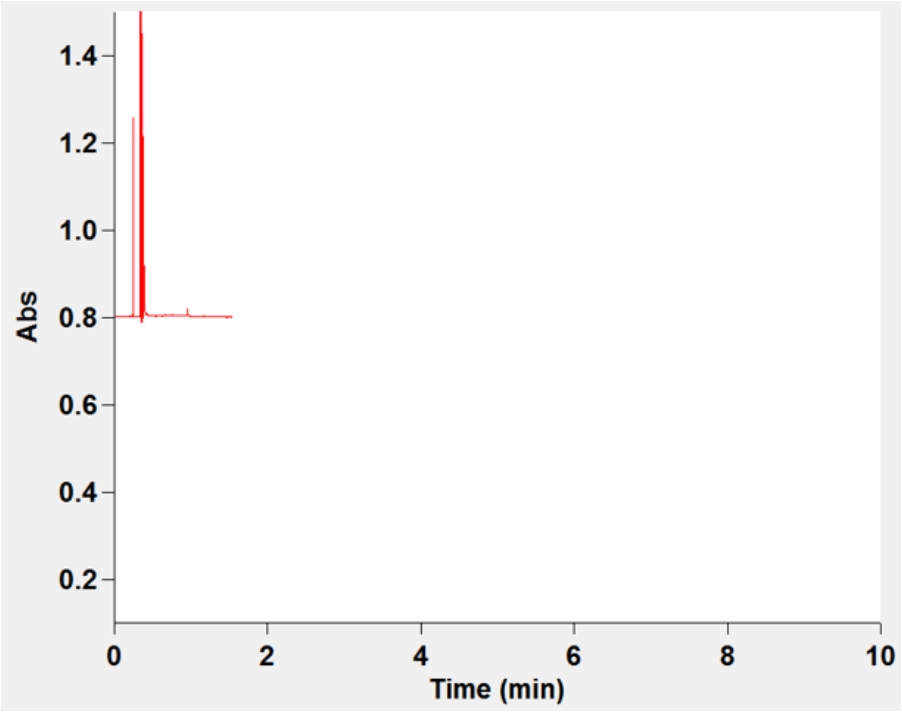

Figure 7.16.38: Shows the chromatogram obtained when measuring IFT25/27^{WT} 0:3 replicate 3. Measured between 1-2 minutes

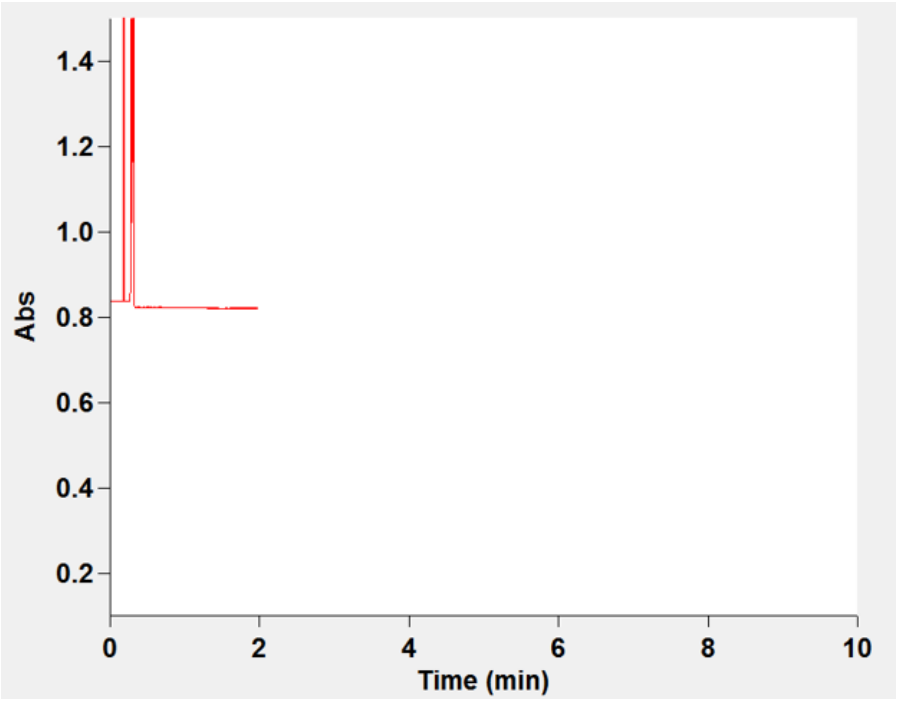

Figure 7.16.39: Shows the chromatogram obtained when measuring IFT25/27^{Y35C} 0:3 replicate 1. Measured between 1-2 minutes

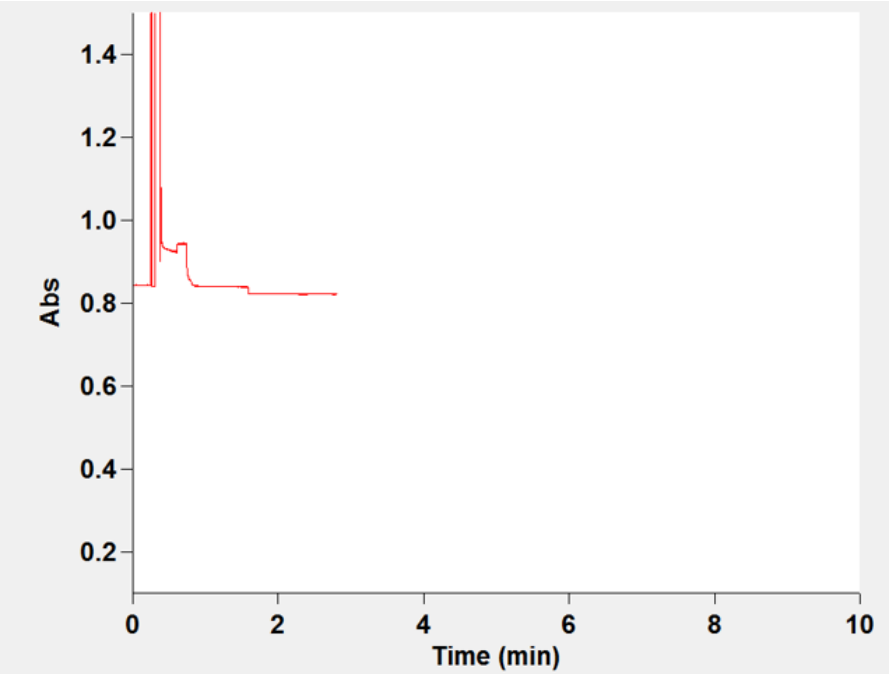

Figure 7.16.40: Shows the chromatogram obtained when measuring IFT25/27^{Y35C} 0:3 replicate 2. Measured between 1-2 minutes

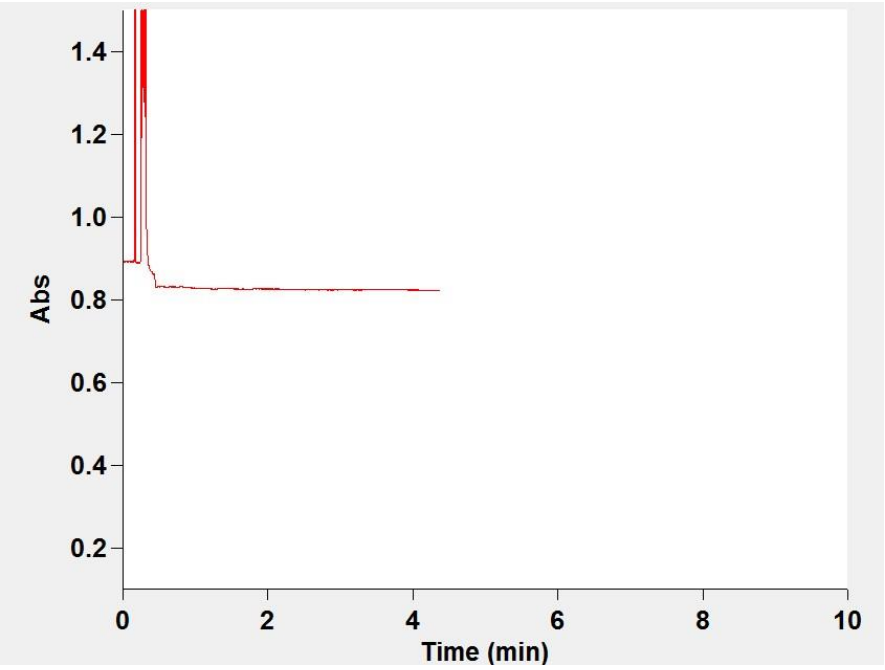

Figure 7.16.41: Shows the chromatogram obtained when measuring IFT25/27^{Y35C} 0:3 replicate 3. Measured between 1-2 minutes

Table 7.16.1: Shows the absorbance recorded for every replicate of the Kinase activity test of the first experiment

	Replicate 1	Replicate 2	Replicate 3
AuB	0.0527	0.0419	0.0447
WT 1:1	0.0654	0.0626	0.0652
Y35C 1:1	0.0521	0.0366	0.053
WT 4:1	0.0794	0.0351	0.0748
Y35C 4:1	0.0532	0.0428	0.0508
Only WT	0.0033	0.009	0.0034
Only Y35C	0.0034	0.0002	0.0037

Table 7.16.2: Shows the absorbance recorded for every replicate of the Kinase activity test of the second experiment

	Replicate 1	Replicate 2	Replicate 3
AuB	0.2187	0.1788	0.1722
WT 1:1	0.15	0.1907	0.1868
Y35C 1:1	0.2357	0.2438	0.2291
WT 3:1	0.2139	0.2234	0.2158
Y35C 3:1	0.1751	0.1624	0.1847
Only WT	0.0009	0.0004	0.0025
Only Y35C	0.0018	0.0001	0.0018